Search for cascade decays of charged sleptons and sneutrinos in final states with three leptons and missing transverse momentum in *pp* collisions at $\sqrt{s} = 13$ TeV with the ATLAS detector

G. Aad *et al.*[*]
(ATLAS Collaboration)

(Received 18 March 2025; accepted 15 May 2025; published 8 July 2025)

A search for cascade decays of charged sleptons and sneutrinos using final states characterized by three leptons (electrons or muons) and missing transverse momentum is presented. The analysis is based on a dataset with 140 fb^{-1} of proton-proton (pp) collisions at a center-of-mass energy of $\sqrt{s} = 13$ TeV recorded by the ATLAS detector at the Large Hadron Collider. This paper focuses on a supersymmetric scenario that is motivated by the muon anomalous magnetic moment observation, dark-mattter relic density abundance, and electroweak naturalness. A mass spectrum involving light Higgsinos and heavier sleptons with a bino at intermediate mass is targeted. No significant deviation from the Standard Model expectation is observed. This search enables us to place stringent constraints on this model, excluding at the 95% confidence level charged slepton and sneutrino masses up to 450 GeV when assuming a lightest neutralino mass of 100 GeV and mass-degenerate selectrons, smuons and sneutrinos.

DOI: 10.1103/6gy3-cb4t

I. INTRODUCTION

Supersymmetry (SUSY) [1–6] postulates a symmetry between bosons and fermions, and predicts the existence of new partners (superpartners) for each Standard Model (SM) particle. In SUSY models conserving R-parity [7], SUSY particles are produced in pairs. The lightest supersymmetric particle (LSP) has to be stable and is weakly interacting, constituting a possible dark-matter candidate [8,9]. The LSP produced at the Large Hadron Collider (LHC) [10] would escape detection and cause momentum imbalance in the form of missing transverse momentum ($\mathbf{p}_{\mathrm{T}}^{\mathrm{miss}}$, the magnitude of which is referred to as $E_{\mathrm{T}}^{\mathrm{miss}}$) in the final state, which is used to discriminate the SUSY signal from the background.

The scalar superpartners of the SM fermions are charged sleptons ($\tilde{\ell}$), sneutrinos ($\tilde{\nu}$), and squarks ($\tilde{q}$), while gluons have fermionic superpartners called gluinos ($\tilde{g}$). In the minimal supersymmetric extension of the SM (MSSM) [11,12], the bino, wino and Higgsino fields are the fermionic superpartners of the $\mathrm{SU}(2) \times \mathrm{U}(1)$ gauge fields in the SM, and the two complex scalar doublets of a minimally extended Higgs sector, respectively. The bino, wino, and Higgsino are collectively referred to as "electroweakinos," and they mix to give the mass eigenstates referred to as charginos $\tilde{\chi}_i^{\pm}$ ($i = 1, 2$) and neutralinos $\tilde{\chi}_j^0$ ($j = 1, 2, 3, 4$), with the subscripts indicating increasing mass.

Electroweakinos and sleptons with masses of several hundred GeV are motivated by various phenomenological arguments: the MSSM parameter space explaining the possible discrepancy between the measured muon anomalous magnetic moment [13] and its SM predictions [14][1] typically includes electroweakinos and smuons with masses from 200 GeV to 1 TeV [16–18]; when the neutralino LSP is the dark-matter candidate, its mass is constrained to be less than a few TeV by the observed relic density [19,20]; the Higgsino mass is also motivated to be of the same order as the Z-boson mass by electroweak naturalness arguments [21–24]. The additional muon anomalous magnetic moment contribution is typically generated through chargino-sneutrino loops and neutralino-smuon loops containing at least three types of supersymmetric particles [16,18].

This paper targets the loop contribution including the bino, Higgsino, and left-handed smuon as shown in Fig. 1, and specifically the mass spectrum involving the Higgsino LSP, heavier left-handed sleptons and sneutrinos, and the bino at a mass in between, as illustrated in Fig. 2. Higgsino-dominated states ($\tilde{\chi}_2^0$, $\tilde{\chi}_1^{\pm}$, $\tilde{\chi}_1^0$) have a mass-compressed spectrum in this model. This mass spectrum is referred to as

[*]Full author list given at the end of the article.

[1]Note that the discrepancy tends to smaller when the lattice QCD results are used for the theory prediction [15].

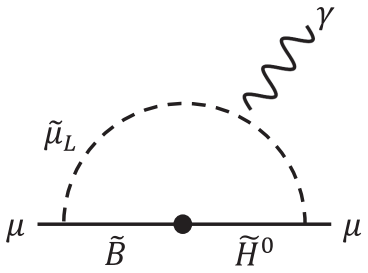

FIG. 1. Neutralino-smuon loop yielding a sizable muon anomalous magnetic moment. The black dot represents the mixing between electroweakinos.

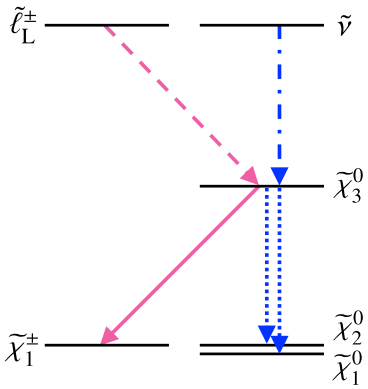

FIG. 2. Mass spectrum and the decay pattern of the considered simplified SBH model. The dashed (dash-dotted) arrow represents the decay emitting a charged lepton (neutrino). The solid (dotted) arrow represents the decay emitting a W (Z or h) boson. Light pink (darker blue) arrows represent the decay emitting a charged (neutral) particle.

the "slepton-bino-Higgsino" (SBH) model in this paper, and can address the observed muon anomalous magnetic moment, dark matter, and electroweak naturalness simultaneously when the involved SUSY particles are lighter than 1 TeV [16]. While the SBH model involving smuons is more motivated by the muon anomalous magnetic moment measurement, a model with selectrons is also considered in this analysis as the electron anomalous magnetic moment measurements [25,26] may also imply a mild deviation from the SM prediction [27–30].

Current constraints on the SBH model primarily originate from direct dark-matter searches using nuclear recoils [31] and SUSY searches at the LHC. The direct dark-matter searches place a stringent constraint for $\Delta m(\tilde{\chi}^0_3,\tilde{\chi}^0_1) \lesssim 100$ GeV, while $\Delta m(\tilde{\chi}^0_3,\tilde{\chi}^0_1) \gtrsim 100$ GeV is still fully viable assuming a local dark-matter density of 0.3 GeV $\cdot$ cm^{-3} [32].

At the LHC, no dedicated searches have been performed for the SBH model; however, some constraints can be set through (i) generic Higgsino LSP searches, using the disappearing track signature [33–35], the mildly displaced track signature [36], and the low-momentum prompt lepton[2] signatures [37–39]; and (ii) several electroweakino and slepton searches using final states with two or three leptons and $E_{\mathrm{T}}^{\mathrm{miss}}$ [38,40–46]. However, their sensitivity to the SBH model is mostly limited to the mass parameter space that is already disfavored by the direct dark-matter searches, i.e. $\Delta m(\tilde{\chi}^0_3,\tilde{\chi}^0_1) \lesssim 100$ GeV. In the SBH model, sleptons rarely decay into Higgsinos directly due to the suppressed slepton-Higgsino Yukawa coupling compared with the slepton-bino electroweak coupling.

This study reports the first dedicated search for the SBH model targeting the cascade decay signature using the proton-proton collision data at a center-of-mass energy of $\sqrt{s} = 13$ TeV collected by the ATLAS detector at the LHC in the years 2015–2018, corresponding to an integrated luminosity of 140 fb^{-1} [47]. Final states with three leptons are explored. Through the optimization of the event selection, and the introduction of new search regions requiring three leptons with the same charge and zero jets containing b-hadrons, a signature explored in this paper for the first time at the LHC, the first unique sensitivity for $\Delta m(\tilde{\chi}^0_3,\tilde{\chi}^0_1) \gtrsim 100$ GeV is achieved.

The paper is structured as follows; the definition of the benchmark signal model is further detailed in Sec. II; a brief overview of the ATLAS detector is provided in Sec. III; the data and the Monte Carlo (MC) simulation samples are described in Sec. IV; the particle reconstruction methods used in the analysis are presented in Sec. V; the event selection strategy and the signal region definition are discussed in Sec. VI; the SM background estimation is described in Sec. VII, followed by a summary of the systematic uncertainties in Sec. VIII; the results of the search and its interpretation are presented in Sec. IX, followed by the conclusion in Sec. X.

II. THE SBH SIGNAL MODEL

The benchmark signal model targeted in the analysis involves the direct pair production of left-handed sleptons and sneutrinos ($\tilde{\ell}^+_{\mathrm{L}}\tilde{\ell}^-_{\mathrm{L}}$, $\tilde{\nu}\,\tilde{\nu}$), or the associated production of a left-handed slepton and a sneutrino ($\tilde{\ell}^{\pm}_{\mathrm{L}}\tilde{\nu}$) mediated by off shell W/Z bosons.

Sleptons and sneutrinos promptly decay into $\tilde{\ell}_{\mathrm{L}} \to \ell\tilde{\chi}^0_3$ and $\tilde{\nu} \to \nu\tilde{\chi}^0_3$, and the $\tilde{\chi}^0_3$ further decays as $\tilde{\chi}^0_3 \to W^{\pm}\tilde{\chi}^{\mp}_1$, $\tilde{\chi}^0_3 \to Z\tilde{\chi}^0_{1,2}$ or $\tilde{\chi}^0_3 \to h\tilde{\chi}^0_{1,2}$, as illustrated in Fig. 2. The decay of the $\tilde{\chi}^0_3$ via a Higgs boson, h, is only kinematically allowed when the mass difference between the bino-dominated state ($\tilde{\chi}^0_3$) and the Higgsino-dominated states ($\tilde{\chi}^{\pm}_1$, $\tilde{\chi}^0_2$) is larger than the Higgs-boson mass. Example signal diagrams with three leptons in the final state are illustrated in Fig. 3. Right-handed sleptons are not considered in this model due to their much smaller production cross section. However, they can be targeted by the same

[2]In this paper, "leptons" refer to electrons or muons.

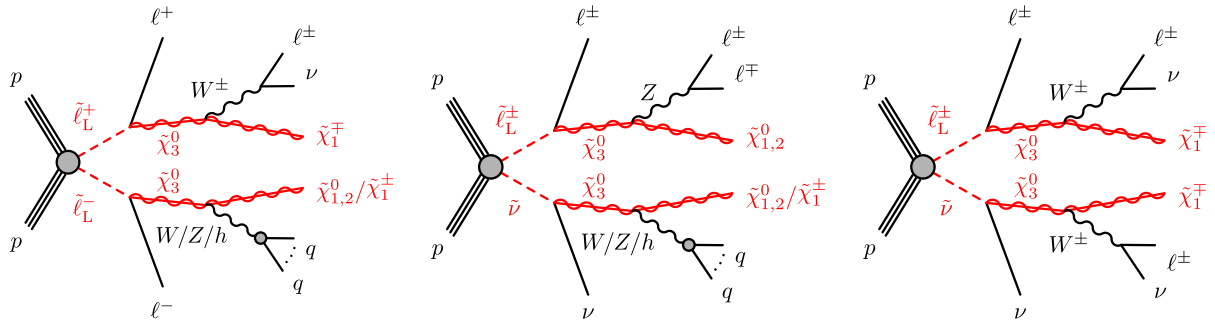

FIG. 3. Diagrams for the targeted cascade signatures in the SBH model. Final states with three light-flavor charged leptons (electrons or muons) are considered in the analysis. The decays of $\tilde{\chi}_2^0$ and $\tilde{\chi}_1^\pm$ are ignored as they only result in low-momentum particles that are almost never reconstructed.

search since they follow the same decay chains as the left-handed ones. The presence of right-handed sleptons would also not influence the decay chains of the left-handed sleptons and sneutrinos.

Leptons can originate from the decay of sleptons, the direct decay of W/Z bosons, or the indirect decay of a Higgs boson (mostly via $h \to WW^*$). The analysis focuses on final states with three leptons as they are found to be the most sensitive compared with the other lepton multiplicity categories. The signatures are also characterized by the presence of $E_{\mathrm{T}}^{\mathrm{miss}}$ originating from the LSPs and neutrinos.

The analysis design and the result interpretation are based on the framework of "simplified models" [48], where the masses of relevant SUSY particles (in this case the $\tilde{\ell}_{\mathrm{L}}$, $\tilde{\nu}$, $\tilde{\chi}_3^0$, $\tilde{\chi}_2^0$, $\tilde{\chi}_1^\pm$, and $\tilde{\chi}_1^0$) are the only free parameters. For the sleptons and sneutrinos, three subscenarios are considered:

(i) $m(\tilde{e}_{\mathrm{L}}) = m(\tilde{\nu}_e) < 1$ TeV with $\tilde{\mu}_{\mathrm{L}}, \tilde{\nu}_\mu$ being decoupled,
(ii) $m(\tilde{\mu}_{\mathrm{L}}) = m(\tilde{\nu}_\mu) < 1$ TeV with $\tilde{e}_{\mathrm{L}}, \tilde{\nu}_e$ being decoupled, and
(iii) $m(\tilde{e}_{\mathrm{L}}) = m(\tilde{\nu}_e) = m(\tilde{\mu}_{\mathrm{L}}) = m(\tilde{\nu}_\mu) < 1$ TeV.

Staus and right-handed sleptons are not considered. The mass splitting between the left-handed sleptons and sneutrinos, and between the Higgsino-dominated states ($\tilde{\chi}_2^0$, $\tilde{\chi}_1^\pm$, $\tilde{\chi}_1^0$) with non-negligible bino mixing, is typically $\mathcal{O}(1\text{–}10)$ GeV [49,50]. The states are treated as mass degenerate in this study, since the low-p_{T} particles from decays in such compressed hierarchies are rarely reconstructed in the analysis. A 100% branching ratio is assumed for $\tilde{\ell}_{\mathrm{L}} \to \ell\tilde{\chi}_3^0$ and $\tilde{\nu} \to \nu\tilde{\chi}_3^0$, which is reasonable given the coupling assumptions. The branching ratios of $\tilde{\chi}_3^0$ are set to:

(i) $\mathcal{B}(\tilde{\chi}_3^0 \to W^{\pm(*)}\tilde{\chi}_1^\mp) = 50\%(50\%)$,
(ii) $\mathcal{B}(\tilde{\chi}_3^0 \to Z^{(*)}\tilde{\chi}_{1,2}^0) = 25\%(50\%)$, and
(iii) $\mathcal{B}(\tilde{\chi}_3^0 \to h\tilde{\chi}_{1,2}^0) = 25\%(0\%)$,

with equal branching ratios into $\tilde{\chi}_1^0$ and $\tilde{\chi}_2^0$, for $\Delta m(\tilde{\chi}_3^0, \tilde{\chi}_1^0) \geq m_h$ ($\Delta m(\tilde{\chi}_3^0, \tilde{\chi}_1^0) < m_h$). The values for $\Delta m(\tilde{\chi}_3^0, \tilde{\chi}_1^0) \geq m_h$ are typical for these masses [51]. The values for $\Delta m(\tilde{\chi}_3^0, \tilde{\chi}_1^0) < m_h$ are set more arbitrarily, but this choice has a negligible impact on the search results. Other SUSY particles are decoupled.

III. THE ATLAS DETECTOR

The ATLAS detector [52] at the LHC covers nearly the entire solid angle around the collision point.[3] It consists of an inner tracking detector surrounded by a thin superconducting solenoid, electromagnetic and hadron calorimeters, and a muon spectrometer incorporating three large superconducting air-core toroidal magnets.

The inner-detector system (ID) is immersed in a 2 T axial magnetic field and provides charged-particle tracking in the range of $|\eta| < 2.5$. The high-granularity silicon pixel detector covers the vertex region and typically provides four measurements per track, the first hit normally being in the insertable B-layer installed before Run 2 [53,54]. It is followed by the semiconductor tracker, which usually provides eight measurements per track. These silicon detectors are complemented by the transition radiation tracker (TRT), which enables radially extended track reconstruction up to $|\eta| < 2.0$. The TRT also provides electron identification information based on the fraction of hits (typically 30 in total) above a higher energy-deposit threshold corresponding to transition radiation.

The calorimeter system covers the pseudorapidity range $|\eta| < 4.9$. Within the region $|\eta| < 3.2$, electromagnetic calorimetry is provided by barrel and endcap high-granularity lead/liquid-argon (LAr) calorimeters, with an

[3]ATLAS uses a right-handed coordinate system with its origin at the nominal interaction point (IP) in the center of the detector and the z-axis along the beam pipe. The x-axis points from the IP to the center of the LHC ring, and the y-axis points upwards. Polar coordinates (r, ϕ) are used in the transverse plane, ϕ being the azimuthal angle around the z-axis. The pseudorapidity is defined in terms of the polar angle θ as $\eta = -\ln\tan(\theta/2)$ and is equal to the rapidity $y = \frac{1}{2}\ln(\frac{E+p_z}{E-p_z})$ in the relativistic limit. Angular distance is measured in units of $\Delta R \equiv \sqrt{(\Delta y)^2 + (\Delta\phi)^2}$.

additional thin LAr presampler covering $|\eta| < 1.8$ to correct for energy loss in material upstream of the calorimeters. Hadron calorimetry is provided by the steel/scintillator-tile calorimeter, segmented into three barrel structures within $|\eta| < 1.7$, and two copper/LAr hadron endcap calorimeters. The solid angle coverage is completed with forward copper/LAr and tungsten/LAr calorimeter modules optimized for electromagnetic and hadronic energy measurements respectively.

The muon spectrometer (MS) comprises separate trigger and high-precision tracking chambers measuring the deflection of muons in a magnetic field generated by the superconducting air-core toroidal magnets. The field integral of the toroids ranges between 2.0 and 6.0 Tm across most of the detector. Three layers of precision chambers, each consisting of layers of monitored drift tubes, cover the region $|\eta| < 2.7$, complemented by cathode-strip chambers in the forward region, where the background is higher. The muon trigger system covers the range $|\eta| < 2.4$ with resistive-plate chambers in the barrel, and thin-gap chambers in the endcap regions.

The luminosity is measured mainly by the LUminosity Cherenkov Integrating Detector 2 (LUCID-2) [55] detector that records Cherenkov light produced by the quartz windows of photomultipliers located close to the beam pipe. Events are selected by the first-level trigger system implemented in custom hardware, followed by selections made by algorithms implemented in software in the high-level trigger [56]. The first-level trigger accepts events from the 40 MHz bunch crossings at a rate below 100 kHz, which the high-level trigger further reduces to record events to disk at about 1 kHz.

A software suite [57] is used in data simulation, in the reconstruction and analysis of real and simulated data, in detector operations, and in the trigger and data acquisition systems of the experiment.

IV. DATA AND MONTE CARLO SIMULATION

The analysis is performed using the pp collision data collected by the ATLAS detector at the LHC between the years 2015 and 2018 at a center-of-mass energy of $\sqrt{s} = 13$ TeV. The dataset corresponds to a total integrated luminosity of 140 fb^{-1} after imposing data quality requirements [47]. In this dataset there are, on average, approximately 34 simultaneous pp collisions in each bunch crossing.

Monte Carlo simulation is used to model the contributions of the signal and the SM processes. It is used to define and optimize the event selection criteria, to estimate the signal and SM background event yields after the selections, and to evaluate the systematic uncertainties associated with the estimation. The generators and parameters used in the MC simulation samples are described below and summarized in Table I.

Events from $W/Z+$jets, diboson and triboson processes [70,74] are simulated using the Sherpa2.2 [71] generator: the fully leptonically decaying diboson events are simulated using Sherpa2.2.12; events of $Z \to ee+$ jets, $Z \to \mu\mu+$ jets, $W+$jets, and semileptonically decaying diboson processes are simulated with Sherpa2.2.11; $Z \to \tau\tau$ samples are simulated with Sherpa2.2.14; triboson processes are simulated using Sherpa2.2.2. The matrix element calculations are matched to the parton shower (PS) simulation using the Catani-Seymour dipole factorization [104,105]. This matching is performed separately for different jet multiplicities and merged into an inclusive sample using an improved Catani-Krauss-Kuhn-Webber (CKKW) matching procedure [106,107] extended to next-to-leading-order (NLO) accuracy in QCD, using the MEPS@NLO prescription [106–109]. The virtual QCD correction for matrix elements at NLO accuracy is provided by the

TABLE I. Summary of the generator configurations for the simulated SM backgrounds and signal samples.

Process	Matrix element	Parton shower	Tune	PDF set	Cross section order
SUSY processes	MadGraph5_aMC@NLO3.3.1 [58]	PYTHIA8.307 [59]	A14 [60,61]	NNPDF2.3LO [62]	NLO + NLL [63–69]
$W/Z+$jets [70]	Sherpa 2.2.11/2.2.14 [71]	Sherpa 2.2.11/2.2.14	Standard	NNPDF3.0NNLO [72]	NNLO [73]
Diboson [74]	Sherpa 2.2.11/2.2.12	Sherpa 2.2.11/2.2.12	Standard	NNPDF3.0NNLO	Generator NLO
Triboson [74]	Sherpa2.2.2	Sherpa2.2.2	Standard	NNPDF3.0NNLO	Generator NLO
$t\bar{t}$ [75]	POWHEG BOX2 [76–78]	PYTHIA8.230	A14	NNPDF2.3LO	NNLO + NNLL [79–85]
Single-top [86–89]	POWHEG BOX2	PYTHIA8.230 [90]	A14	NNPDF2.3LO	NNLO + NNLL [88,89,91,92]
$t\bar{t}W$	Sherpa2.2.10	Sherpa2.2.10	Standard	NNPDF3.0NNLO	Generator NLO
$t\bar{t}Z, tZ, tWZ$	MadGraph5_aMC@NLO2.3	PYTHIA8.210	A14	NNPDF3.0NNLO	Generator NLO
$t\bar{t}WW$, 3-top, 4-top	MadGraph5_aMC@NLO2.2	PYTHIA8.186 [93]	A14	NNPDF2.3LO	Generator LO
$t\bar{t}h$ [94]	POWHEG BOX2	PYTHIA8.230	A14	NNPDF2.3LO	Generator NLO
Higgs (ggF)	POWHEG BOX2	PYTHIA8.212	AZNLO [95]	CTEQ6L1 [96]	NNNLO+NLO(EWK) [97–103]
Higgs (Vh)	POWHEG BOX2	PYTHIA8.230	AZNLO	CTEQ6L1	NNLO + NLO(EWK) [97]

OpenLoops library [110,111]. Virtual electroweak loop-terms are included at NLO accuracy for the $W/Z+$jets and diboson processes. The NNPDF3.0NNLO [72] set of parton distribution functions (PDFs) is used together with a dedicated set of tuned PS parameters ("tune") developed by the Sherpa authors [105]. The $W/Z+$jets (diboson) samples are calculated for up to two (one) additional partons at NLO and up to four (three) additional partons at leading order (LO) in QCD, and the triboson samples are calculated at NLO in QCD for the inclusive processes and at LO in QCD for up to two additional parton emissions. The diboson samples include the loop-induced and electroweak production. The Higgs boson contributions are not included in the diboson and triboson samples. The cross sections calculated by the event generators are used for all these samples except for $W/Z+$jets, which are normalized to a next-to-next-to-leading-order (NNLO) cross section prediction [73].

The $t\bar{t}$, $t\bar{t}h$ and the single-top t-channel, s-channel and tW processes are modeled using POWHEG BOX2 + PYTHIA8.230 [76–78,90]. The h_{damp} parameter[4] is set to 1.5 times the top-quark mass [112]. The samples are generated employing the five-flavor scheme (four-flavor for the single-top t-channel), and a diagram removal scheme [113] is used to remove the interference and overlap of the tW process with the $t\bar{t}$ production. The $t\bar{t}W$ process is simulated using the Sherpa2.2.10 generator. The matrix elements are calculated for up to one additional parton at NLO and up to two partons at LO using Comix [104] and OpenLoops, and merged with the Sherpa parton shower using the MEPS@NLO prescription with a merging scale of 30 GeV. Other top-quark-involved processes ($t\bar{t}Z$, tZ, tWZ, $t\bar{t}WW$, 3-top and 4-top) are modeled using MadGraph5_aMC@NLO2 + PYTHIA8 [58,93]. Samples of Higgs boson production via gluon-gluon fusion and associated production are simulated using POWHEG BOX2 + PYTHIA8.

The SUSY signal production is generated with LO matrix elements with up to two extra partons using MadGraph5_aMC@NLO3.3.1 interfaced with PYTHIA8.307 [59] with the A14 [60] tune to perform the SUSY particle decays, parton showering, hadronization, and the underlying event simulation. The parton luminosities used are provided by the NNPDF2.3LO PDF set [62]. Jet-parton matching is performed following the CKKW-L prescription [114,115], with a matching scale set to one-quarter of the mass of the pair-produced SUSY particles. The generated signal events are required to have at least two leptons. The signal cross sections are calculated up to NLO in α_{s} adding the resummation of soft gluon emission at next-to-leading-logarithm accuracy (NLO + NLL) [63–69]. The nominal cross sections and their uncertainties are taken from an envelope of cross section predictions using different PDF sets and factorization and renormalization scales, as described in Ref. [116]. For example, for a slepton/sneutrino mass of 400 GeV, the production cross sections for $\tilde{\ell}_{\mathrm{L}}^{+}\tilde{\ell}_{\mathrm{L}}^{-}$ and $\tilde{\ell}_{\mathrm{L}}^{\pm}\tilde{\nu}$ are 1.33 ± 0.04 fb and 4.82 ± 0.19 fb respectively, for each generation of the left-handed slepton.

The simulation of b- and c-hadron decays in the samples generated with POWHEG BOX or MadGraph5_aMC@NLO is performed with EvtGen 1.6.0 [117].

All MC events are propagated through a full simulation of the ATLAS detector [118] using Geant4 [119] to model the interactions of particles with the detector, except those from the SUSY signal and 4-top processes for which a parametrized simulation of the ATLAS calorimeter [118,120] is used. The effect of multiple interactions in the same and neighboring bunch crossings (pileup) is modeled by overlaying simulated minimum-bias collisions onto each hard-scattering event. The minimum-bias events are generated with PYTHIA8.186 using the A3 tune [121] and MSTW2008LO PDF set [122]. For each simulated hard-scatter process a separate MC sample is generated to reflect the conditions of the 2015 + 2016, the 2017, and the 2018 datasets. The number of overlaid minimum-bias collisions is sampled for each event according to the distribution of the average number of interactions per bunch crossing measured in that dataset.

V. EVENT RECONSTRUCTION

The collision data were collected with triggers requiring at least a single electron or a single muon reconstructed by the trigger system, with various lepton transverse momentum (p_{T}) thresholds depending upon their relative quality including isolation [56,123,124]. To ensure trigger efficiencies are well understood in the analysis phase space, tighter quality and p_{T} requirements are applied to fully reconstructed "signal" leptons, which are defined below. Each event for which the trigger was activated is required to have at least one electron (muon) with a fully calibrated p_{T} above 27, 61, or 141 GeV (27.3 or 52.5 GeV), with larger-p_{T} requirements corresponding to reduced lepton-quality requirements of the trigger. For the 2015 data, the p_{T} requirement is lowered to 26, 61, or 121 GeV (21 or 52.5 GeV) for the electron (muon).

Both the data and MC events are required to have at least one reconstructed vertex that is associated with two or more tracks of transverse momentum $p_{\mathrm{T}}>500$ MeV. The primary vertex of each event is selected as the vertex with the largest Σp_{T}^2 of its associated tracks, and used as the pivot of object reconstructions [125].

The primary objects considered in this analysis are electrons, muons, and jets. Two levels of selection criteria are defined for leptons and jets; the looser "baseline" criteria and the tighter signal criteria. Baseline objects are

[4]The h_{damp} parameter is a resummation damping factor and one of the parameters that controls the matching of POWHEG matrix elements to the parton shower and thus effectively regulates the high-p_{T} radiation against which the $t\bar{t}$ system recoils.

used for resolving ambiguities between overlapping objects and calculating $\mathbf{p}_{\mathrm{T}}^{\mathrm{miss}}$. Baseline objects are also used as inputs to the data-driven estimation of *fake* leptons, which, in this paper, collectively refer to hadrons misidentified as leptons and nonprompt leptons originating from photon conversion or b-/c-hadron decays. Tighter signal criteria are applied to the final leptons and jets considered in the analysis to ensure a high selection purity.

Baseline electrons are reconstructed from three-dimensional energy clusters in the electromagnetic calorimeter that are matched to an ID track and calibrated *in situ* using $Z \to ee$ decays [126]. In addition, baseline electrons are required to meet the "loose and B-layer likelihood" quality criteria [126], satisfy $p_{\mathrm{T}} > 4.5$ GeV, and be within the ID acceptance ($|\eta| < 2.47$) excluding the barrel/endcap transition region of the electromagnetic calorimeter ($1.37 < |\eta| < 1.52$).

Baseline muons are reconstructed from a combined fit of tracks formed in the MS and ID, calibrated *in situ* using $Z \to \mu\mu$ and $J/\psi \to \mu\mu$ decays [127], and are required to meet the "medium" quality criteria [127], satisfy $p_{\mathrm{T}} > 3$ GeV, and $|\eta| < 2.5$.

Each baseline electron or muon is also required to have a trajectory consistent with the primary vertex to suppress pileup. For this purpose, the transverse impact parameter (d_0) of a lepton is defined as the distance in the transverse plane between the beam line and the closest point of the associated ID track. The longitudinal impact parameter (z_0) then corresponds to the z-coordinate distance between that point and the primary vertex. A selection of $|z_0 \sin\theta| < 0.5$ mm, where θ is the polar angle of the track, is required for each lepton to ensure it is compatible with the primary vertex.

Baseline jets are reconstructed from particle-flow objects using the anti-k_t algorithm [128,129] with a radius parameter of $R = 0.4$. The particle-flow algorithm combines information about ID tracks and energy deposits in the calorimeters to form the input for jet reconstruction [130]. The jet energy scale and resolution are first corrected to particle level using MC simulation and then calibrated *in situ* through $Z +$ jets, $\gamma +$ jets, and multijet measurements [131]. Baseline jets are required to satisfy $p_{\mathrm{T}} > 20$ GeV and $|\eta| < 4.5$. To suppress jets originating from pileup, jets with $p_{\mathrm{T}} < 60$ GeV and $|\eta| < 2.5$ are required to satisfy the "FixedEffPt" working point of the track-based jet vertex tagger [132,133]. The identification of baseline jets containing b-hadrons (b-jets) is performed using the "DL1dv01" multivariate discriminant built using information from track impact parameters, the presence of displaced secondary vertices, and the reconstructed flight paths of b- and c-hadrons inside the jet [134]. The identification criteria are tuned to an average identification efficiency of 85% as obtained for b-jets in simulated $t\bar{t}$ events, corresponding to rejection factors of 29, 2.6, and 3.9 for jets originating from light quarks and gluons, c-quarks, and τ-leptons, respectively [134]. Hadronically decaying taus are reconstructed and treated as jets in this analysis.

While photons are not used directly in the analysis, baseline photons are defined for the calculation of $\mathbf{p}_{\mathrm{T}}^{\mathrm{miss}}$. Baseline photons are required to meet the tight quality criteria [126], satisfy $p_{\mathrm{T}} > 25$ GeV, and fall within the ID acceptance ($|\eta| < 2.37$) and excluding the calorimeter's transition region ($1.37 < |\eta| < 1.52$).

To prevent the reconstruction of a single particle as multiple objects, the following overlap-removal procedure is applied. First, any electron that shares an ID track with an electron with higher p_{T} is removed. Next, any electron that shares a track with a muon in the ID is removed. Jets are removed if they are within $\Delta R = 0.2$ of an electron and are not b-tagged. The remaining electrons are removed if they are within $\Delta R = \min(0.4, 0.04 + 10\ \mathrm{GeV}/p_{\mathrm{T}}(e))$ of a jet to reject fake leptons. For the overlap of a jet with a nearby muon, the jet is discarded only if it is within $\Delta R = 0.2$ of a muon and is not b-tagged. Finally, muons within $\Delta R = \min(0.4, 0.04 + 10\ \mathrm{GeV}/p_{\mathrm{T}}(\mu))$ of any remaining jets are discarded.

The $\mathbf{p}_{\mathrm{T}}^{\mathrm{miss}}$ of each event is defined as the negative vector sum of the transverse momenta of all identified baseline objects (electrons, muons, jets, and photons), and an additional soft term constructed from all tracks associated with the primary vertex that are not associated with any baseline objects [135]. The $\mathbf{p}_{\mathrm{T}}^{\mathrm{miss}}$ is therefore adjusted to include the full calibration of the reconstructed baseline objects while minimizing any pileup dependence in the soft term.

Signal electrons must meet the tight quality criteria [126]. The track associated with each signal electron or muon must satisfy a requirement on d_0 and its uncertainty σ_{d_0} such that $|d_0/\sigma_{d_0}| < 5(3)$ for electrons (muons), ensuring the selection of leptons with prompt, well-reconstructed tracks. In order to reduce the rate of electrons with wrongly reconstructed charge (*charge-flip*), the `ECIDS` discriminant [126] is used, which exploits further information related to the electron track reconstruction and its compatibility with the primary vertex and the electron cluster. Finally, signal leptons must be sufficiently well isolated from additional detector activity by satisfying a tight requirement on both calorimeter-based and track-based isolation variables [126,127]. Any event containing a baseline lepton that fails to meet the signal criteria is rejected to reduce the contamination from fake-lepton events. At least one of the signal leptons must be identified as having activated a trigger and must satisfy the larger p_{T} requirement of that trigger.

Signal jets are required to have $|\eta| < 2.8$, and events are rejected if they contain a jet that fails to meet the loose quality criteria [136], reducing contamination from electronic noise bursts and noncollision backgrounds. All MC simulation samples are corrected using per-event weights to account for small differences with respect to the data, in

signal-lepton identification, reconstruction, isolation and triggering efficiencies [126,127], as well as in signal-jet pileup rejection [132] and flavor-identification efficiencies [134].

VI. EVENT SELECTION

Events with exactly three leptons are selected. A common preselection is applied for all the signal regions (SRs) requiring the leading (subleading) lepton in the event to satisfy $p_{\mathrm{T}} > 28(20)$ GeV, while the third lepton must have $p_{\mathrm{T}} > 10$ GeV. In addition, events with at least one b-jet are rejected in SRs to suppress the contribution of $t\bar{t}$ and single-top processes. The choice of three-lepton final states is based on the highest significance to the SBH model compared with two-lepton and four-lepton final states, which either have typically 200 times higher background yields or five times lower signal yields. The lepton-p_{T} requirements are driven by the p_{T} threshold of the single-lepton trigger and the suppression of the fake-lepton backgrounds which tend to have low-p_{T} leptons.

Three orthogonal SRs are developed to target different signal production and decay modes, varying the requirement on the charge and flavor combination of the leptons. A summary of the selection criteria is presented in Table II.

The signal region `SROS-on` targets the $\tilde{\ell}^{\pm}_{\mathrm{L}}\tilde{\nu}$ production followed by a $\tilde{\chi}^0_3$ decay emitting an on-shell Z boson. At least one same-flavor opposite-charge (SFOS) lepton pair with an invariant mass $m_{\ell\ell}$ consistent with the Z-boson mass ($|m_{\ell\ell} - m_Z| \leq 10$ GeV) is required.

The signal region `SROS-off` targets the $\tilde{\ell}^{+}_{\mathrm{L}}\tilde{\ell}^{-}_{\mathrm{L}}$ production followed by a $\tilde{\chi}^0_3$ decay emitting a W boson, and the $\tilde{\ell}^{\pm}_{\mathrm{L}}\tilde{\nu}$ production followed by a $\tilde{\chi}^0_3$ decay emitting an off shell Z boson resulting from a compressed mass splitting $\Delta m(\tilde{\chi}^0_3, \tilde{\chi}^0_1) < m_Z$. This SR is defined by the presence of one or more SFOS lepton pairs in the event with none of them having an invariant mass consistent with the Z-boson mass.

The signal region `SRSS` requires all three leptons to have the same charge, targeting the $\tilde{\ell}^{\pm}_{\mathrm{L}}\tilde{\nu}$ production with the $\tilde{\chi}^0_3$ decays resulting in a pair of same-charge W bosons. The diagrams of the signals targeted by each SR are summarized in Fig. 3: Fig. 3(a) is for `SROS-off`, Fig. 3(b) for `SROS-on`, and Fig. 3(c) for `SRSS`.

The `SROS-on` and `SROS-off` (collectively referred to as `SROS`) are subject to the following additional selections. A significantly large missing transverse energy, $E^{\mathrm{miss}}_{\mathrm{T}} > 150$ GeV, is required to reflect the presence of $\tilde{\chi}^0_1$ and neutrinos in the signals events while rejecting a large part of the SM processes without neutrinos, particularly $Z+$jets events that include a fake lepton. The fully leptonically decaying WZ process is the leading SM background in `SROS` due to the single neutrino from the W decay. This background is suppressed by requiring a large transverse mass m_{T} defined by:

$$m_{\mathrm{T}} = \sqrt{2p_{\mathrm{T}}(\ell_W)E^{\mathrm{miss}}_{\mathrm{T}}(1-\cos(\Delta\phi(\ell_W, \mathbf{p}^{\mathrm{miss}}_{\mathrm{T}})))},$$

where ℓ_W is the lepton candidate from the W decay defined by the leftover lepton when forming an SFOS lepton pair. Since, in the WZ events, $\mathbf{p}^{\mathrm{miss}}_{\mathrm{T}}$ represents the p_{T} of the neutrino, the m_{T} distribution exhibits a kinematic edge at the W mass reflecting the W's Jacobian peak. Multiple ℓ_W

TABLE II. Summary of selections for signal region definition. Merged cells indicate common selections. Dots indicate that no requirement is applied to the variable. The number of SFOS and DFOS lepton pairs are represented by n_{SFOS} and n_{DFOS} respectively. If more than one SFOS lepton pair is in the event, the invariant mass closest to the Z-boson mass is quoted for $m_{\ell\ell}$. `SROS-on` and `SROS-off` are divided into three $m_{3\ell}$ bins and further divided into four channels by lepton flavor. `SRSS` is divided into three channels according to the lepton flavor.

	`SROS-on`				`SROS-off`				`SRSS`		
Variables	eee	$ee\mu$	$e\mu\mu$	$\mu\mu\mu$	eee	$ee\mu$	$e\mu\mu$	$\mu\mu\mu$	eee	$ee\mu$	$2\mu(e\mu\mu+\mu\mu\mu)$
Trigger	Single-lepton										
$n^{\mathrm{baseline}}_{\ell}$, $n^{\mathrm{signal}}_{\ell}$	$=3$										
$p^{\ell_1}_{\mathrm{T}}$, $p^{\ell_2}_{\mathrm{T}}$, $p^{\ell_3}_{\mathrm{T}}$ [GeV]	>28, 20, 10										
$n_{b\text{-jets}}$	$=0$										
n_{SFOS}	≥ 1				≥ 1				$=0$		
n_{DFOS}	…				…				$=0$		
$m_{\ell\ell}$ [GeV]	$\in [81.2, 101.2]$				$\notin [81.2, 101.2]$				…		
$m^{\mathrm{min}}_{\mathrm{T}}$ [GeV]	>125				>125				…		
$E^{\mathrm{miss}}_{\mathrm{T}}$ [GeV]	>150				>150				>50		
$m_{3\ell}$ binning [GeV][a]	a: $\in [30, 200)$ b: $\in [200, 400)$ c: $\in [400, +\infty)$								…		

[a]The $m_{3\ell}$ binning applies separately to each flavor channel of `SROS`.

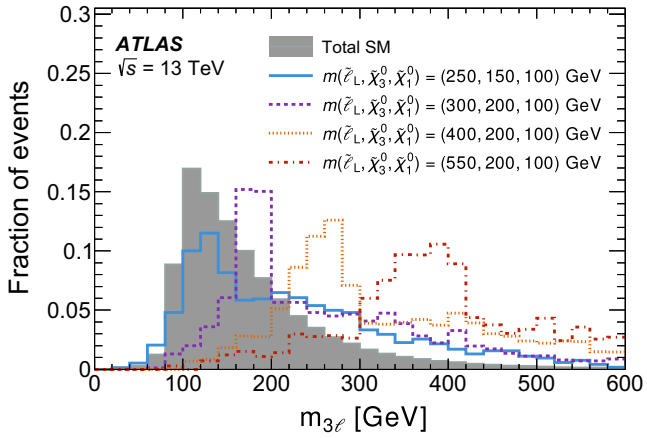

FIG. 4. Distribution of $m_{3\ell}$ for the SM backgrounds and several signal hypotheses, normalized to unity. All SM backgrounds are included and no uncertainties are shown. A preselection is applied requesting exactly three baseline and signal leptons, and of at least one SFOS lepton pair.

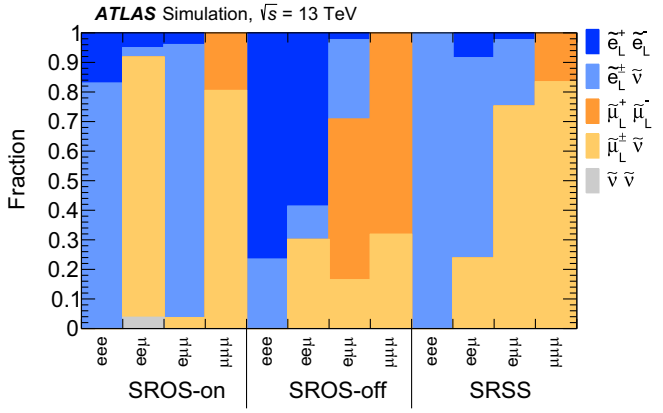

FIG. 5. Relative fractions of signal production modes populating the SR channels. A signal with $m(\tilde{\ell}_{\mathrm{L}}, \tilde{\chi}_3^0, \tilde{\chi}_1^0) = (300, 200, 100)$ GeV is shown as an example. Mass-degenerate $\tilde{e}_{\mathrm{L}}$, $\tilde{\mu}_{\mathrm{L}}$ and $\tilde{\nu}$ are considered. The $m_{3\ell}$ bins are merged and SRSS-2μ is divided into SRSS-$e\mu\mu$ and SRSS-$\mu\mu\mu$ for illustration.

can be defined when the three leptons have the same flavor. To account for such cases, the minimum m_{T} of all ℓ_W candidates ($m_{\mathrm{T}}^{\mathrm{min}}$) in SROS must satisfy $m_{\mathrm{T}}^{\mathrm{min}} > 125$ GeV.

A multibin strategy is applied in each SROS using the trilepton invariant mass, $m_{3\ell}$, and the lepton flavor combination to maximize the sensitivity across the model phase space. First, each SROS is divided into $m_{3\ell}$ bins, exploiting the cutoff structure of the signal as illustrated in Fig. 4. The position of the cutoff corresponds to the mass splitting between the $\tilde{\ell}_{\mathrm{L}}$ and $\tilde{\chi}_1^0$, when the three leptons originate from the same side of the decay chain as shown in Fig. 3(b). In contrast, the distribution of backgrounds, dominated by WZ events, smoothly falls without particular structures. Each SROS is further divided into four channels by lepton flavor combination ($eee, ee\mu, e\mu\mu, \mu\mu\mu$) to maximize the sensitivity to the single-slepton-flavor models.

In the SRSS, events are required to have three same-charge leptons. The region with three same-charge leptons and zero b-jets has never been investigated before at the LHC. The dominant SM backgrounds in this region are events with a charge-flip electron or a fake lepton. The charge-flip-electron events majorly come from the WZ process when the charge of one of the electrons from $Z \to ee$ is misidentified. An $E_{\mathrm{T}}^{\mathrm{miss}} > 50$ GeV cut is imposed to exploit the real missing transverse momentum from the neutralinos and neutrinos in the targeted signals. The SRSS is further divided into three channels according to the lepton flavor combination, eee, $ee\mu$ and 2μ, with the latter containing both the $e\mu\mu$ and $\mu\mu\mu$ channels to ease the background estimation due to extremely low background levels in these regions.

The breakdown of signal events per production mode in the various SR channels is summarized in Fig. 5. The selection production signals tend to populate the eee and $e\mu\mu$ channels in SROS-on, and the eee and $ee\mu$ channels in SROS-off and SRSS. Conversely, the smuon production signals are more likely to fall into the $ee\mu$ and $\mu\mu\mu$ channels in SROS-on, and the $e\mu\mu$ and $\mu\mu\mu$ channels in SROS-off and SRSS. The selection acceptance times efficiency for SROS-on, SROS-off and SRSS are respectively 5.4×10^{-3}, 3.2×10^{-3}, and 1.0×10^{-3}, for a signal point with $m(\tilde{\ell}_{\mathrm{L}}, \tilde{\chi}_3^0, \tilde{\chi}_1^0) = (400, 200, 100)$ GeV.

VII. BACKGROUND ESTIMATION AND VALIDATION

The SM backgrounds in this analysis are classified into two categories: "irreducible backgrounds" where the three leptons are all real and promptly produced with the charge correctly assigned; and "reducible backgrounds" where one or more of the leptons are either a charge-flip or a fake lepton. The irreducible backgrounds are particularly relevant in SROS accounting for 90% of the total background, and are estimated using MC simulations corrected to data. The reducible backgrounds account for almost all background in SRSS. These are estimated with dedicated data-driven approaches since the instrumental effects causing them are generally difficult to model. The $t\bar{t}$ background is exceptionally estimated with MC despite involving one fake lepton, since its MC modeling is found to be good, as shown in Sec. VII C.

A. Irreducible background estimation

The dominant irreducible background process is WZ production. A partially data-driven method is used for its estimation. The WZ MC is normalized to the data in a control region (CR), CRWZ, designed with the same selection as SROS except for $m_{\mathrm{T}}^{\mathrm{min}}$ being shifted to $40\ \mathrm{GeV} \leq m_{\mathrm{T}}^{\mathrm{min}} < 80$ GeV. Dedicated validation regions (VRs) are set to validate the normalization and its extrapolation to the SROS. These are defined either in the phase

TABLE III. Summary of the selection criteria for the CR and VRs for WZ, for the SROS-on and SROS-off selection. Merged cells indicate common selections. Dots indicate that no requirement is applied to the variable. The number of SFOS lepton pairs is represented by n_{SFOS}. If more than one SFOS lepton pair is in the event, the invariant mass closest to the Z-boson mass is quoted for $m_{\ell\ell}$. VRs are divided into three $m_{3\ell}$ bins to match the SROS binning.

Variables	CRWZ	VRWZ-on-$m_{\mathrm{T}}^{\mathrm{min}}$	VRWZ-on-$E_{\mathrm{T}}^{\mathrm{miss}}$	VRWZ-off-$m_{\mathrm{T}}^{\mathrm{min}}$	VRWZ-off-$E_{\mathrm{T}}^{\mathrm{miss}}$
Trigger	Single-lepton				
$n_\ell^{\mathrm{baseline}}$, n_ℓ^{signal}	$=3$				
$p_{\mathrm{T}}^{\ell_1}$, $p_{\mathrm{T}}^{\ell_2}$, $p_{\mathrm{T}}^{\ell_3}$ [GeV]	$>28, 20, 10$				
$n_{b\text{-jets}}$	$=0$				
n_{SFOS}	≥ 1				
$m_{\ell\ell}$ [GeV]	…	$\in [81.2, 101.2]$		$\notin [81.2, 101.2]$	
$m_{\mathrm{T}}^{\mathrm{min}}$ [GeV]	$\in [40, 80)$	$\in [80, 125)$	$\in [125, +\infty)$	$\in [80, 125)$	$\in [125, +\infty)$
$E_{\mathrm{T}}^{\mathrm{miss}}$ [GeV]	$\in [150, +\infty)$	$\in [150, +\infty)$	$\in [80, 150)$	$\in [50, +\infty)$	$\in [20, 150)$
n_{jets}	…	…	$=0$	…	$=0$
$m_{3\ell}$ binning [GeV]	…	a: $\in [30, 200)$ b: $\in [200, 400)$ c: $\in [400, +\infty)$			
WZ purity	94%	93%	80%	87%	54%

space between the CRWZ and SROS (80 GeV $\leq m_{\mathrm{T}}^{\mathrm{min}} <$ 125 GeV), or in the low $E_{\mathrm{T}}^{\mathrm{miss}}$ phase space with respect to the SROS ($E_{\mathrm{T}}^{\mathrm{miss}} < 150$ GeV). The selections are summarized in Table III and the region segmentation is illustrated in Figs. 6(a) and 6(b). The $E_{\mathrm{T}}^{\mathrm{miss}}$ range of the VRs is enlarged in the off shell Z region to suppress signal contamination. While the CRWZ is inclusive in $m_{3\ell}$, the VRs follow the same splitting in $m_{3\ell}$ as in the SROS. The WZ purity is about 94% in CRWZ and 54%–93% in VRs. The signal contamination is at most 3.2% in CRWZ and 12% in the VRs, with the largest signal contamination found in VRWZ-off-$m_{\mathrm{T}}^{\mathrm{min}}$-c.

The other rare irreducible SM processes, including triboson (VVV), Higgs boson production, top-pair production in association with a boson ($t\bar{t}X$), 3-top, 4-top, and single-top production, are estimated from MC simulations with SM cross-sections in all analysis regions.

The WZ normalization factor extracted from CRWZ is found to be 1.07 ± 0.06. The estimated background and the observed data in the relevant VRs are shown in Fig. 7, and some example kinematic distributions in the VRs are presented in Fig. 8. Good agreement is generally observed.

B. Charge-flip background estimation

Charge-flip leptons are predominantly electrons which emit bremmstrahlung while propagating through the detector material [126,138], creating electron-positron pairs. The production of these secondary particles can lead to distortions of the primary electron track, when hits from secondary particles are included in the fit, or when the track from a secondary particle is wrongly selected as the primary track.

The charge-flip background is only relevant in SRSS. The MC modeling of charge flip is not always reliable since they are sensitive to details of the detector modeling. In this analysis, the per-electron charge-flip probability is measured using $Z \to ee$ data and a MC correction factor ("scale factor") is derived as a function of the p_{T} and $|\eta|$ of the electron. The scaled MC simulation is then used to estimate the charge-flip background in SRSS.

The charge-flip probability measurement in the $Z \to ee$ data is based on a likelihood fit as described in Ref. [126]. The measured probability is then compared with the $Z \to ee$ MC simulation to derive the scale factors. Typically the charge-flip probability is of the order of $\mathcal{O}(10^{-5})$ in the low-p_{T} region, increases with increasing p_{T} and $|\eta|$, and may reach as high as $\mathcal{O}(0.1)$. High-p_{T} electrons are more likely to cause charge-flip, as their tracks are approximately straight and more susceptible to small angular perturbations. The higher charge-flip probability in high-$|\eta|$ electrons is due to denser detector materials in this region. Systematic uncertainties in the charge-flip scale factors are assigned based on the statistical uncertainties of the data sample, modeling uncertainties in the background subtraction, and uncertainties related to the parametrization of charge-flip probabilities. Examples of the measured charge-flip probabilities and the scale factors are illustrated in Fig. 9.

An additional uncertainty is assigned to account for the physics process dependency of the charge-flip probabilities when applying scale factors in the analysis. While the scale factors are measured using $Z \to ee$ events, the main charge-flip source in SRSS is WZ. Though charge-flip probabilities are found to be statistically consistent between $Z \to ee$ and WZ, to ensure the difference is covered, a 20%

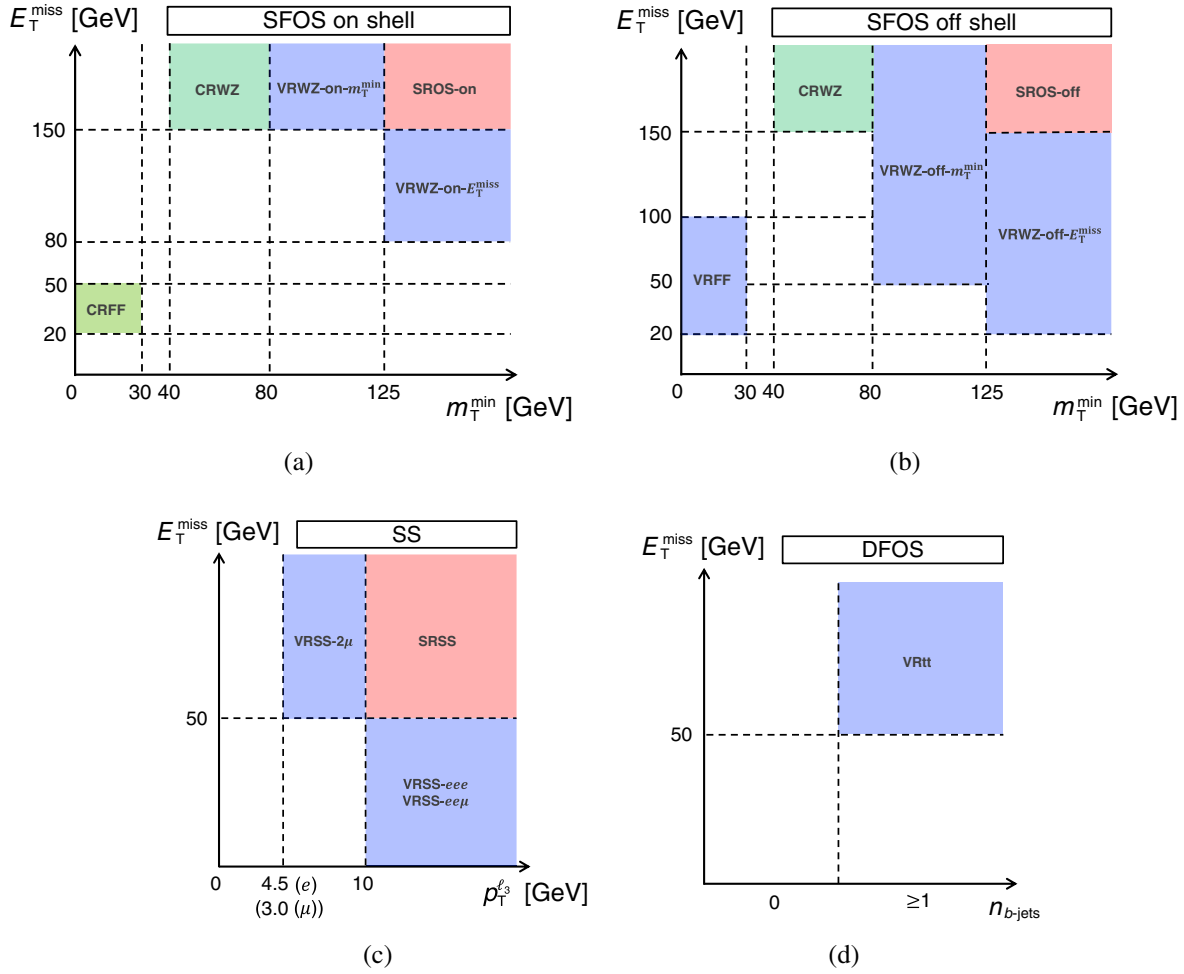

FIG. 6. Schematics illustrating the selection of the CRs and the VRs used to estimate (a),(b) the WZ and fake background in SROS, (c) the charge-flip and fake backgrounds in SRSS, and (d) the $t\bar{t}$ background in SROS.

systematic uncertainty is assigned to account for possible physics-process dependency. This is evaluated based on a MC closure test, comparing the MC yields of same-sign WZ events to those of reweighted opposite-sign WZ events, using MC-derived charge-flip probabilities of the $Z \to ee$ process.

The validation regions VRSS-eee and VRSS-$ee\mu$ are defined to test the charge-flip estimation in SRSS, by inverting the E_T^{miss} selection with respect to SRSS-eee and SRSS-$ee\mu$, respectively. To further boost the data event statistics, a set of supplementary validation regions, VRSS-noECIDS, are defined by removing the Electron Charge ID Selector (ECIDS) requirement to the leading lepton. The selection is summarized in Table IV and the region segmentation is illustrated in Fig. 6(c). The signal contamination in VRSS-eee and VRSS-$ee\mu$ is below 8% of the total expected background. The observed and expected event yields for these VRs are summarized in Fig. 10 with an example kinematic distribution shown in Fig. 11(a). Reasonable agreement is observed.

C. Fake-lepton background estimation

Fake leptons are defined as either hadrons misidentified as leptons, or nonprompt real leptons from photon conversion or b- or c-hadron decays. Electrons from final-state-radiation or bremsstrahlung photons originating from a prompt electron are not considered as fake leptons.[5] A data-driven method, referred to as the "fake-factor (FF) method" [139,140], is used to estimate the fake-lepton backgrounds. A lepton anti-ID requirement is defined for the fake-factor method, corresponding to leptons that satisfy the baseline criteria but not the signal criteria. The FF is defined as the ratio of the probability that a given lepton candidate satisfies the signal lepton

[5]Events with such electrons are not targeted by the fake-factor method but are instead taken directly from MC simulation, which is considered to adequately model such processes. These events have a minor contribution in SRSS, and are negligible in all other regions.

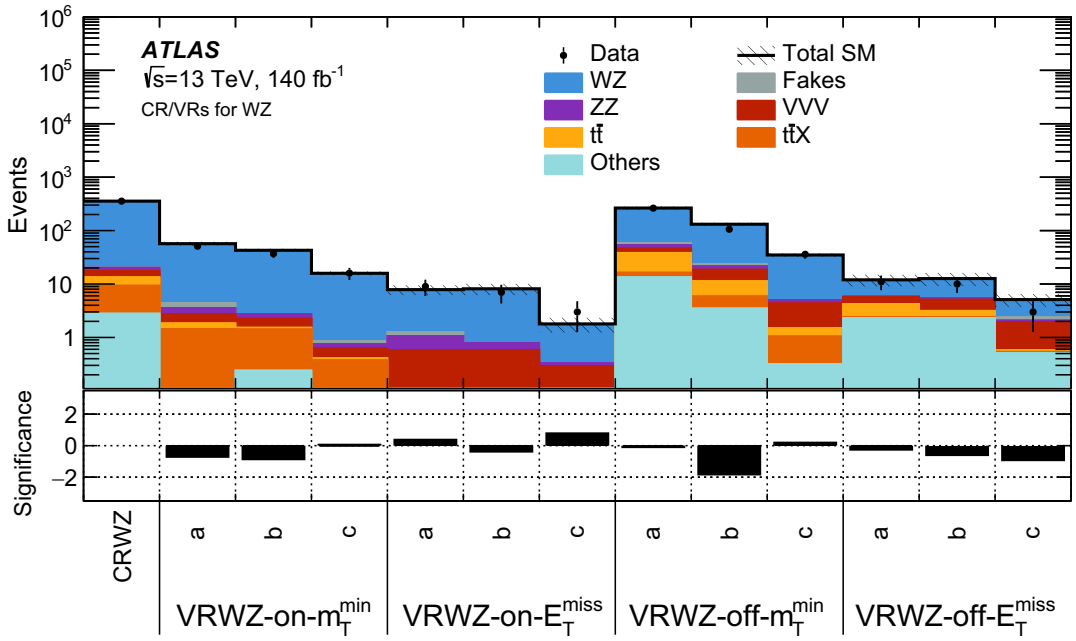

FIG. 7. Expected SM backgrounds and the data yields in the CRWZ, VRWZ-on-m_T^{min}, VRWZ-on-E_T^{miss}, VRWZ-off-m_T^{min}, and VRWZ-off-E_T^{miss} designed to provide and validate the WZ estimation in SROS. The expected backgrounds are obtained from a background-only fit described in Sec. IX A. The "Others" category contains the production of Higgs boson, 3-top, 4-top, and single-top processes. The hatched band includes all statistical and systematic uncertainties discussed in Sec. VIII. The bottom panel shows the statistical significance [137] of the difference between the observed events and the SM expectation.

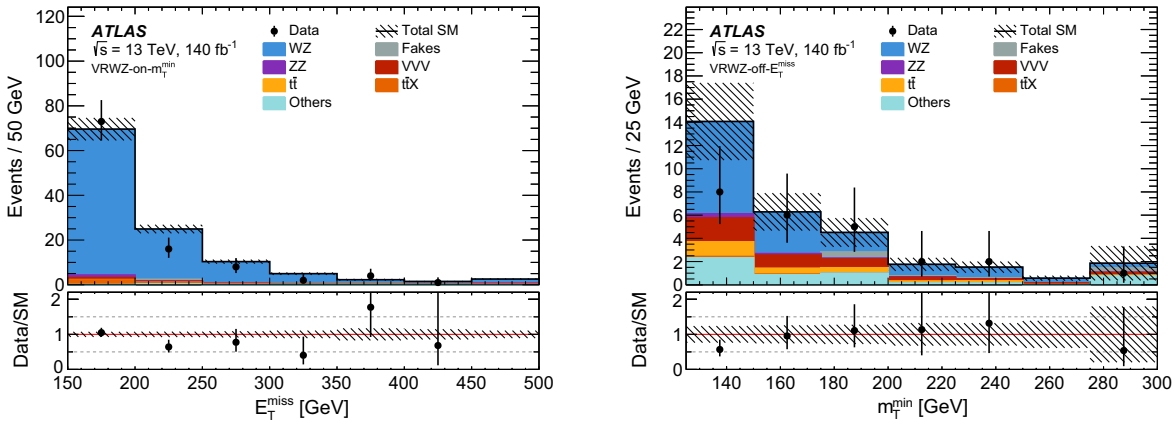

FIG. 8. Example kinematic distributions for the expected backgrounds and the data, obtained from a background-only fit described in Sec. IX A. The figure shows (a) the E_T^{miss} distribution in VRWZ-on-m_T^{min} and (b) the m_T^{min} distribution in VRWZ-off-E_T^{miss}. The last bin includes the overflow. The Others category contains the production of Higgs boson, 3-top, 4-top, and single-top processes. The hatched band includes all statistical and systematic uncertainties discussed in Sec. VIII. The bottom panel shows the ratio of the observed data to the predicted yields.

requirement to the probability that it fulfills the anti-ID requirement.

The FF is measured using data in a control region, CRFF, designed to be enriched with $Z+$jets events associated with a fake lepton. The selection is summarized in Table IV and the region segmentation is illustrated in Fig. 6(a). After selecting exactly three baseline leptons with at least one SFOS lepton pair, the Z-boson candidate in the event is identified as the SFOS pair yielding the invariant mass closest to the Z-boson mass, and the remaining lepton is tagged as the fake-lepton candidate. Either of the two leptons from the Z-boson candidate must activate the

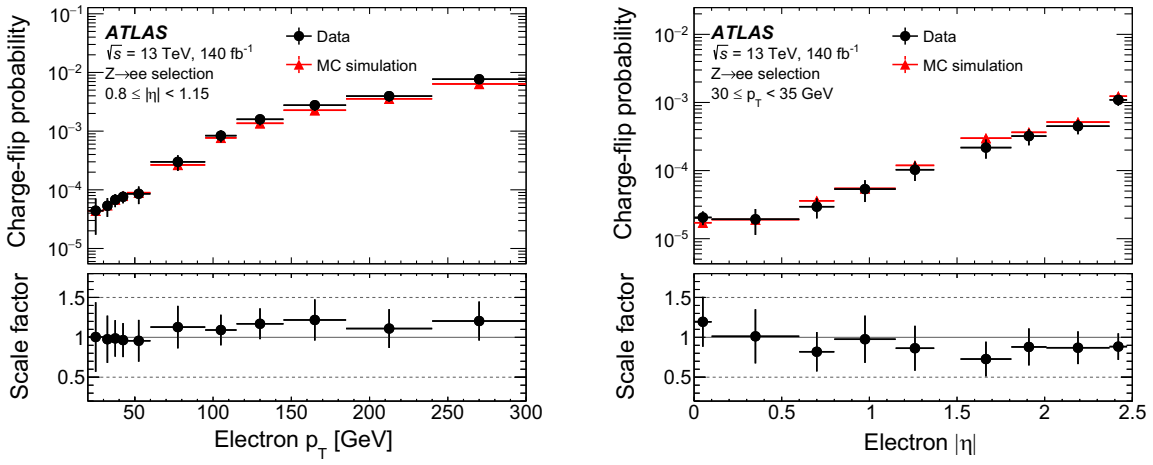

(a) (b)

FIG. 9. Charge-flip (upper panel) probabilities in data and MC simulation and (lower panel) scale factors (a) as a function of the electron p_{T} for a specific electron $|\eta|$ slice ($0.8 \leq |\eta| < 1.15$) or (b) as a function of the electron $|\eta|$ for a specific electron p_{T} slice ($30 \leq p_{\mathrm{T}} < 35$ GeV). For (a), the highest-p_{T} bin includes the overflow. The uncertainties in the data charge-flip probabilities and the scale factors include both the statistical and systematic components, while the uncertainties in MC simulation charge-flip probabilities include only the statistical uncertainty.

single-lepton trigger to remove the bias from trigger selection on the fake leptons. To suppress the WZ contribution in CRFF, the $m_{\mathrm{T}}^{\mathrm{min}}$ and $E_{\mathrm{T}}^{\mathrm{miss}}$ selections are imposed. Additionally, a requirement of $m_{3\ell} > 105$ GeV is applied to suppress $Z \to \ell\ell\gamma^* \to 4\ell$. The FF is extracted as the fraction of fake-lepton candidates satisfying to that failing the signal lepton criteria.

The fake-lepton background estimation in a given region is then obtained by applying the FF to the data events in its corresponding anti-ID region, defined by requiring at least one anti-ID lepton as opposed to three signal leptons in the target region. An exceptional treatment is applied to the estimation in SRSS-2μ, where the FF is applied to the MC simulated events in the anti-ID region with two signal and one anti-ID leptons, instead of the data events. This is due to the small data statistics in SRSS-2μ anti-ID region, which would result in a large uncertainty. This exception is validated by verifying the MC modeling in the anti-ID region with a loosened kinematic selection, and confirming the similar origin composition of fake leptons in SRSS-2μ and its anti-ID region using MC simulation.

The FFs are derived separately per lepton flavor, and are parametrized as a function of lepton p_{T}. Typical FF values are 0.04–0.08 (0.08–0.12) for electrons (muons) in a p_{T}

TABLE IV. Definitions of the CR and VRs involved in the fake and charge-flip lepton estimation. Merged cells indicate common selections. Dots indicate that no requirement is applied to the variable. The number of SFOS and DFOS lepton pairs are represented by n_{SFOS} and n_{DFOS} respectively. If more than one SFOS lepton pair is in the event, the invariant mass closest to the Z-boson mass is quoted for $m_{\ell\ell}$.

		VRFF				VRtt		VRSS(-noECIDS)		VRSS
Variables	CRFF	eee	$ee\mu$	$e\mu\mu$	$\mu\mu\mu$	$ee\mu$	$e\mu\mu$	eee	$ee\mu$	$2\mu(e\mu\mu + \mu\mu\mu)$
Trigger						Single-lepton				
$n_\ell^{\mathrm{baseline}}$, n_ℓ^{signal}						$= 3$				
$p_{\mathrm{T}}^{\ell_1}$, $p_{\mathrm{T}}^{\ell_2}$ [GeV]		> 10, 10						> 28, 20		
$p_{\mathrm{T}}^{\ell_3}$ [GeV]		> 10				> 10		> 10		< 10
$n_{b\text{-jets}}$		$= 0$				≥ 1		$= 0$		$= 0$
n_{SFOS}	≥ 1	≥ 1				$= 0$		$= 0$		$= 0$
n_{DFOS}	...	...				≥ 1		$= 0$		$= 0$
$m_{\ell\ell}$ [GeV]	$\in [81.2, 101.2]$	$\notin [81.2, 101.2]$				...		...		...
$m_{\mathrm{T}}^{\mathrm{min}}$ [GeV]	< 30	< 30				...		...		...
$E_{\mathrm{T}}^{\mathrm{miss}}$ [GeV]	$\in [20, 50)$	$\in [20, 100)$				> 50		< 50		> 50
$m_{3\ell}$ [GeV]	> 105	> 105				...		...		...

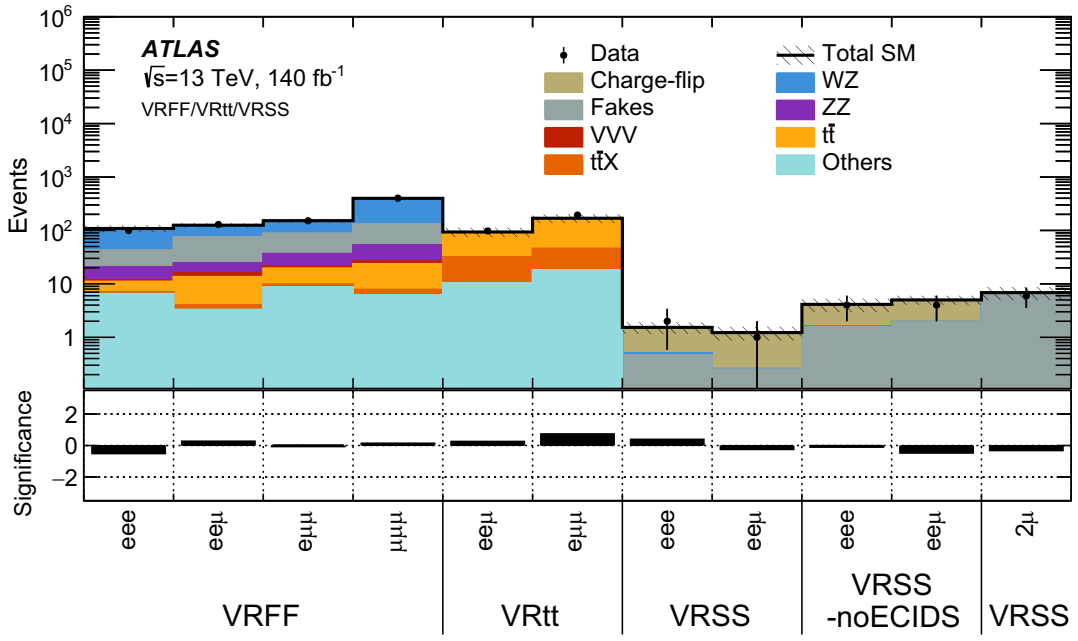

FIG. 10. Expected SM backgrounds and the data yields in the VRFF, VRtt, and VRSS. The expected backgrounds are obtained from a background-only fit described in Sec. IX A. The Others category contains the production of Higgs boson, 3-top, 4-top, and single-top processes. The hatched band includes all statistical and systematic uncertainties discussed in Sec. VIII. The bottom panel shows the statistical significance [137] of the difference between the observed events and the SM expectation.

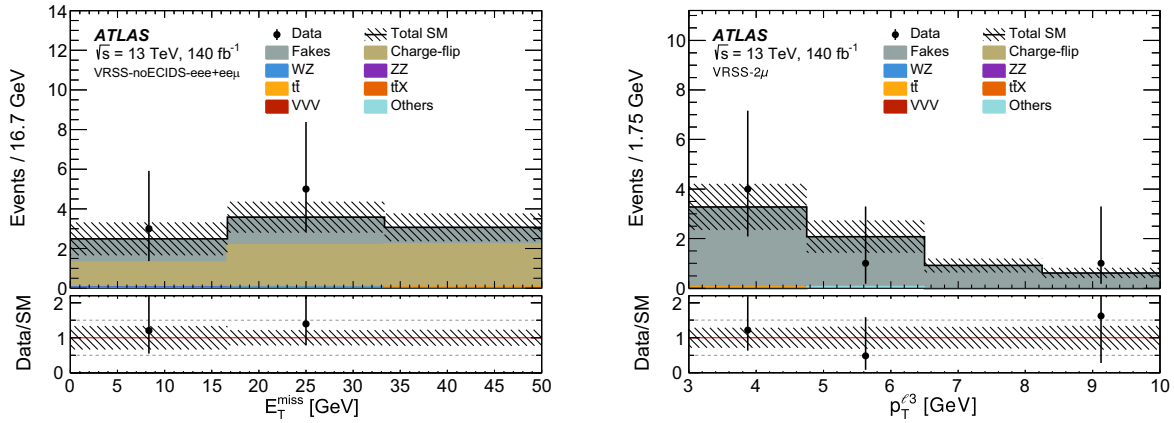

FIG. 11. Example kinematic distributions for the expected backgrounds and the data, obtained from a background-only fit described in Sec. IX A. The figure shows (a) the $E_{\mathrm{T}}^{\mathrm{miss}}$ distribution in the merged region of VRSS-noECIDS-eee and VRSS-noECIDS-$ee\mu$ and (b) the $p_{\mathrm{T}}^{\ell_3}$ distribution in VRSS-2μ. The Others category contains the production of Higgs boson, 3-top, 4-top, and single-top processes. The hatched band includes all statistical and systematic uncertainties discussed in Sec. VIII. The bottom panel shows the ratio of the observed data to the predicted yields.

range of 4.5–50 (3.0–30) GeV. FFs are parameterized inclusively in lepton's η since no significant η dependency is found. In both the FF measurement and the FF application procedure, contributions from $t\bar{t}$ and irreducible background processes are subtracted using MC simulation samples.

The data-driven fake estimation is subject to the statistical uncertainties of the data in the anti-ID regions to which the FFs are applied, and the uncertainties in the FF values. The FF uncertainties include the statistical uncertainty of the data in CRFF, an uncertainty obtained by varying the choice of the $E_{\mathrm{T}}^{\mathrm{miss}}$ requirement in CRFF to account for the potential fake-lepton composition change in data, and an uncertainty in the subtraction of the WZ process in CRFF evaluated by varying the WZ normalization by 10% [141]. These FF uncertainties are propagated

by varying the FF in the estimation. An additional systematic uncertainty is considered to account for the difference in the fake-lepton origin compositions between the CRFF and the SRs. This is evaluated based on an MC closure test, comparing the MC prediction in an SR to the FF method estimation using the MC-derived FFs.

The fake-lepton estimates derived for SROS and SRSS are validated in VRFF and VRSS-2μ, respectively. The selection is summarized in Table IV and the region segmentation is shown in Figs. 6(b) and 6(c). The VRFF is defined in the off shell Z region to enhance the fake-lepton fraction, and is separated by lepton flavor. The purity of the fake-lepton background in VRFF is about 25%, while the contamination from signals is negligible. The VRSS-2μ is defined by inverting the selection on the third leading lepton p_{T} ($p_{\mathrm{T}} < 10$ GeV) with respect to SRSS-2μ. The signal contamination in VRSS-2μ is at most 15%. The observed and expected event yields for these VRs are summarized in Fig. 10 with an example kinematic distribution shown in Fig. 11(c). Reasonable agreement is observed.

The $t\bar{t}$ MC modeling is validated in VRtt, enhancing the $t\bar{t}$ contribution by requiring a different-flavor opposite-charge (DFOS) lepton pair, moderate $E_{\mathrm{T}}^{\mathrm{miss}}$, and the presence of one or more b-jets. The $t\bar{t}$ purity is about 70% in VRtt. Selection requirements for VRtt are summarized in Table IV and illustrated in Fig. 6(d). The observed and expected event yields for VRFF are summarized in Fig. 10.

VIII. SYSTEMATIC UNCERTAINTIES

Systematic uncertainties in the predicted event yields are considered for both the signal and background processes, and propagated to the final results through the profile likelihood described in Sec. IX A. Several sources of systematic uncertainty are considered. They are grouped into experimental uncertainties, theoretical uncertainties, MC statistical uncertainties, WZ normalization uncertainty, and uncertainties from the data-driven methods applied in this analysis. The contribution to the analysis sensitivity is generally minor, since the total uncertainty in the SRs is dominated by the statistical uncertainty.

The experimental uncertainties encompass possible differences between data and simulations in all analysis elements including trigger, pileup, and reconstructed objects. The leading experimental uncertainty originates from the electron identification efficiencies in the electron-dominated SRs, and the jet energy resolution in the muon-dominated SRs. For leptons, uncertainties in the reconstruction efficiencies [126], identification efficiencies [142], isolation efficiencies, energy scales [126,143], resolutions, and trigger efficiencies are considered. The uncertainties related to electrons typically yield a relative uncertainty in the total expected background of 10% for the electron-dominated SROS. For jets, uncertainties in the vertex tagger efficiency [132], energy scale [131], energy resolution [144], and efficiencies of the flavor tagging [134,145,146] are considered. The uncertainties related to jets typically yield a relative uncertainty in the total expected background of 5% for the muon-dominated SROS. Uncertainties associated with the objects used to compute the $E_{\mathrm{T}}^{\mathrm{miss}}$ are propagated through the computation, and additional uncertainties in the scale and resolution of the soft term are also included [135]. The uncertainty in the combined 2015–2018 integrated luminosity is 0.83% [47], obtained primarily using the luminosity measurements of the LUCID-2 detector [55].

The theoretical uncertainties comprise the cross section uncertainty and the MC generator modeling uncertainty. Signals and the background processes that are not normalized in the CR are subject to cross section uncertainties. For the triboson background, a $+45/-40\%$ uncertainty is applied to WWW process, a $+35/-30\%$ uncertainty to WWZ, a $+192/-100\%$ uncertainty to WZZ, and a $+440/-100\%$ uncertainty to ZZZ, based on their cross section measurement by the CMS Collaboration [147].[6] Cross section uncertainties of 13%, 12%, and 10% are applied for the minor backgrounds $t\bar{t}W$, $t\bar{t}Z$, and $t\bar{t}h$, respectively [97,149–151], and a conservative uncertainty of 50% is applied to all other rare top processes, which has little impact on final results. For the signal samples, theoretical uncertainties in the cross section are applied, ranging from 2% at 120 GeV to 6% at 700 GeV, as detailed in Sec. IV.

The MC generator modeling uncertainties for the dominant background processes, WZ, ZZ, and $t\bar{t}$, and the signal processes are also evaluated. For the WZ background, which is normalized to data in CRWZ, these uncertainties are implemented as transfer factor uncertainties that reflect differences in the SR-to-CR or VR-to-CR ratio of yields, and therefore provide an uncertainty in the assumed shape of MC distributions across analysis regions. The uncertainties due to the choice of the renormalization and factorization scales [152] are assessed by varying the relevant generator parameters up and down by a factor of two with respect to the nominal values. Uncertainties related to these variations, the choice of PDF sets [153], and the strong coupling constant (α_{s}) value are derived by taking the envelope of the variation in the event yields [153]. For the WZ and ZZ backgrounds, uncertainties due to the virtual NLO electroweak corrections are assessed by varying the nominal scheme (*additive*) to alternative schemes (*multiplicative* and *exponentiated*). Additional shape uncertainties are related to the assumptions made in the event generators and PS models. For the WZ and ZZ backgrounds, the Sherpa parameters related to

[6]The ATLAS Collaboration has also produced compatible results [148] in which the ZZZ process is however not separately measured.

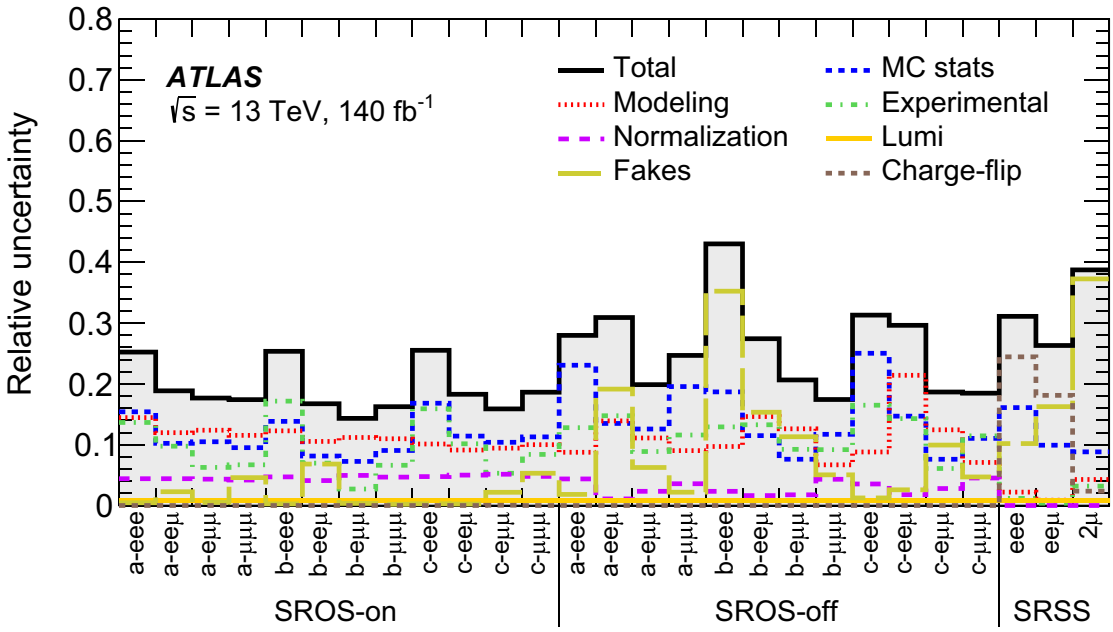

FIG. 12. Breakdown of the total systematic uncertainties in the background prediction for all SR channels after the background-only fit, relative to the total expected background. "MC stats" stands for the statistical uncertainties due to a limited number of simulated events. The "Modeling" uncertainty groups the uncertainties due to the theoretical uncertainties, including the WZ transfer factor uncertainties. Uncertainties related to the experimental effects are grouped as "Experimental" uncertainty. The "Normalization" category includes the statistical uncertainty of the data count in CRWZ and the uncertainty from the fitted WZ normalization factor. "Lumi" stands for the luminosity uncertainty. "Fakes" represents the uncertainties for the fake background estimation for which the bin-to-bin fluctuations are due to the small number of events in the anti-ID regions. The uncertainties in the charge-flip background estimation are grouped as "Charge-flip" uncertainty. Individual uncertainty categories can be (anti-)correlated.

the PS matching scale and resummation scale are varied up and down by a factor of two with respect to the nominal values. For the $t\bar{t}$ background, the uncertainties related to the modeling of the hard scatter and to the PS are derived by comparing the PYTHIA8 and Herwig7 predictions, and the modeling uncertainties in the amount of initial-state radiation and final-state radiation are assessed by varying the related generator parameters. The shape uncertainty in the signals are estimated by varying by a factor of two the MadGraph5_aMC@NLO parameters corresponding to the renormalization, factorization, and CKKW-L matching scales, as well as the PYTHIA8 shower tune parameters.

Other uncertainties include the MC statistical uncertainties, which are the largest contribution to the systematic uncertainty, mainly from the limited size of the WZ background sample. The uncertainties associated to the WZ normalization factor includes the statistical uncertainty of the data count in CRWZ. The uncertainties related to the data-driven estimation of the charge-flip and fake backgrounds are separately evaluated, and detailed in Secs. VII B and VII C. A summary of systematic uncertainties in the predicted background event yields in the SRs is shown in Fig. 12.

IX. RESULTS

A. Statistical analysis

The determination of the background and signal event yields is done through a profile log-likelihood fit [154] simultaneously in the CRWZ and all SR channels relevant to a given interpretation, using the HistFitter [155] framework. Systematic uncertainties are treated as Gaussian-distributed nuisance parameters in the likelihood, while the statistical uncertainties of the MC samples are treated as Poisson-distributed nuisance parameters. The experimental uncertainties are treated as correlated between regions and processes. The theoretical uncertainties in the background and signal predictions are treated as correlated between regions but as process independent. The statistical uncertainties due to limited MC or data statistics are considered uncorrelated between regions and processes.

Three types of fit configurations are used to derive the results.

(i) A *background-only fit* is performed considering only the CRWZ and assuming no signal contribution. The normalization of the WZ background is allowed to float and is constrained by the fit using the data in the

CR. The WZ normalization factor and nuisance parameters are profiled by maximizing the likelihood.

(ii) A *discovery fit* performs the hypothesis test for a generic beyond-the-SM (BSM) signal, setting an upper limit on the number of events and visible cross section for the signal. The fit considers only a single flavor-merged inclusive SR at once. The CRWZ is also added to the fit to constrain the WZ normalization if the SR belongs to SROS. The signal contribution is allowed only in the SR, and the signal-strength parameter is bounded to be positive.

(iii) An *exclusion fit* is performed to derive the exclusion limit for a given signal hypothesis. The SR channels and CRWZ are fit simultaneously to determine the WZ normalization factor and constrain the systematic uncertainties. The signal contamination in the CRWZ is also taken into account according to the model predictions.

For each discovery or exclusion fit, the compatibility of the observed data with the background-only or signal-plus-background hypotheses is quantified by calculating a one-sided p-value with the profile likelihood ratio used as a test statistic [154]. The limits are derived using the CL_s prescription [156] where the 95% confidence level (CL) exclusion is defined by $CL_s < 0.05$.

B. Event yields in the signal regions

The observed data yields in each SR channel together with their SM background expectations, determined after the background-only fit, are summarized in Tables V–VII as well as visualized in Fig. 13. No significant deviation

TABLE V. Observed and expected yields after the background-only fit in SROS-on. The Others category contains the production of Higgs boson, 3-top, 4-top, and single-top processes. The combined statistical and systematic uncertainties are presented.

Region	SROS-on-a-eee	SROS-on-a-$ee\mu$	SROS-on-a-$e\mu\mu$	SROS-on-a-$\mu\mu\mu$
Observed data	0	1	2	6
Fitted SM	1.0 ± 0.3	2.1 ± 0.4	2.6 ± 0.5	3.4 ± 0.6
WZ	0.77 ± 0.20	1.6 ± 0.3	2.0 ± 0.4	2.4 ± 0.5
ZZ	<0.005	0.090 ± 0.034	<0.005	0.14 ± 0.05
VVV	0.17 ± 0.13	0.26 ± 0.19	0.47 ± 0.28	0.40 ± 0.31
$t\bar{t}$	<0.05	<0.05	$0.04 \pm^{0.04}_{0.04}$	<0.05
$t\bar{t}X$	0.059 ± 0.029	0.14 ± 0.06	0.13 ± 0.05	0.28 ± 0.09
Fakes	<0.005	$0.00 \pm^{0.05}_{0.00}$	$0.000 \pm^{0.014}_{0.000}$	$0.11 \pm^{0.15}_{0.11}$
Others	$0.019 \pm^{0.021}_{0.019}$	<0.007	0.011 ± 0.005	<0.006

Region	SROS-on-b-eee	SROS-on-b-$ee\mu$	SROS-on-b-$e\mu\mu$	SROS-on-b-$\mu\mu\mu$
Observed data	4	4	9	5
Fitted SM	1.3 ± 0.3	2.7 ± 0.5	4.6 ± 0.7	3.9 ± 0.6
WZ	1.0 ± 0.3	1.9 ± 0.3	3.9 ± 0.6	3.1 ± 0.6
ZZ	<0.005	0.11 ± 0.04	0.012 ± 0.009	0.21 ± 0.06
VVV	0.18 ± 0.13	0.34 ± 0.23	0.46 ± 0.28	0.42 ± 0.30
$t\bar{t}$	<0.05	$0.04 \pm^{0.04}_{0.04}$	$0.04 \pm^{0.05}_{0.04}$	<0.05
$t\bar{t}X$	0.05 ± 0.04	0.18 ± 0.05	0.15 ± 0.07	0.13 ± 0.06
Fakes	<0.003	$0.14 \pm^{0.19}_{0.14}$	$0.000 \pm^{0.016}_{0.000}$	<0.008
Others	<0.002	<0.005	<0.006	<0.004

Region	SROS-on-c-eee	SROS-on-c-$ee\mu$	SROS-on-c-$e\mu\mu$	SROS-on-c-$\mu\mu\mu$
Observed data	1	2	1	3
Fitted SM	0.81 ± 0.21	1.9 ± 0.3	2.7 ± 0.4	2.2 ± 0.4
WZ	0.66 ± 0.19	1.6 ± 0.3	2.4 ± 0.4	1.8 ± 0.4
ZZ	<0.005	0.031 ± 0.028	0.013 ± 0.007	0.073 ± 0.028
VVV	0.09 ± 0.06	0.19 ± 0.10	0.18 ± 0.11	0.20 ± 0.13
$t\bar{t}$	<0.05	<0.05	$0.06 \pm^{0.08}_{0.06}$	<0.05
$t\bar{t}X$	0.052 ± 0.026	0.036 ± 0.024	0.031 ± 0.022	$0.011 \pm^{0.023}_{0.011}$
Fakes	<0.002	<0.004	$0.02 \pm^{0.06}_{0.02}$	$0.09 \pm^{0.11}_{0.09}$
Others	<0.002	<0.002	<0.001	<0.001

from the SM background prediction is found in any of the SR channels. The maximum deviation of the data from the background expectation is in SROS-on-b-*eee* with a local 1.8σ data excess, followed by a local 1.7σ excess in SROS-on-b-$e\mu\mu$; the significances are computed following the prescription in Ref. [137]. One event is found in SRSS-2μ, whose lepton-flavor combination is $e\mu\mu$.

Postfit distributions, after the background-only fit, of the key kinematic variables are shown in Fig. 14. In particular, Figs. 14(d) and 14(e) show the $E_{\mathrm{T}}^{\mathrm{miss}}$ and $m_{\mathrm{T}}^{\mathrm{min}}$ distribution in SROS-on-b-$e\mu\mu$. The overflow bin in $m_{\mathrm{T}}^{\mathrm{min}}$ distribution, $m_{\mathrm{T}}^{\mathrm{min}} \in [275, +\infty)$, which has the largest signal contribution shows a good agreement with the SM prediction and the excess in $E_{\mathrm{T}}^{\mathrm{miss}}$ distribution is only seen in $E_{\mathrm{T}}^{\mathrm{miss}} \in [150, 175)$ GeV bin, suggesting that this small excess is unlikely to be explained by the targeted SBH model.

To illustrate the sensitivity to various SBH signals throughout the regions, the MC predictions of representative simplified signal points are overlaid in the figures. The sensitivity to selectron signals is driven by the *eee* and $e\mu\mu$ channel in SROS-on, *eee* and $ee\mu$ channel in SROS-off, and *eee* and $ee\mu$ channel in SRSS. On the other hand, the sensitivity to smuon signals is dominated by the $ee\mu$ and $\mu\mu\mu$ channel in SROS-on, $e\mu\mu$ and $\mu\mu\mu$ channel in SROS-off, and 2μ channel in SRSS. The SRSS-2μ shows an especially significant signal-to-background ratio for smuon signals.

TABLE VI. Observed and expected yields after the background-only fit in SROS-off. The Others category contains the production of Higgs boson, 3-top, 4-top, and single-top processes. The combined statistical and systematic uncertainties are presented.

Region	SROS-off-a-*eee*	SROS-off-a-$ee\mu$	SROS-off-a-$e\mu\mu$	SROS-off-a-$\mu\mu\mu$
Observed data	0	3	2	1
Fitted SM	0.39 ± 0.11	1.4 ± 0.4	3.8 ± 0.8	1.0 ± 0.3
WZ	0.30 ± 0.10	0.26 ± 0.12	1.5 ± 0.2	0.62 ± 0.21
ZZ	<0.005	0.027 ± 0.019	0.027 ± 0.016	0.053 ± 0.034
VVV	0.06 ± 0.04	0.31 ± 0.16	0.48 ± 0.20	0.15 ± 0.08
$t\bar{t}$	<0.05	0.41 ± 0.24	1.1 ± 0.4	0.13 ± 0.10
$t\bar{t}X$	0.028 ± 0.017	0.08 ± 0.04	0.16 ± 0.06	0.046 ± 0.020
Fakes	<0.007	0.28 ± 0.27	$0.00^{+0.24}_{-0.00}$	$0.000^{+0.022}_{-0.000}$
Others	<0.01	0.032 ± 0.012	0.5 ± 0.5	0.0101 ± 0.0034
Region	SROS-off-b-*eee*	SROS-off-b-$ee\mu$	SROS-off-b-$e\mu\mu$	SROS-off-b-$\mu\mu\mu$
Observed data	0	3	6	1
Fitted SM	0.75 ± 0.33	1.6 ± 0.4	3.6 ± 0.7	1.5 ± 0.3
WZ	0.30 ± 0.10	0.45 ± 0.14	1.1 ± 0.2	1.1 ± 0.2
ZZ	<0.005	0.049 ± 0.029	0.034 ± 0.023	0.058 ± 0.029
VVV	0.17 ± 0.11	0.57 ± 0.28	1.1 ± 0.5	0.23 ± 0.11
$t\bar{t}$	<0.05	0.18 ± 0.11	0.61 ± 0.25	<0.05
$t\bar{t}X$	<0.01	0.15 ± 0.05	0.24 ± 0.07	0.064 ± 0.031
Fakes	$0.20^{+0.27}_{-0.20}$	$0.15^{+0.25}_{-0.15}$	0.5 ± 0.4	$0.02^{+0.08}_{-0.02}$
Others	$0.07^{+0.11}_{-0.07}$	0.040 ± 0.016	0.039 ± 0.011	<0.01
Region	SROS-off-c-*eee*	SROS-off-c-$ee\mu$	SROS-off-c-$e\mu\mu$	SROS-off-c-$\mu\mu\mu$
Observed data	0	1	1	3
Fitted SM	0.27 ± 0.08	0.96 ± 0.28	3.0 ± 0.6	1.9 ± 0.4
WZ	0.16 ± 0.07	0.29 ± 0.09	1.4 ± 0.2	1.5 ± 0.3
ZZ	<0.005	0.020 ± 0.013	0.09 ± 0.04	0.04 ± 0.04
VVV	0.063 ± 0.026	0.52 ± 0.25	0.9 ± 0.4	0.31 ± 0.15
$t\bar{t}$	<0.05	$0.04^{+0.05}_{-0.04}$	0.09 ± 0.07	<0.05
$t\bar{t}X$	0.039 ± 0.029	0.08 ± 0.04	0.12 ± 0.05	$0.02^{+0.05}_{-0.02}$
Fakes	<0.003	$0.000^{+0.025}_{-0.000}$	0.33 ± 0.30	$0.05^{+0.09}_{-0.05}$
Others	<0.002	<0.005	<0.01	<0.004

TABLE VII. Observed and expected event yields after the background-only fit in SRSS. The combined statistical and systematic uncertainties are presented.

Region	SRSS-*eee*	SRSS-*eμμ*	SRSS-2*μ*
Observed data	1	2	1
Fitted SM	0.85 ± 0.26	2.0 ± 0.5	0.66 ± 0.26
Charge-flip	0.74 ± 0.25	1.4 ± 0.4	0.015 ± 0.006
Fakes	$0.06^{+0.09}_{-0.06}$	0.57 ± 0.33	0.55 ± 0.25
WZ	< 0.01	0.032 ± 0.027	< 0.005
VVV	< 0.01	$0.012^{+0.018}_{-0.012}$	$0.016^{+0.022}_{-0.016}$
$t\bar{t}$	$0.04^{+0.04}_{-0.04}$	< 0.05	0.08 ± 0.06

C. Model-independent limits on new physics in inclusive regions

Model-independent upper limits are derived by performing the discovery fits as described in Sec. IX A. The nominal flavor-binned SR channels are merged to form seven flavor-merged inclusive SRs. The discovery fit is performed for each flavor-merged inclusive SR to derive the expected and the observed 95% CL upper limits on the number of the generic BSM signal events (S^{95}_{exp} and S^{95}_{obs}) as well as the one-sided p-value of the background-only hypothesis. Pseudo-experiments with toy MC are used for the calculation. An upper limit on the cross-section, $\langle \epsilon\sigma \rangle^{95}_{\text{obs}}$ where ϵ represents the efficiency times acceptance of the flavor-merged inclusive SR for the given signal, is obtained by dividing S^{95}_{obs} by the integrated luminosity. The upper limits and the p value associated with each flavor-merged inclusive SR are summarized in Table VIII.

D. Model-dependent exclusion limits

The constraints on the SBH models are derived by combining all the SR channels discussed in Sec. VI. The model-dependent 95% CL exclusion limits are

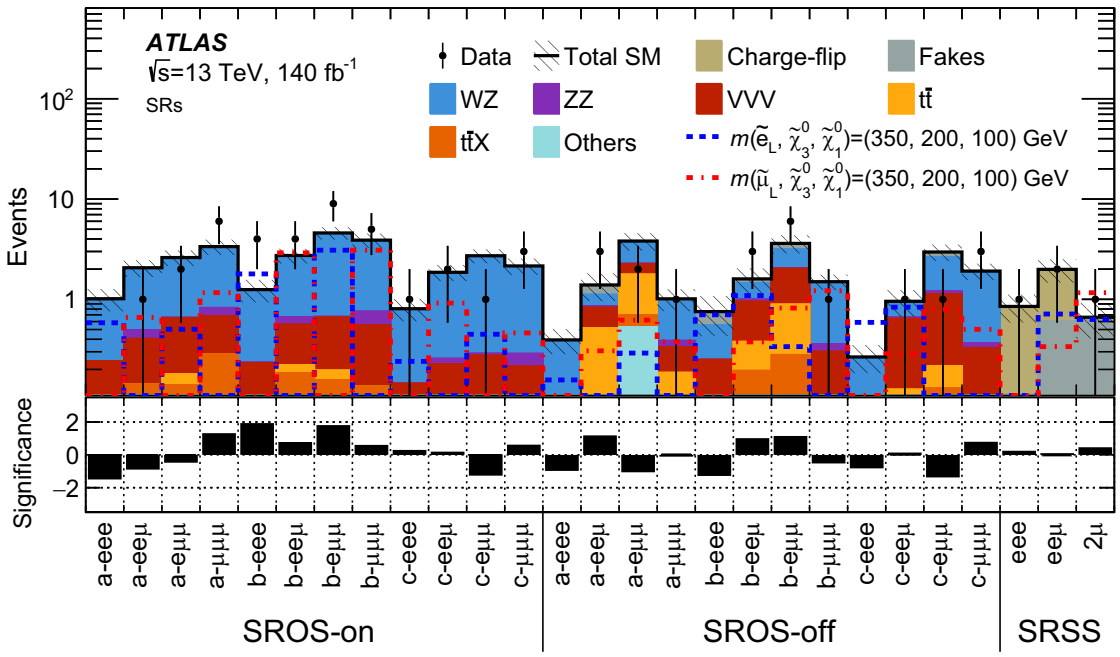

FIG. 13. Comparison of the observed data and the expected SM background yields in the SR channels. The bin indices a, b, c represent $m_{3\ell} \in [30, 200]$, $m_{3\ell} \in [200, 400)$, and $m_{3\ell} \in [400, +\infty)$, respectively. The SM prediction is taken from the background-only fit. The Others category contains the production of Higgs boson, 3-top, 4-top, and single-top processes. The hatched band includes all statistical and systematic uncertainties. Distributions for SBH $\tilde{e}_{\text{L}}$ and $\tilde{\mu}_{\text{L}}$ signals are overlaid, with masses $m(\tilde{\ell}_{\text{L}}, \tilde{\chi}^0_3, \tilde{\chi}^0_1) = (350, 200, 100)$ GeV. The bottom panel shows the statistical significance [137] of the difference between the observed events and the SM expectation. A difference of about 1.8σ (1.7σ) is observed in SROS-on-b-*eee* (SROS-on-b-*eμμ*).

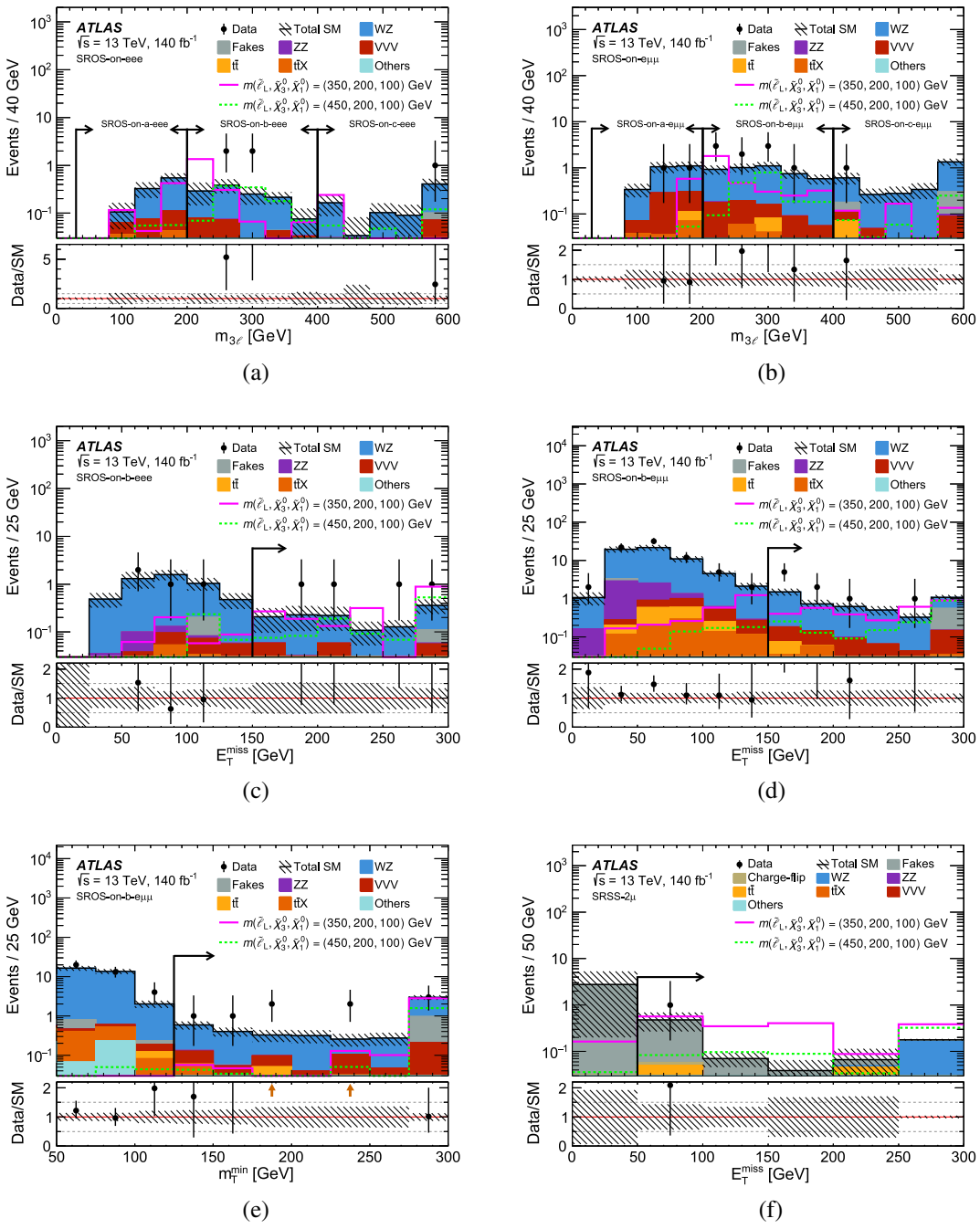

FIG. 14. Distributions of $m_{3\ell}$ in (a) SROS-on-eee and (b) SROS-on-$e\mu\mu$, of $E_{\mathrm{T}}^{\mathrm{miss}}$ in (c) SROS-on-b-eee and (d) SROS-on-b-$e\mu\mu$, of (e) $m_{\mathrm{T}}^{\mathrm{min}}$ in SROS-on-b-$e\mu\mu$, and of (f) $E_{\mathrm{T}}^{\mathrm{miss}}$ in SRSS-2μ. The SR selections are applied for each distribution, except for the variable shown, for which the selection is indicated by a black arrow. The last bin includes the overflow. The Others category contains the production of Higgs boson, 3-top, 4-top, and single-top processes. Distributions for SBH signals are overlaid. The bottom panels show the ratio of the observed data to the predicted total background yields. Ratio values outside the graph range are indicated by brown arrows. The hatched band includes all statistical and systematic uncertainties.

calculated by performing the exclusion fits as described in Sec. IX A. Given the large number of signal points tested, an asymptotic approximation [154] is employed in the $\mathrm{CL_s}$ calculation instead of the full calculation using pseudoexperiments. The difference between the $\mathrm{CL_s}$ obtained from the two methods is at most 40%, which can be translated into a difference of up to 10% in the cross section upper limit.

TABLE VIII. Observed (N_{obs}) and expected (N_{exp}) yields after the background-only fit for the flavor-merged inclusive SRs. The third and fourth columns list the 95% CL upper limits on the visible cross section (σ_{vis}^{95}) and on the number of signal events (S_{obs}^{95}). The fifth column (S_{exp}^{95}) shows the 95% CL upper limit on the number of signal events, given the expected number of background events and its $\pm 1\sigma$ variations. The last two columns indicate the CL_{b} value, i.e. the confidence level observed for the background-only hypothesis, and the discovery p value ($p(s=0)$) with its associated statistical significance Z. If the observed yield is below the expected yield, the p value is capped at 0.5.

Region	N_{obs}	N_{exp}	$\langle\epsilon\sigma\rangle_{\text{obs}}^{95}$ [fb]	S_{obs}^{95}	S_{exp}^{95}	CL_{b}	$p(s=0)$ (Z)
SROS-on-a	9	8.94 ± 1.33	0.06	8.1	$7.6^{+3.1}_{-2.1}$	0.58	0.49 (0.01)
SROS-on-b	22	12.33 ± 1.67	0.14	19.2	$9.9^{+3.9}_{-2.3}$	0.98	0.01 (2.24)
SROS-on-c	7	7.49 ± 0.99	0.05	6.8	$7.0^{+2.9}_{-2.1}$	0.46	0.50 (0.00)
SROS-off-a	6	6.33 ± 1.08	0.04	6.1	$6.6^{+2.9}_{-1.9}$	0.39	0.50 (0.00)
SROS-off-b	10	7.47 ± 1.25	0.07	9.3	$7.4^{+2.8}_{-2.0}$	0.78	0.24 (0.71)
SROS-off-c	5	5.72 ± 0.91	0.04	5.7	$6.2^{+2.8}_{-1.6}$	0.41	0.50 (0.00)
SRSS	4	3.50 ± 0.78	0.04	6.1	$5.4^{+2.0}_{-1.4}$	0.65	0.33 (0.43)

The SROS is mainly sensitive to models with sufficiently large $\Delta m(\tilde{\ell}_{\text{L}}, \tilde{\chi}_3^0)$ and $\Delta m(\tilde{\chi}_3^0, \tilde{\chi}_1^0)$. On the other hand SRSS is optimal for models with small $\Delta m(\tilde{\ell}_{\text{L}}, \tilde{\chi}_3^0)$, and rapidly loses sensitivity with decreasing $\Delta m(\tilde{\chi}_3^0, \tilde{\chi}_1^0)$.

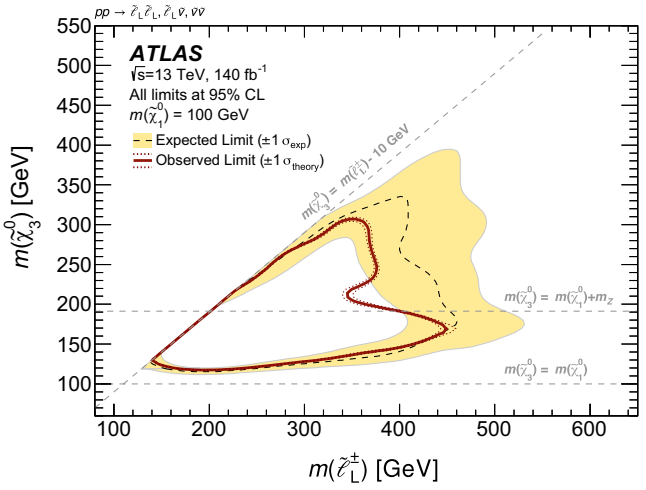

FIG. 15. Observed and expected exclusion limits on the SBH model where mass-degenerate $\tilde{e}_{\text{L}}$, $\tilde{\mu}_{\text{L}}$ and $\tilde{\nu}$ are considered. The expected 95% CL exclusion limit is shown as a dashed black line, with the yellow band indicating $\pm 1\sigma_{\text{exp}}$ including all uncertainties except for the signal cross-section uncertainty. The observed 95% CL exclusion limit is shown as a red solid line, with the dotted red lines indicating $\pm 1\sigma_{\text{theory}}$ due to the signal cross section uncertainty. The limits are shown projected onto the $m(\tilde{\ell}_{\text{L}})$ vs $m(\tilde{\chi}_3^0)$ plane, with $m(\tilde{\chi}_1^0)$ assumed to be 100 GeV.

The expected and observed exclusion limit obtained for the simplified model with mass-degenerate selectrons, smuons and sneutrinos is shown in Fig. 15. The observed bounds are weaker than the expected especially in $\Delta m(\tilde{\chi}_3^0, \tilde{\chi}_1^0) \geq m_Z$ region due to the excess of data with respect to the SM background expectation seen in SROS-on-b-*eee* and SROS-on-b-*eμμ*. The one-sided p value for the background-only hypothesis with signal hypothesis $m(\tilde{\ell}_{\text{L}}, \tilde{\chi}_3^0, \tilde{\chi}_1^0) = (350, 200, 100)$ GeV assuming mass-degenerate selectrons, smuons and sneutrinos is 0.07. A left-handed slepton/sneutrino mass up to 375 GeV is excluded in $\Delta m(\tilde{\chi}_3^0, \tilde{\chi}_1^0) \geq m_Z$ region and up to 450 GeV in $\Delta m(\tilde{\chi}_3^0, \tilde{\chi}_1^0) < m_Z$ region at 95% CL when $m(\tilde{\chi}_1^0)$ is 100 GeV. The exclusion limits are also set for $\tilde{e}_{\text{L}}$ and $\tilde{\mu}_{\text{L}}$ separately by assuming that either $\tilde{\mu}_{\text{L}}$ or $\tilde{e}_{\text{L}}$ is decoupled. These are shown in Fig. 16. These results extend the sensitivity to the SBH model compared with previous searches [38,40,46], particularly in the $\Delta m(\tilde{\chi}_3^0, \tilde{\chi}_1^0) \gtrsim 100$ GeV region which is not disfavored by direct dark-matter searches. The expected and observed exclusion limits on the $\tilde{\chi}_1^0$ mass are shown in Fig. 17 onto the $\Delta m(\tilde{\ell}_{\text{L}}, \tilde{\chi}_3^0)$ vs $\Delta m(\tilde{\chi}_3^0, \tilde{\chi}_1^0)$ plane. The observed (expected) maximum excluded $\tilde{\chi}_1^0$ mass is 205 (215) GeV for $\Delta m(\tilde{\chi}_3^0, \tilde{\chi}_1^0) = \Delta m(\tilde{\ell}_{\text{L}}, \tilde{\chi}_3^0) = 70$ GeV.

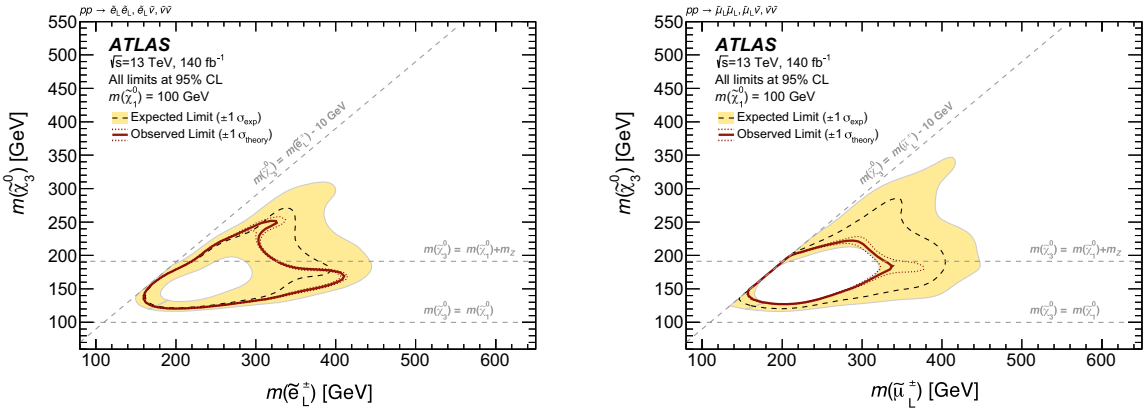

FIG. 16. Observed and expected exclusion limits on the SBH model where only one of (a) $\tilde{e}_{\mathrm{L}}$ and (b) $\tilde{\mu}_{\mathrm{L}}$ is considered and the other being decoupled. The expected 95% CL exclusion limit is shown as a dashed black line, with the yellow band indicating $\pm 1\sigma_{\mathrm{exp}}$ including all uncertainties except for the signal cross section uncertainty. The observed 95% CL exclusion limit is shown as a red solid line, with the dotted red lines indicating $\pm 1\sigma_{\mathrm{theory}}$ due to the signal cross section uncertainty. The limits are shown projected onto the $m(\tilde{\ell}_{\mathrm{L}})$ vs $m(\tilde{\chi}_3^0)$ plane, with $m(\tilde{\chi}_1^0)$ assumed to be 100 GeV.

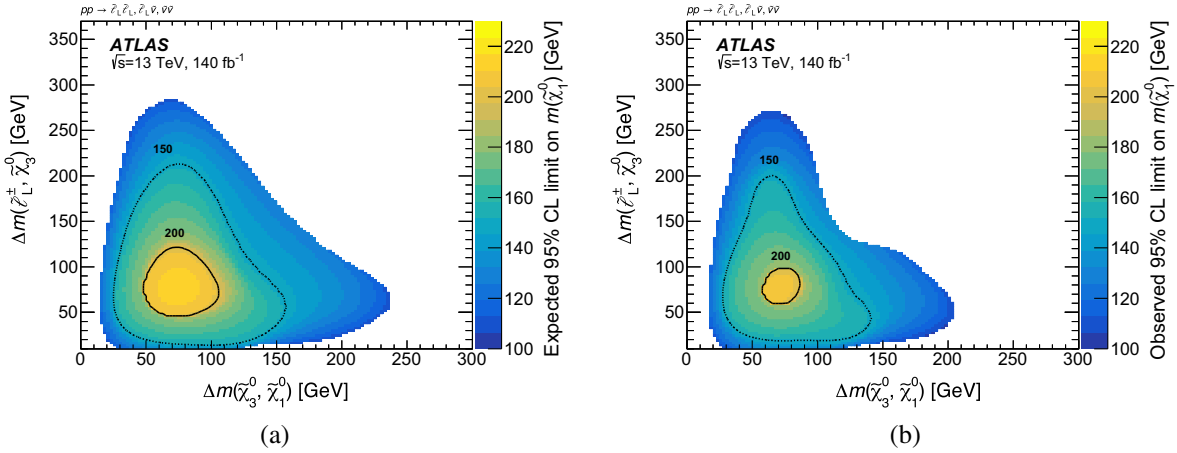

FIG. 17. The (a) expected and (b) observed lower limit on the $\tilde{\chi}_1^0$ mass at 95% CL. The limits are shown onto the $\Delta m(\tilde{\ell}_{\mathrm{L}}, \tilde{\chi}_3^0)$ vs $\Delta m(\tilde{\chi}_3^0, \tilde{\chi}_1^0)$ plane. The dotted (solid) contour line indicate 150 (200) GeV limit of $\tilde{\chi}_1^0$ mass. In the white region, the lower limit on the $\tilde{\chi}_1^0$ mass is below 100 GeV.

X. CONCLUSION

This paper presents the first dedicated search for the directly produced left-handed sleptons and sneutrinos followed by a cascade decay into light Higgsinos via a binolike neutralino, motivated by the observed anomaly in the muon anomalous magnetic moment, dark matter, and electroweak naturalness arguments. The dataset of pp collisions at $\sqrt{s} = 13$ TeV collected by the ATLAS experiment at the LHC from 2015 to 2018 is used, corresponding to an integrated luminosity of 140 fb^{-1}. By introducing search regions requiring three leptons with the same charge and optimizing the event selection strategy, the sensitivity to the targeted model is improved compared with previous searches, particularly in the $\Delta m(\tilde{\chi}_3^0, \tilde{\chi}_1^0) \gtrsim 100$ GeV region. No significant deviations from the Standard Model expectations are observed and 95% CL limits are set on the masses of relevant supersymmetric particles. For $m(\tilde{\chi}_1^0) = 100$ GeV, left-handed charged slepton and sneutrino masses up to 450 GeV are excluded assuming mass-degenerate selectrons, smuons and sneutrinos. The highest excluded $\tilde{\chi}_1^0$ mass is 205 GeV, for $\Delta m(\tilde{\chi}_3^0, \tilde{\chi}_1^0) = \Delta m(\tilde{\ell}_{\mathrm{L}}, \tilde{\chi}_3^0) = 70$ GeV.

ACKNOWLEDGMENTS

We thank CERN for the very successful operation of the LHC and its injectors, as well as the support staff at CERN and at our institutions worldwide without whom ATLAS

could not be operated efficiently. The crucial computing support from all WLCG partners is acknowledged gratefully, in particular from CERN, the ATLAS Tier-1 facilities at TRIUMF/SFU (Canada), NDGF (Denmark, Norway, Sweden), CC-IN2P3 (France), KIT/GridKA (Germany), INFN-CNAF (Italy), NL-T1 (Netherlands), PIC (Spain), RAL (United Kingdom) and BNL (USA), the Tier-2 facilities worldwide and large non-WLCG resource providers. Major contributors of computing resources are listed in Ref. [157]. We gratefully acknowledge the support of ANPCyT, Argentina; YerPhI, Armenia; ARC, Australia; BMWFW and FWF, Austria; ANAS, Azerbaijan; CNPq and FAPESP, Brazil; NSERC, NRC and CFI, Canada; CERN; ANID, Chile; CAS, MOST and NSFC, China; Minciencias, Colombia; MEYS CR, Czech Republic; DNRF and DNSRC, Denmark; IN2P3-CNRS and CEA-DRF/IRFU, France; SRNSFG, Georgia; BMBF, HGF and MPG, Germany; GSRI, Greece; RGC and Hong Kong SAR, China; ICHEP and Academy of Sciences and Humanities, Israel; INFN, Italy; MEXT and JSPS, Japan; CNRST, Morocco; NWO, Netherlands; RCN, Norway; MNiSW, Poland; FCT, Portugal; MNE/IFA, Romania; MSTDI, Serbia; MSSR, Slovakia; ARIS and MVZI, Slovenia; DSI/NRF, South Africa; MICIU/AEI, Spain; SRC and Wallenberg Foundation, Sweden; SERI, SNSF and Cantons of Bern and Geneva, Switzerland; NSTC, Taipei; TENMAK, Türkiye; STFC/UKRI, United Kingdom; DOE and NSF, USA. Individual groups and members have received support from BCKDF, CANARIE, CRC and DRAC, Canada; CERN-CZ, FORTE and PRIMUS, Czech Republic; COST, ERC, ERDF, Horizon 2020, ICSC-NextGenerationEU and Marie Skłodowska-Curie Actions, European Union; Investissements d'Avenir Labex, Investissements d'Avenir Idex and ANR, France; DFG and AvH Foundation, Germany; Herakleitos, Thales and Aristeia programmes co-financed by EU-ESF and the Greek NSRF, Greece; BSF-NSF and MINERVA, Israel; NCN and NAWA, Poland; La Caixa Banking Foundation, CERCA Programme Generalitat de Catalunya and PROMETEO and GenT Programmes Generalitat Valenciana, Spain; Göran Gustafssons Stiftelse, Sweden; The Royal Society and Leverhulme Trust, United Kingdom. In addition, individual members wish to acknowledge support from Armenia: Yerevan Physics Institute (FAPERJ); CERN: European Organization for Nuclear Research (CERN DOCT); Chile: Agencia Nacional de Investigación y Desarrollo (FONDECYT 1230812, FONDECYT 1230987, and FONDECYT 1240864); China: Chinese Ministry of Science and Technology (MOST-2023YFA1605700 and MOST-2023YFA1609300), National Natural Science Foundation of China (NSFC-12175119 and NSFC-12275265); Czech Republic: Czech Science Foundation (GACR-24-11373S), Ministry of Education Youth and Sports (ERC-CZ-LL2327 and FORTE CZ.02.01.01/00/22_008/0004632), PRIMUS Research Programme (PRIMUS/21/SCI/017); EU: H2020 European Research Council (ERC-101002463); European Union: European Research Council (ERC-948254, ERC-101089007, ERC, BARD, and 101116429), European Regional Development Fund (SMASH COFUND 101081355 and SLO ERDF), Horizon 2020 Framework Programme (MUCCA-CHIST-ERA-19-XAI-00), European Union, Future Artificial Intelligence Research (FAIR-NextGenerationEU PE00000013), Horizon 2020 (EuroHPC-EHPC-DEV-2024D11-051), Italian Center for High Performance Computing, Big Data and Quantum Computing (ICSC, NextGenerationEU); France: Agence Nationale de la Recherche (ANR-21-CE31-0013, ANR-21-CE31-0022, and ANR-22-EDIR-0002); Germany: Baden-Württemberg Stiftung (BW Stiftung-Postdoc Eliteprogramme), Deutsche Forschungsgemeinschaft (DFG-469666862 and DFG-CR 312/5-2); China: Research Grants Council (GRF); Italy: Istituto Nazionale di Fisica Nucleare (ICSC, NextGenerationEU), Ministero dell'Università e della Ricerca (NextGenEU I53D23000820006 M4C2.1.1); Japan: Japan Society for the Promotion of Science (JSPS KAKENHI JP22H01227, JSPS KAKENHI JP22H04944, JSPS KAKENHI JP22KK0227, and JSPS KAKENHI JP23KK0245); Norway: Research Council of Norway (RCN-314472); Poland: Ministry of Science and Higher Education (IDUB AGH, POB8, D4 No. 9722), Polish National Science Centre (NCN 2021/42/E/ST2/00350, NCN OPUS 2023/51/B/ST2/02507, NCN OPUS nr 2022/47/B/ST2/03059, NCN UMO-2019/34/E/ST2/00393, UMO-2020/37/B/ST2/01043, UMO-2022/47/O/ST2/00148, UMO-2023/49/B/ST2/04085, UMO-2023/51/B/ST2/00920, and UMO-2024/53/N/ST2/00869); Portugal: Foundation for Science and Technology (FCT); Spain: Generalitat Valenciana (Artemisa, FEDER, IDIFEDER/2018/048), Ministry of Science and Innovation (MCIN and NextGenEU PCI2022-135018-2, MICIN and FEDER PID2021-125273NB, RYC2019-028510-I, RYC2020-030254-I, RYC2021-031273-I, and RYC2022-038164-I); Sweden: Carl Trygger Foundation (Carl Trygger Foundation CTS 22:2312), Swedish Research Council (Swedish Research Council 2023-04654, VR 2021-03651, VR 2022-03845, VR 2022-04683, VR 2023-03403, and VR 2024-05451), Knut and Alice Wallenberg Foundation (KAW 2018.0458, KAW 2022.0358, and KAW 2023.0366); Switzerland: Swiss National Science Foundation (SNSF-PCEFP2_194658); United Kingdom: Leverhulme Trust (Leverhulme Trust RPG-2020-004), Royal Society (NIF-R1-231091); USA: U.S. Department of Energy (ECA DE-AC02-76SF00515), Neubauer Family Foundation.

DATA AVAILABILITY

The data that support the findings of this article are not publicly available. The data are available from the authors upon reasonable request.

[1] Y. Golfand and E. Likhtman, Extension of the algebra of Poincare group generators and violation of P invariance, Pis'ma Zh. Eksp. Teor. Fiz. **13**, 452 (1971) [JETP Lett. **13**, 323 (1971)].

[2] D. Volkov and V. Akulov, Is the neutrino a goldstone particle?, Phys. Lett. **46B**, 109 (1973).

[3] J. Wess and B. Zumino, Supergauge transformations in four dimensions, Nucl. Phys. **B70**, 39 (1974).

[4] J. Wess and B. Zumino, Supergauge invariant extension of quantum electrodynamics, Nucl. Phys. **B78**, 1 (1974).

[5] S. Ferrara and B. Zumino, Supergauge invariant Yang-Mills theories, Nucl. Phys. **B79**, 413 (1974).

[6] A. Salam and J. Strathdee, Super-symmetry and non-Abelian gauges, Phys. Lett. **51B**, 353 (1974).

[7] G. R. Farrar and P. Fayet, Phenomenology of the production, decay, and detection of new hadronic states associated with supersymmetry, Phys. Lett. **76B**, 575 (1978).

[8] H. Goldberg, Constraint on the photino mass from cosmology, Phys. Rev. Lett. **50**, 1419 (1983); **103**, 099905(E) (2009).

[9] J. Ellis, J. Hagelin, D. V. Nanopoulos, K. Olive, and M. Srednicki, Supersymmetric relics from the big bang, Nucl. Phys. **B238**, 453 (1984).

[10] L. Evans and P. Bryant, LHC machine, J. Instrum. **3**, S08001 (2008).

[11] P. Fayet, Supersymmetry and weak, electromagnetic and strong interactions, Phys. Lett. **64B**, 159 (1976).

[12] P. Fayet, Spontaneously broken supersymmetric theories of weak, electromagnetic and strong interactions, Phys. Lett. **69B**, 489 (1977).

[13] Muon $g-2$ Collaboration, Measurement of the positive muon anomalous magnetic moment to 0.20 ppm, Phys. Rev. Lett. **131**, 161802 (2023).

[14] T. Aoyama *et al.*, The anomalous magnetic moment of the muon in the standard model, Phys. Rep. **887**, 1 (2020).

[15] G. Colangelo *et al.*, Prospects for precise predictions of a_μ in the standard model, arXiv:2203.15810.

[16] T. Moroi, Muon anomalous magnetic dipole moment in the minimal supersymmetric standard model, Phys. Rev. D **53**, 6565 (1996); **56**, 4424(E) (1997).

[17] L. L. Everett, G. L. Kane, S. Rigolin, and L.-T. Wang, Implications of muon $g-2$ for supersymmetry and for discovering superpartners directly, Phys. Rev. Lett. **86**, 3484 (2001).

[18] M. Endo, K. Hamaguchi, S. Iwamoto, and T. Kitahara, Muon $g-2$ vs LHC Run 2 in supersymmetric models, J. High Energy Phys. 04 (**2020**) 165.

[19] J. Hisano, S. Matsumot, M. Nagai, O. Saito, and M. Senami, Non-perturbative effect on thermal relic abundance of dark matter, Phys. Lett. B **646**, 34 (2007).

[20] T. Han, S. Mukhopadhyay, and X. Wang, Electroweak dark matter at future hadron colliders, Phys. Rev. D **98**, 035026 (2018).

[21] R. Barbieri and D. Pappadopulo, S-particles at their naturalness limits, J. High Energy Phys. 10 (2009) 061.

[22] H. Baer, V. Barger, and P. Huang, Hidden SUSY at the LHC: The light Higgsino-world scenario and the role of a lepton collider, J. High Energy Phys. 11 (2011) 031.

[23] M. Papucci, J. T. Ruderman, and A. Weiler, Natural SUSY endures, J. High Energy Phys. 09 (2012) 035.

[24] H. Baer, V. Barger, P. Huang, A. Mustafayev, and X. Tata, Radiative natural supersymmetry with a 125 GeV Higgs boson, Phys. Rev. Lett. **109**, 161802 (2012).

[25] X. Fan, T. G. Myers, B. A. D. Sukra, and G. Gabrielse, Measurement of the electron magnetic moment, Phys. Rev. Lett. **130**, 071801 (2023).

[26] D. Hanneke, S. Fogwell, and G. Gabrielse, New measurement of the electron magnetic moment and the fine structure constant, Phys. Rev. Lett. **100**, 120801 (2008).

[27] T. Aoyama, T. Kinoshita, and M. Nio, Theory of the anomalous magnetic moment of the electron, Atoms **7**, 28 (2019).

[28] T. Aoyama, T. Kinoshita, and M. Nio, Revised and improved value of the QED tenth-order electron anomalous magnetic moment, Phys. Rev. D **97**, 036001 (2018).

[29] L. Morel, Z. Yao, P. Cladé, and S. Guellati-Khélifa, Determination of the fine-structure constant with an accuracy of 81 parts per trillion, Nature (London) **588**, 61 (2020).

[30] R. H. Parker, C. Yu, W. Zhong, B. Estey, and H. Müller, Measurement of the fine-structure constant as a test of the standard model, Science **360**, 191 (2018).

[31] LUX-ZEPLIN Collaboration, First dark matter search results from the LUX-ZEPLIN (LZ) experiment, Phys. Rev. Lett. **131**, 041002 (2023).

[32] D. Baxter *et al.*, Recommended conventions for reporting results from direct dark matter searches, Eur. Phys. J. C **81**, 907 (2021).

[33] ATLAS Collaboration, Search for long-lived charginos based on a disappearing-track signature using 136 fb^{-1} of pp collisions at $\sqrt{s}=13$ TeV with the ATLAS detector, Eur. Phys. J. C **82**, 606 (2022).

[34] CMS Collaboration, Search for disappearing tracks as a signature of new long-lived particles in proton–proton collisions at $\sqrt{s}=13$ TeV, J. High Energy Phys. 08 (2018) 016.

[35] CMS Collaboration, Search for disappearing tracks in proton–proton collisions at $\sqrt{s} = 13$ TeV, Phys. Lett. B **806**, 135502 (2020).

[36] ATLAS Collaboration, Search for nearly mass-degenerate Higgsinos using low-momentum mildly displaced tracks in pp collisions at $\sqrt{s} = 13$ TeV with the ATLAS detector, Phys. Rev. Lett. **132**, 221801 (2024).

[37] ATLAS Collaboration, Search for electroweak production of supersymmetric states in scenarios with compressed mass spectra at $\sqrt{s} = 13$ TeV with the ATLAS detector, Phys. Rev. D **97**, 052010 (2018).

[38] ATLAS Collaboration, Search for chargino–neutralino pair production in final states with three leptons and missing transverse momentum in $\sqrt{s} = 13$ TeV pp collisions with the ATLAS detector, Eur. Phys. J. C **81**, 1118 (2021).

[39] CMS Collaboration, Search for electroweak production of charginos and neutralinos in proton–proton collisions at $\sqrt{s} = 13$ TeV, J. High Energy Phys. 04 (2022) 147.

[40] ATLAS Collaboration, Search for electroweak production of charginos and sleptons decaying into final states with two leptons and missing transverse momentum in $\sqrt{s} =$ 13 TeV pp collisions using the ATLAS detector, Eur. Phys. J. C **80**, 123 (2020).

[41] ATLAS Collaboration, Search for direct production of charginos, neutralinos and sleptons in final states with two leptons and missing transverse momentum in pp collisions at $\sqrt{s} = 8$ TeV with the ATLAS detector, J. High Energy Phys. 05 (2014) 071.

[42] ATLAS Collaboration, Search for electroweak production of supersymmetric particles in final states with two or three leptons at $\sqrt{s} = 13$ TeV with the ATLAS detector, Eur. Phys. J. C **78**, 995 (2018).

[43] ATLAS Collaboration, Search for direct pair production of sleptons and charginos decaying to two leptons and neutralinos with mass splittings near the W-boson mass in $\sqrt{s} = 13$ TeV pp collisions with the ATLAS detector, J. High Energy Phys. 06 (**2023**) 031.

[44] CMS Collaboration, Searches for electroweak production of charginos, neutralinos, and sleptons decaying to leptons and W, Z, and Higgs bosons in pp collisions at 8 TeV, Eur. Phys. J. C **74**, 3036 (2014).

[45] CMS Collaboration, Search for supersymmetric partners of electrons and muons in proton–proton collisions at $\sqrt{s} = 13$ TeV, Phys. Lett. B **790**, 140 (2019).

[46] ATLAS Collaboration, Search for trilepton resonances from chargino and neutralino pair production in $\sqrt{s} =$ 13 TeV pp collisions with the ATLAS detector, Phys. Rev. D **103**, 112003 (2021).

[47] ATLAS Collaboration, Luminosity determination in pp collisions at $\sqrt{s} = 13$ TeV using the ATLAS detector at the LHC, Eur. Phys. J. C **83**, 982 (2023).

[48] J. Alwall, P. C. Schuster, and N. Toro, Simplified models for a first characterization of new physics at the LHC, Phys. Rev. D **79**, 075020 (2009).

[49] S. P. Martin, A supersymmetry primer, Adv. Ser. Dir. High Energy Phys. **18**, 1 (1998).

[50] S. P. Martin, Implications of purity constraints on light Higgsinos, Phys. Rev. D **109**, 095045 (2024).

[51] H. Baer, V. Barger, X. Tata, and K. Zhang, Winos from natural SUSY at the high luminosity LHC, Phys. Rev. D **109**, 015027 (2024).

[52] ATLAS Collaboration, The ATLAS Experiment at the CERN Large Hadron Collider, J. Instrum. **3**, S08003 (2008).

[53] ATLAS Collaboration, ATLAS insertable B-layer: Technical design report, Reports No. ATLAS-TDR-19, No. CERN-LHCC-2010-013, 2010, https://cds.cern.chrecord/1291633; Addendum: Reports No. ATLAS-TDR-19-ADD-1, CERN-LHCC-2012-009, 2012, https://cds.cern.ch/record/1451888.

[54] B. Abbott *et al.*, Production and integration of the ATLAS insertable B-layer, J. Instrum. **13**, T05008 (2018).

[55] G. Avoni *et al.*, The new LUCID-2 detector for luminosity measurement and monitoring in ATLAS, J. Instrum. **13**, P07017 (2018).

[56] ATLAS Collaboration, Performance of the ATLAS trigger system in 2015, Eur. Phys. J. C **77**, 317 (2017).

[57] ATLAS Collaboration, Software and computing for Run 3 of the ATLAS experiment at the LHC, Eur. Phys. J. C **85**, 234 (2025).

[58] J. Alwall, R. Frederix, S. Frixione, V. Hirschi, F. Maltoni, O. Mattelaer, H.-S. Shao, T. Stelzer, P. Torrielli, and M. Zaro, The automated computation of tree-level and next-to-leading order differential cross sections, and their matching to parton shower simulations, J. High Energy Phys. 07 (2014) 079.

[59] C. Bierlich *et al.*, A comprehensive guide to the physics and usage of PYTHIA 8.3, SciPost Phys. Codebases **8**, 1 (2022).

[60] ATLAS Collaboration, ATLAS PYTHIA 8 tunes to 7 TeV data, Report No. ATL-PHYS-PUB-2014-021, 2014, https://cds.cern.ch/record/1966419.

[61] ATLAS Collaboration, Studies on top-quark Monte Carlo modelling with Sherpa and MG5_aMC@NLO, Report No. ATL-PHYS-PUB-2017-007, 2017, https://cds.cern.ch/record/2261938.

[62] R. D. Ball *et al.* (NNPDF Collaboration), Parton distributions with LHC data, Nucl. Phys. **B867**, 244 (2013).

[63] J. Debove, B. Fuks, and M. Klasen, Threshold resummation for gaugino pair production at hadron colliders, Nucl. Phys. **B842**, 51 (2011).

[64] B. Fuks, M. Klasen, D. R. Lamprea, and M. Rothering, Gaugino production in proton–proton collisions at a center-of-mass energy of 8 TeV, J. High Energy Phys. 10 (2012) 081.

[65] B. Fuks, M. Klasen, D. R. Lamprea, and M. Rothering, Precision predictions for electroweak superpartner production at hadron colliders with resummino, Eur. Phys. J. C **73**, 2480 (2013).

[66] J. Fiaschi and M. Klasen, Neutralino-chargino pair production at NLO + NLL with resummation-improved parton density functions for LHC Run II, Phys. Rev. D **98**, 055014 (2018).

[67] G. Bozzi, B. Fuks, and M. Klasen, Threshold resummation for slepton-pair production at hadron colliders, Nucl. Phys. **B777**, 157 (2007).

[68] B. Fuks, M. Klasen, D. R. Lamprea, and M. Rothering, Revisiting slepton pair production at the Large Hadron Collider, J. High Energy Phys. 01 (2014) 168.

[69] J. Fiaschi and M. Klasen, Slepton pair production at the LHC in NLO + NLL with resummation-improved parton densities, J. High Energy Phys. 03 (2018) 094.
[70] ATLAS Collaboration, ATLAS simulation of boson plus jets processes in Run 2, Report No. ATL-PHYS-PUB-2017-006, 2017, https://cds.cern.ch/record/2261937.
[71] E. Bothmann *et al.*, Event generation with Sherpa 2.2, SciPost Phys. **7**, 034 (2019).
[72] R. D. Ball *et al.* (NNPDF Collaboration), Parton distributions for the LHC Run II, J. High Energy Phys. 04 (2015) 040.
[73] C. Anastasiou, L. Dixon, K. Melnikov, and F. Petriello, High-precision QCD at hadron colliders: Electroweak gauge boson rapidity distributions at next-to-next-to leading order, Phys. Rev. D **69**, 094008 (2004).
[74] ATLAS Collaboration, Multi-boson simulation for 13 TeV ATLAS analyses, Report No. ATL-PHYS-PUB-2017-005, 2017.
[75] S. Frixione, G. Ridolfi, and P. Nason, A positive-weight next-to-leading-order Monte Carlo for heavy flavour hadroproduction, J. High Energy Phys. 09 (2007) 126.
[76] P. Nason, A new method for combining NLO QCD with shower Monte Carlo algorithms, J. High Energy Phys. 11 (2004) 040.
[77] S. Frixione, P. Nason, and C. Oleari, Matching NLO QCD computations with parton shower simulations: The POWHEG method, J. High Energy Phys. 11 (2007) 070.
[78] S. Alioli, P. Nason, C. Oleari, and E. Re, A general framework for implementing NLO calculations in shower Monte Carlo programs: The POWHEG BOX, J. High Energy Phys. 06 (2010) 043.
[79] M. Beneke, P. Falgari, S. Klein, and C. Schwinn, Hadronic top-quark pair production with NNLL threshold resummation, Nucl. Phys. **B855**, 695 (2012).
[80] M. Cacciari, M. Czakon, M. Mangano, A. Mitov, and P. Nason, Top-pair production at hadron colliders with next-to-next-to-leading logarithmic soft-gluon resummation, Phys. Lett. B **710**, 612 (2012).
[81] P. Bärnreuther, M. Czakon, and A. Mitov, Percent-level-precision physics at the tevatron: Next-to-next-to-leading order QCD corrections to $q\bar{q} \to t\bar{t} + X$, Phys. Rev. Lett. **109**, 132001 (2012).
[82] M. Czakon and A. Mitov, NNLO corrections to top-pair production at hadron colliders: The all-fermionic scattering channels, J. High Energy Phys. 12 (2012) 054.
[83] M. Czakon and A. Mitov, NNLO corrections to top pair production at hadron colliders: The quark-gluon reaction, J. High Energy Phys. 01 (2013) 080.
[84] M. Czakon, P. Fiedler, and A. Mitov, Total top-quark pair-production cross section at hadron colliders through $\mathcal{O}(\alpha_S^4)$, Phys. Rev. Lett. **110**, 252004 (2013).
[85] M. Czakon and A. Mitov, Top++: A program for the calculation of the top-pair cross-section at hadron colliders, Comput. Phys. Commun. **185**, 2930 (2014).
[86] E. Re, Single-top Wt-channel production matched with parton showers using the POWHEG method, Eur. Phys. J. C **71**, 1547 (2011).
[87] R. Frederix, E. Re, and P. Torrielli, Single-top t-channel hadroproduction in the four-flavour scheme with POWHEG and aMC@NLO, J. High Energy Phys. 09 (2012) 130.
[88] M. Aliev, H. Lacker, U. Langenfeld, S. Moch, P. Uwer, and M. Wiedermann, HATHOR—HAdronic Top and Heavy quarks crOss section calculatoR, Comput. Phys. Commun. **182**, 1034 (2011).
[89] P. Kant, O. M. Kind, T. Kintscher, T. Lohse, T. Martini, S. Mölbitz, P. Rieck, and P. Uwer, HatHor for single top-quark production: Updated predictions and uncertainty estimates for single top-quark production in hadronic collisions, Comput. Phys. Commun. **191**, 74 (2015).
[90] T. Sjöstrand, S. Ask, J. R. Christiansen, R. Corke, N. Desai, P. Ilten, S. Mrenna, S. Prestel, C. O. Rasmussen, and P. Z. Skands, An introduction to PYTHIA 8.2, Comput. Phys. Commun. **191**, 159 (2015).
[91] N. Kidonakis, Two-loop soft anomalous dimensions for single top quark associated production with a W^- or H^-, Phys. Rev. D **82**, 054018 (2010).
[92] N. Kidonakis, Top quark production, in *Proceedings of the Helmholtz International Summer School on Physics of Heavy Quarks and Hadrons (HQ 2013)* (JINR, Dubna, Russia, 2013), p. 139, 10.3204/DESY-PROC-2013-03/Kidonakis.
[93] T. Sjöstrand, S. Mrenna, and P. Skands, A brief introduction to PYTHIA 8.1, Comput. Phys. Commun. **178**, 852 (2008).
[94] H. B. Hartanto, B. Jäger, L. Reina, and D. Wackeroth, Higgs boson production in association with top quarks in the POWHEG BOX, Phys. Rev. D **91**, 094003 (2015).
[95] ATLAS Collaboration, Measurement of the Z/γ^* boson transverse momentum distribution in pp collisions at $\sqrt{s} =$ 7 TeV with the ATLAS detector, J. High Energy Phys. 09 (2014) 145.
[96] J. Pumplin, D. R. Stump, J. Huston, H.-L. Lai, P. Nadolsky, and W.-K. Tung, New generation of parton distributions with uncertainties from global QCD analysis, J. High Energy Phys. 07 (2002) 012.
[97] D. de Florian *et al.*, *Handbook of LHC Higgs Cross Sections: 4. Deciphering the Nature of the Higgs Sector, CERN Reports: Monographs* (CERN, Geneva, Switzerland, 2017), 10.23731/CYRM-2017-002.
[98] C. Anastasiou, C. Duhr, F. Dulat, E. Furlan, T. Gehrmann, F. Herzog, A. Lazopoulos, and B. Mistlberger, High precision determination of the gluon fusion Higgs boson cross-section at the LHC, J. High Energy Phys. 05 (2016) 058.
[99] C. Anastasiou, C. Duhr, F. Dulat, F. Herzog, and B. Mistlberger, Higgs boson gluon-fusion production in QCD at three loops, Phys. Rev. Lett. **114**, 212001 (2015).
[100] F. Dulat, A. Lazopoulos, and B. Mistlberger, iHixs 2—Inclusive Higgs cross sections, Comput. Phys. Commun. **233**, 243 (2018).
[101] U. Aglietti, R. Bonciani, G. Degrassi, and A. Vicini, Two-loop light fermion contribution to Higgs production and decays, Phys. Lett. B **595**, 432 (2004).
[102] S. Actis, G. Passarino, C. Sturm, and S. Uccirati, NLO electroweak corrections to Higgs boson production at hadron colliders, Phys. Lett. B **670**, 12 (2008).
[103] M. Bonetti, K. Melnikov, and L. Tancredi, Higher order corrections to mixed QCD-EW contributions to Higgs boson production in gluon fusion, Phys. Rev. D **97**, 056017 (2018); **97**, 099906(E) (2018).

[104] T. Gleisberg and S. Höche, Comix, a new matrix element generator, J. High Energy Phys. 12 (2008) 039.

[105] S. Schumann and F. Krauss, A parton shower algorithm based on Catani–Seymour dipole factorisation, J. High Energy Phys. 03 (2008) 038.

[106] S. Catani, F. Krauss, B. R. Webber, and R. Kuhn, QCD matrix elements + parton showers, J. High Energy Phys. 11 (2001) 063.

[107] S. Höche, F. Krauss, S. Schumann, and F. Siegert, QCD matrix elements and truncated showers, J. High Energy Phys. 05 (2009) 053.

[108] S. Höche, F. Krauss, M. Schönherr, and F. Siegert, A critical appraisal of NLO + PS matching methods, J. High Energy Phys. 09 (2012) 049.

[109] S. Höche, F. Krauss, M. Schönherr, and F. Siegert, QCD matrix elements + parton showers. The NLO case, J. High Energy Phys. 04 (2013) 027.

[110] F. Cascioli, P. Maierhöfer, and S. Pozzorini, Scattering amplitudes with OpenLoops, Phys. Rev. Lett. **108**, 111601 (2012).

[111] A. Denner, S. Dittmaier, and L. Hofer, Collier: A Fortran-based complex one-loop library in extended regularizations, Comput. Phys. Commun. **212**, 220 (2017).

[112] ATLAS Collaboration, Studies on top-quark Monte Carlo modelling for Top2016, Report No. ATL-PHYS-PUB-2016-020, 2016, https://cds.cern.ch/record/2216168.

[113] S. Frixione, E. Laenen, P. Motylinski, C. White, and B. R. Webber, Single-top hadroproduction in association with a W boson, J. High Energy Phys. 07 (2008) 029.

[114] L. Lönnblad, Correcting the colour-dipole cascade model with fixed order matrix elements, J. High Energy Phys. 05 (2002) 046.

[115] L. Lönnblad and S. Prestel, Matching tree-level matrix elements with interleaved showers, J. High Energy Phys. 03 (2012) 019.

[116] C. Borschensky, M. Krämer, A. Kulesza, M. Mangano, S. Padhi, T. Plehn, and X. Portell, Squark and gluino production cross sections in pp collisions at $\sqrt{s} = 13$, 14, 33 and 100 TeV, Eur. Phys. J. C **74**, 3174 (2014).

[117] D. J. Lange, The EvtGen particle decay simulation package, Nucl. Instrum. Methods Phys. Res., Sect. A **462**, 152 (2001).

[118] ATLAS Collaboration, The ATLAS simulation infrastructure, Eur. Phys. J. C **70**, 823 (2010).

[119] S. Agostinelli *et al.*, Geant4—A simulation toolkit, Nucl. Instrum. Methods Phys. Res., Sect. A **506**, 250 (2003).

[120] ATLAS Collaboration, AtlFast3: The next generation of fast simulation in ATLAS, Comput. Software Big Sci. **6**, 7 (2022).

[121] ATLAS Collaboration, The PYTHIA 8 A3 tune description of ATLAS minimum bias and inelastic measurements incorporating the Donnachie–Landshoff diffractive model, Report No. ATL-PHYS-PUB-2016-017, 2016, https://cds.cern.ch/record/2206965.

[122] A. D. Martin, W. J. Stirling, R. S. Thorne, and G. Watt, Parton distributions for the LHC, Eur. Phys. J. C **63**, 189 (2009).

[123] ATLAS Collaboration, Performance of electron and photon triggers in ATLAS during LHC Run 2, Eur. Phys. J. C **80** (2020) 47.

[124] ATLAS Collaboration, Performance of the ATLAS muon triggers in Run 2, J. Instrum. **15**, P09015 (2020).

[125] ATLAS Collaboration, Vertex reconstruction performance of the ATLAS detector at $\sqrt{s} = 13$ TeV, Report No. ATL-PHYS-PUB-2015-026, 2015, https://cds.cern.ch/record/2037717.

[126] ATLAS Collaboration, Electron and photon performance measurements with the ATLAS detector using the 2015-2017 LHC proton–proton collision data, J. Instrum. **14**, P12006 (2019).

[127] ATLAS Collaboration, Muon reconstruction performance of the ATLAS detector in proton–proton collision data at $\sqrt{s} = 13$ TeV, Eur. Phys. J. C **76**, 292 (2016).

[128] M. Cacciari, G. P. Salam, and G. Soyez, FastJet user manual, Eur. Phys. J. C **72**, 1896 (2012).

[129] M. Cacciari, G. P. Salam, and G. Soyez, The anti-k_t jet clustering algorithm, J. High Energy Phys. 04 (2008) 063.

[130] ATLAS Collaboration, Jet reconstruction and performance using particle flow with the ATLAS detector, Eur. Phys. J. C **77**, 466 (2017).

[131] ATLAS Collaboration, Jet energy scale measurements and their systematic uncertainties in proton–proton collisions at $\sqrt{s} = 13$ TeV with the ATLAS detector, Phys. Rev. D **96**, 072002 (2017).

[132] ATLAS Collaboration, Performance of pile-up mitigation techniques for jets in pp collisions at $\sqrt{s} = 8$ TeV using the ATLAS detector, Eur. Phys. J. C **76**, 581 (2016).

[133] ATLAS Collaboration, Tagging and suppression of pileup jets with the ATLAS detector, Report No. ATLAS-CONF-2014-018, 2014, https://cds.cern.ch/record/1700870.

[134] ATLAS Collaboration, ATLAS b-jet identification performance and efficiency measurement with $t\bar{t}$ events in pp collisions at $\sqrt{s} = 13$ TeV, Eur. Phys. J. C **79**, 970 (2019).

[135] ATLAS Collaboration, The performance of missing transverse momentum reconstruction and its significance with the ATLAS detector using 140 fb^{-1} of $\sqrt{s} = 13$ TeV pp collisions, arXiv:2402.05858.

[136] ATLAS Collaboration, Selection of jets produced in 13 TeV proton–proton collisions with the ATLAS detector, Report No. ATLAS-CONF-2015-029, 2015, https://cds.cern.ch/record/2037702.

[137] R. D. Cousins, J. T. Linnemann, and J. Tucker, Evaluation of three methods for calculating statistical significance when incorporating a systematic uncertainty into a test of the background-only hypothesis for a Poisson process, Nucl. Instrum. Methods Phys. Res., Sect. A **595**, 480 (2008).

[138] ATLAS Collaboration, Search for doubly charged Higgs boson production in multi-lepton final states using 139 fb^{-1} of proton–proton collisions at $\sqrt{s} = 13$ TeV with the ATLAS detector, Eur. Phys. J. C **83**, 605 (2023).

[139] ATLAS Collaboration, Measurement of the WW cross section in $\sqrt{s} = 7$ TeV pp collisions with the ATLAS detector and limits on anomalous gauge couplings, Phys. Lett. B **712**, 289 (2012).

[140] ATLAS Collaboration, Prospects for Higgs boson searches using the $H \to WW^{(*)} \to \ell\nu\ell\nu$ decay mode with the ATLAS detector at 10 TeV, Report No. ATL-PHYS-PUB-2010-005, 2010, https://cds.cern.ch/record/1270568.

[141] ATLAS Collaboration, Measurement of $W^{\pm}Z$ production cross sections and gauge boson polarisation in pp collisions at $\sqrt{s} = 13$ TeV with the ATLAS detector, Eur. Phys. J. C **79**, 535 (2019).
[142] ATLAS Collaboration, Muon reconstruction and identification efficiency in ATLAS using the full Run 2 pp collision data set at $\sqrt{s} = 13$ TeV, Eur. Phys. J. C **81**, 578 (2021).
[143] ATLAS Collaboration, Electron and photon energy calibration with the ATLAS detector using LHC Run 2 data, J. Instrum. **19**, P02009 (2024).
[144] ATLAS Collaboration, Jet energy scale and resolution measured in proton–proton collisions at $\sqrt{s} = 13$ TeV with the ATLAS detector, Eur. Phys. J. C **81**, 689 (2021).
[145] ATLAS Collaboration, Measurement of the c-jet mistagging efficiency in $t\bar{t}$ events using pp collision data at $\sqrt{s} = 13$ TeV collected with the ATLAS detector, Eur. Phys. J. C **82**, 95 (2022).
[146] ATLAS Collaboration, Calibration of the light-flavour jet mistagging efficiency of the b-tagging algorithms with $Z +$ jets events using 139 fb^{-1} of ATLAS proton–proton collision data at $\sqrt{s} = 13$ TeV, Eur. Phys. J. C **83**, 728 (2023).
[147] CMS Collaboration, Observation of the production of three massive gauge bosons at $\sqrt{s} = 13$ TeV, Phys. Rev. Lett. **125**, 151802 (2020).
[148] ATLAS Collaboration, Observation of VVZ production at $\sqrt{s} = 13$ TeV with the ATLAS detector, arXiv: 2412.15123.
[149] ATLAS Collaboration, Measurement of the total and differential cross-sections of $t\bar{t}W$ production in pp collisions at $\sqrt{s} = 13$ TeV with the ATLAS detector, J. High Energy Phys. 05 (2024) 131.
[150] ATLAS Collaboration, Inclusive and differential cross-section measurements of $t\bar{t}Z$ production in pp collisions at $\sqrt{s} = 13$ TeV with the ATLAS detector, including EFT and spin-correlation interpretations, J. High Energy Phys. 07 (2024) 163.
[151] ATLAS Collaboration, A detailed map of Higgs boson interactions by the ATLAS experiment ten years after the discovery, Nature (London) **607**, 52 (2022).
[152] E. Bothmann, M. Schönherr, and S. Schumann, Reweighting QCD matrix-element and parton-shower calculations, Eur. Phys. J. C **76**, 590 (2016).
[153] J. Butterworth *et al.*, PDF4LHC recommendations for LHC Run II, J. Phys. G **43**, 023001 (2016).
[154] G. Cowan, K. Cranmer, E. Gross, and O. Vitells, Asymptotic formulae for likelihood-based tests of new physics, Eur. Phys. J. C **71**, 1554 (2011).
[155] M. Baak, G. J. Besjes, D. Côté, A. Koutsman, J. Lorenz, and D. Short, HistFitter software framework for statistical data analysis, Eur. Phys. J. C **75**, 153 (2015).
[156] A. L. Read, Presentation of search results: The CL_S technique, J. Phys. G **28**, 2693 (2002).
[157] ATLAS Collaboration, ATLAS computing acknowledgements, Report No. ATL-SOFT-PUB-2025-001, 2025, https://cds.cern.ch/record/2922210.

G. Aad,[104] E. Aakvaag,[17] B. Abbott,[123] S. Abdelhameed,[119a] K. Abeling,[55] N. J. Abicht,[49] S. H. Abidi,[30] M. Aboelela,[45] A. Aboulhorma,[36e] H. Abramowicz,[157] Y. Abulaiti,[120] B. S. Acharya,[69a,69b,b] A. Ackermann,[63a] C. Adam Bourdarios,[4] L. Adamczyk,[86a] S. V. Addepalli,[149] M. J. Addison,[103] J. Adelman,[118] A. Adiguzel,[22c] T. Adye,[137] A. A. Affolder,[139] Y. Afik,[40] M. N. Agaras,[13] A. Aggarwal,[102] C. Agheorghiesei,[28c] F. Ahmadov,[39,c] S. Ahuja,[97] X. Ai,[143b] G. Aielli,[76a,76b] A. Aikot,[169] M. Ait Tamlihat,[36e] B. Aitbenchikh,[36a] M. Akbiyik,[102] T. P. A. Åkesson,[100] A. V. Akimov,[151] D. Akiyama,[174] N. N. Akolkar,[25] S. Aktas,[22a] G. L. Alberghi,[24b] J. Albert,[171] P. Albicocco,[53] G. L. Albouy,[60] S. Alderweireldt,[52] Z. L. Alegria,[124] M. Aleksa,[37] I. N. Aleksandrov,[39] C. Alexa,[28b] T. Alexopoulos,[10] F. Alfonsi,[24b] M. Algren,[56] M. Alhroob,[173] B. Ali,[135] H. M. J. Ali,[93,d] S. Ali,[32] S. W. Alibocus,[94] M. Aliev,[34c] G. Alimonti,[71a] W. Alkakhi,[55] C. Allaire,[66] B. M. M. Allbrooke,[152] J. S. Allen,[103] J. F. Allen,[52] P. P. Allport,[21] A. Aloisio,[72a,72b] F. Alonso,[92] C. Alpigiani,[142] Z. M. K. Alsolami,[93] A. Alvarez Fernandez,[102] M. Alves Cardoso,[56] M. G. Alviggi,[72a,72b] M. Aly,[103] Y. Amaral Coutinho,[83b] A. Ambler,[106] C. Amelung,[37] M. Amerl,[103] C. G. Ames,[111] T. Amezza,[130] D. Amidei,[108] B. Amini,[54] K. Amirie,[161] A. Amirkhanov,[39] S. P. Amor Dos Santos,[133a] K. R. Amos,[169] D. Amperiadou,[158] S. An,[84] C. Anastopoulos,[145] T. Andeen,[11] J. K. Anders,[94] A. C. Anderson,[59] A. Andreazza,[71a,71b] S. Angelidakis,[9] A. Angerami,[42] A. V. Anisenkov,[39] A. Annovi,[74a] C. Antel,[56] E. Antipov,[151] M. Antonelli,[53] F. Anulli,[75a] M. Aoki,[84] T. Aoki,[159] M. A. Aparo,[152] L. Aperio Bella,[48] M. Apicella,[31] C. Appelt,[157] A. Apyan,[27] S. J. Arbiol Val,[87] C. Arcangeletti,[53] A. T. H. Arce,[51] J-F. Arguin,[110] S. Argyropoulos,[158] J.-H. Arling,[48] O. Arnaez,[4] H. Arnold,[151] G. Artoni,[75a,75b] H. Asada,[113] K. Asai,[121] S. Asai,[159] N. A. Asbah,[37] R. A. Ashby Pickering,[173] A. M. Aslam,[97] K. Assamagan,[30] R. Astalos,[29a] K. S. V. Astrand,[100] S. Atashi,[165] R. J. Atkin,[34a] H. Atmani,[36f] P. A. Atmasiddha,[131] K. Augsten,[135] A. D. Auriol,[41] V. A. Austrup,[103] G. Avolio,[37] K. Axiotis,[56] G. Azuelos,[110,e] D. Babal,[29b] H. Bachacou,[138] K. Bachas,[158,f] A. Bachiu,[35] E. Bachmann,[50] M. J. Backes,[63a] A. Badea,[40] T. M. Baer,[108] P. Bagnaia,[75a,75b] M. Bahmani,[19] D. Bahner,[54] K. Bai,[126]

J. T. Baines,[137] L. Baines,[96] O. K. Baker,[178] E. Bakos,[16] D. Bakshi Gupta,[8] L. E. Balabram Filho,[83b] V. Balakrishnan,[123] R. Balasubramanian,[4] E. M. Baldin,[38] P. Balek,[86a] E. Ballabene,[24b,24a] F. Balli,[138] L. M. Baltes,[63a] W. K. Balunas,[33] J. Balz,[102] I. Bamwidhi,[119b] E. Banas,[87] M. Bandieramonte,[132] A. Bandyopadhyay,[25] S. Bansal,[25] L. Barak,[157] M. Barakat,[48] E. L. Barberio,[107] D. Barberis,[18b] M. Barbero,[104] M. Z. Barel,[117] T. Barillari,[112] M-S. Barisits,[37] T. Barklow,[149] P. Baron,[125] D. A. Baron Moreno,[103] A. Baroncelli,[62] A. J. Barr,[129] J. D. Barr,[98] F. Barreiro,[101] J. Barreiro Guimarães da Costa,[14] M. G. Barros Teixeira,[133a] S. Barsov,[38] F. Bartels,[63a] R. Bartoldus,[149] A. E. Barton,[93] P. Bartos,[29a] A. Basan,[102] M. Baselga,[49] S. Bashiri,[87] A. Bassalat,[66,g] M. J. Basso,[162a] S. Bataju,[45] R. Bate,[170] R. L. Bates,[59] S. Batlamous,[101] M. Battaglia,[139] D. Battulga,[19] M. Bauce,[75a,75b] M. Bauer,[79] P. Bauer,[25] L. T. Bayer,[48] L. T. Bazzano Hurrell,[31] J. B. Beacham,[112] T. Beau,[130] J. Y. Beaucamp,[92] P. H. Beauchemin,[164] P. Bechtle,[25] H. P. Beck,[20,h] K. Becker,[173] A. J. Beddall,[82] V. A. Bednyakov,[39] C. P. Bee,[151] L. J. Beemster,[16] M. Begalli,[83d] M. Begel,[30] J. K. Behr,[48] J. F. Beirer,[37] F. Beisiegel,[25] M. Belfkir,[119b] G. Bella,[157] L. Bellagamba,[24b] A. Bellerive,[35] C. D. Bellgraph,[68] P. Bellos,[21] K. Beloborodov,[38] D. Benchekroun,[36a] F. Bendebba,[36a] Y. Benhammou,[157] K. C. Benkendorfer,[61] L. Beresford,[48] M. Beretta,[53] E. Bergeaas Kuutmann,[167] N. Berger,[4] B. Bergmann,[135] J. Beringer,[18a] G. Bernardi,[5] C. Bernius,[149] F. U. Bernlochner,[25] F. Bernon,[37] A. Berrocal Guardia,[13] T. Berry,[97] P. Berta,[136] A. Berthold,[50] A. Berti,[133a] R. Bertrand,[104] S. Bethke,[112] A. Betti,[75a,75b] A. J. Bevan,[96] L. Bezio,[56] N. K. Bhalla,[54] S. Bharthuar,[112] S. Bhatta,[151] P. Bhattarai,[149] Z. M. Bhatti,[120] K. D. Bhide,[54] V. S. Bhopatkar,[124] R. M. Bianchi,[132] G. Bianco,[24b,24a] O. Biebel,[111] M. Biglietti,[77a] C. S. Billingsley,[45] Y. Bimgdi,[36f] M. Bindi,[55] A. Bingham,[177] A. Bingul,[22b] C. Bini,[75a,75b] G. A. Bird,[33] M. Birman,[175] M. Biros,[136] S. Biryukov,[152] T. Bisanz,[49] E. Bisceglie,[24b,24a] J. P. Biswal,[137] D. Biswas,[147] I. Bloch,[48] A. Blue,[59] U. Blumenschein,[96] J. Blumenthal,[102] V. S. Bobrovnikov,[39] M. Boehler,[54] B. Boehm,[172] D. Bogavac,[13] A. G. Bogdanchikov,[38] L. S. Boggia,[130] V. Boisvert,[97] P. Bokan,[37] T. Bold,[86a] M. Bomben,[5] M. Bona,[96] M. Boonekamp,[138] A. G. Borbély,[59] I. S. Bordulev,[38] G. Borissov,[93] D. Bortoletto,[129] D. Boscherini,[24b] M. Bosman,[13] K. Bouaouda,[36a] N. Bouchhar,[169] L. Boudet,[4] J. Boudreau,[132] E. V. Bouhova-Thacker,[93] D. Boumediene,[41] R. Bouquet,[57b,57a] A. Boveia,[122] J. Boyd,[37] D. Boye,[30] I. R. Boyko,[39] L. Bozianu,[56] J. Bracinik,[21] N. Brahimi,[4] G. Brandt,[177] O. Brandt,[33] B. Brau,[105] J. E. Brau,[126] R. Brener,[175] L. Brenner,[117] R. Brenner,[167] S. Bressler,[175] G. Brianti,[78a,78b] D. Britton,[59] D. Britzger,[112] I. Brock,[25] R. Brock,[109] G. Brooijmans,[42] A. J. Brooks,[68] E. M. Brooks,[162b] E. Brost,[30] L. M. Brown,[171,162a] L. E. Bruce,[61] T. L. Bruckler,[129] P. A. Bruckman de Renstrom,[87] B. Brüers,[48] A. Bruni,[24b] G. Bruni,[24b] D. Brunner,[47a,47b] M. Bruschi,[24b] N. Bruscino,[75a,75b] T. Buanes,[17] Q. Buat,[142] D. Buchin,[112] A. G. Buckley,[59] O. Bulekov,[82] B. A. Bullard,[149] S. Burdin,[94] C. D. Burgard,[49] A. M. Burger,[91] B. Burghgrave,[8] O. Burlayenko,[54] J. Burleson,[168] J. T. P. Burr,[33] J. C. Burzynski,[148] E. L. Busch,[42] V. Büscher,[102] P. J. Bussey,[59] J. M. Butler,[26] C. M. Buttar,[59] J. M. Butterworth,[98] W. Buttinger,[137] C. J. Buxo Vazquez,[109] A. R. Buzykaev,[39] S. Cabrera Urbán,[169] L. Cadamuro,[66] D. Caforio,[58] H. Cai,[132] Y. Cai,[24b,114c,24a] Y. Cai,[114a] V. M. M. Cairo,[37] O. Cakir,[3a] N. Calace,[37] P. Calafiura,[18a] G. Calderini,[130] P. Calfayan,[35] G. Callea,[59] L. P. Caloba,[83b] D. Calvet,[41] S. Calvet,[41] R. Camacho Toro,[130] S. Camarda,[37] D. Camarero Munoz,[27] P. Camarri,[76a,76b] C. Camincher,[171] M. Campanelli,[98] A. Camplani,[43] V. Canale,[72a,72b] A. C. Canbay,[3a] E. Canonero,[97] J. Cantero,[169] Y. Cao,[168] F. Capocasa,[27] M. Capua,[44b,44a] A. Carbone,[71a,71b] R. Cardarelli,[76a] J. C. J. Cardenas,[8] M. P. Cardiff,[27] G. Carducci,[44b,44a] T. Carli,[37] G. Carlino,[72a] J. I. Carlotto,[13] B. T. Carlson,[132,i] E. M. Carlson,[171] J. Carmignani,[94] L. Carminati,[71a,71b] A. Carnelli,[4] M. Carnesale,[37] S. Caron,[116] E. Carquin,[140f] I. B. Carr,[107] S. Carrá,[71a] G. Carratta,[24b,24a] A. M. Carroll,[126] M. P. Casado,[13,j] M. Caspar,[48] F. L. Castillo,[4] L. Castillo Garcia,[13] V. Castillo Gimenez,[169] N. F. Castro,[133a,133e] A. Catinaccio,[37] J. R. Catmore,[128] T. Cavaliere,[4] V. Cavaliere,[30] L. J. Caviedes Betancourt,[23b] Y. C. Cekmecelioglu,[48] E. Celebi,[82] S. Cella,[37] V. Cepaitis,[56] K. Cerny,[125] A. S. Cerqueira,[83a] A. Cerri,[74a,74b,k] L. Cerrito,[76a,76b] F. Cerutti,[18a] B. Cervato,[71a,71b] A. Cervelli,[24b] G. Cesarini,[53] S. A. Cetin,[82] P. M. Chabrillat,[130] J. Chan,[18a] W. Y. Chan,[159] J. D. Chapman,[33] E. Chapon,[138] B. Chargeishvili,[155b] D. G. Charlton,[21] C. Chauhan,[136] Y. Che,[114a] S. Chekanov,[6] S. V. Chekulaev,[162a] G. A. Chelkov,[39,l] B. Chen,[157] B. Chen,[171] H. Chen,[114a] H. Chen,[30] J. Chen,[144a] J. Chen,[148] M. Chen,[129] S. Chen,[89] S. J. Chen,[114a] X. Chen,[144a] X. Chen,[15,m] Z. Chen,[62] C. L. Cheng,[176] H. C. Cheng,[64a] S. Cheong,[149] A. Cheplakov,[39] E. Cheremushkina,[48] E. Cherepanova,[117] R. Cherkaoui El Moursli,[36e] E. Cheu,[7] K. Cheung,[65]

L. Chevalier,[138] V. Chiarella,[53] G. Chiarelli,[74a] G. Chiodini,[70a] A. S. Chisholm,[21] A. Chitan,[28b] M. Chitishvili,[169] M. V. Chizhov,[39,n] K. Choi,[11] Y. Chou,[142] E. Y. S. Chow,[116] K. L. Chu,[175] M. C. Chu,[64a] X. Chu,[14,114c] Z. Chubinidze,[53] J. Chudoba,[134] J. J. Chwastowski,[87] D. Cieri,[112] K. M. Ciesla,[86a] V. Cindro,[95] A. Ciocio,[18a] F. Cirotto,[72a,72b] Z. H. Citron,[175] M. Citterio,[71a] D. A. Ciubotaru,[28b] A. Clark,[56] P. J. Clark,[52] N. Clarke Hall,[98] C. Clarry,[161] S. E. Clawson,[48] C. Clement,[47a,47b] Y. Coadou,[104] M. Cobal,[69a,69c] A. Coccaro,[57b] R. F. Coelho Barrue,[133a] R. Coelho Lopes De Sa,[105] S. Coelli,[71a] L. S. Colangeli,[161] B. Cole,[42] P. Collado Soto,[101] J. Collot,[60] R. Coluccia,[70a,70b] P. Conde Muiño,[133a,133g] M. P. Connell,[34c] S. H. Connell,[34c] E. I. Conroy,[129] F. Conventi,[72a,o] H. G. Cooke,[21] A. M. Cooper-Sarkar,[129] L. Corazzina,[75a,75b] F. A. Corchia,[24b,24a] A. Cordeiro Oudot Choi,[142] L. D. Corpe,[41] M. Corradi,[75a,75b] F. Corriveau,[106,p] A. Cortes-Gonzalez,[19] M. J. Costa,[169] F. Costanza,[4] D. Costanzo,[145] B. M. Cote,[122] J. Couthures,[4] G. Cowan,[97] K. Cranmer,[176] L. Cremer,[49] D. Cremonini,[24b,24a] S. Crépé-Renaudin,[60] F. Crescioli,[130] T. Cresta,[73a,73b] M. Cristinziani,[147] M. Cristoforetti,[78a,78b] V. Croft,[117] J. E. Crosby,[124] G. Crosetti,[44b,44a] A. Cueto,[101] H. Cui,[98] Z. Cui,[7] W. R. Cunningham,[59] F. Curcio,[169] J. R. Curran,[52] M. J. Da Cunha Sargedas De Sousa,[57b,57a] J. V. Da Fonseca Pinto,[83b] C. Da Via,[103] W. Dabrowski,[86a] T. Dado,[37] S. Dahbi,[154] T. Dai,[108] D. Dal Santo,[20] C. Dallapiccola,[105] M. Dam,[43] G. D'amen,[30] V. D'Amico,[111] J. Damp,[102] J. R. Dandoy,[35] D. Dannheim,[37] G. D'anniballe,[74a,74b] M. Danninger,[148] V. Dao,[151] G. Darbo,[57b] S. J. Das,[30] F. Dattola,[48] S. D'Auria,[71a,71b] A. D'Avanzo,[72a,72b] T. Davidek,[136] J. Davidson,[173] I. Dawson,[96] K. De,[8] C. De Almeida Rossi,[161] R. De Asmundis,[72a] N. De Biase,[48] S. De Castro,[24b,24a] N. De Groot,[116] P. de Jong,[117] H. De la Torre,[118] A. De Maria,[114a] A. De Salvo,[75a] U. De Sanctis,[76a,76b] F. De Santis,[70a,70b] A. De Santo,[152] J. B. De Vivie De Regie,[60] J. Debevc,[95] D. V. Dedovich,[39] J. Degens,[94] A. M. Deiana,[45] J. Del Peso,[101] L. Delagrange,[130] F. Deliot,[138] C. M. Delitzsch,[49] M. Della Pietra,[72a,72b] D. Della Volpe,[56] A. Dell'Acqua,[37] L. Dell'Asta,[71a,71b] M. Delmastro,[4] C. C. Delogu,[102] P. A. Delsart,[60] S. Demers,[178] M. Demichev,[39] S. P. Denisov,[38] H. Denizli,[22a,q] L. D'Eramo,[41] D. Derendarz,[87] F. Derue,[130] P. Dervan,[94] K. Desch,[25] F. A. Di Bello,[57b,57a] A. Di Ciaccio,[76a,76b] L. Di Ciaccio,[4] A. Di Domenico,[75a,75b] C. Di Donato,[72a,72b] A. Di Girolamo,[37] G. Di Gregorio,[37] A. Di Luca,[78a,78b] B. Di Micco,[77a,77b] R. Di Nardo,[77a,77b] K. F. Di Petrillo,[40] M. Diamantopoulou,[35] F. A. Dias,[117] M. A. Diaz,[140a,140b] A. R. Didenko,[39] M. Didenko,[169] S. D. Diefenbacher,[18a] E. B. Diehl,[108] S. Díez Cornell,[48] C. Diez Pardos,[147] C. Dimitriadi,[150] A. Dimitrievska,[21] A. Dimri,[151] J. Dingfelder,[25] T. Dingley,[129] I-M. Dinu,[28b] S. J. Dittmeier,[63b] F. Dittus,[37] M. Divisek,[136] B. Dixit,[94] F. Djama,[104] T. Djobava,[155b] C. Doglioni,[103,100] A. Dohnalova,[29a] Z. Dolezal,[136] K. Domijan,[86a] K. M. Dona,[40] M. Donadelli,[83d] B. Dong,[109] J. Donini,[41] A. D'Onofrio,[72a,72b] M. D'Onofrio,[94] J. Dopke,[137] A. Doria,[72a] N. Dos Santos Fernandes,[133a] P. Dougan,[103] M. T. Dova,[92] A. T. Doyle,[59] M. A. Draguet,[129] M. P. Drescher,[55] E. Dreyer,[175] I. Drivas-koulouris,[10] M. Drnevich,[120] M. Drozdova,[56] D. Du,[62] T. A. du Pree,[117] Z. Duan,[114a] F. Dubinin,[39] M. Dubovsky,[29a] E. Duchovni,[175] G. Duckeck,[111] P. K. Duckett,[98] O. A. Ducu,[28b] D. Duda,[52] A. Dudarev,[37] E. R. Duden,[27] M. D'uffizi,[103] L. Duflot,[66] M. Dührssen,[37] I. Duminica,[28g] A. E. Dumitriu,[28b] M. Dunford,[63a] S. Dungs,[49] K. Dunne,[47a,47b] A. Duperrin,[104] H. Duran Yildiz,[3a] M. Düren,[58] A. Durglishvili,[155b] D. Duvnjak,[35] B. L. Dwyer,[118] G. I. Dyckes,[18a] M. Dyndal,[86a] B. S. Dziedzic,[37] Z. O. Earnshaw,[152] G. H. Eberwein,[129] B. Eckerova,[29a] S. Eggebrecht,[55] E. Egidio Purcino De Souza,[83e] G. Eigen,[17] K. Einsweiler,[18a] T. Ekelof,[167] P. A. Ekman,[100] S. El Farkh,[36b] Y. El Ghazali,[62] H. El Jarrari,[37] A. El Moussaouy,[36a] V. Ellajosyula,[167] M. Ellert,[167] F. Ellinghaus,[177] N. Ellis,[37] J. Elmsheuser,[30] M. Elsawy,[119a] M. Elsing,[37] D. Emeliyanov,[137] Y. Enari,[84] I. Ene,[18a] S. Epari,[110] D. Ernani Martins Neto,[87] F. Ernst,[37] M. Errenst,[177] M. Escalier,[66] C. Escobar,[169] E. Etzion,[157] G. Evans,[133a,133b] H. Evans,[68] L. S. Evans,[97] A. Ezhilov,[38] S. Ezzarqtouni,[36a] F. Fabbri,[24b,24a] L. Fabbri,[24b,24a] G. Facini,[98] V. Fadeyev,[139] R. M. Fakhrutdinov,[38] D. Fakoudis,[102] S. Falciano,[75a] L. F. Falda Ulhoa Coelho,[133a] F. Fallavollita,[112] G. Falsetti,[44b,44a] J. Faltova,[136] C. Fan,[168] K. Y. Fan,[64b] Y. Fan,[14] Y. Fang,[14,114c] M. Fanti,[71a,71b] M. Faraj,[69a,69b] Z. Farazpay,[99] A. Farbin,[8] A. Farilla,[77a] T. Farooque,[109] J. N. Farr,[178] S. M. Farrington,[137,52] F. Fassi,[36e] D. Fassouliotis,[9] L. Fayard,[66] P. Federic,[136] P. Federicova,[134] O. L. Fedin,[38,l] M. Feickert,[176] L. Feligioni,[104] D. E. Fellers,[18a] C. Feng,[143a] Z. Feng,[117] M. J. Fenton,[165] L. Ferencz,[48] B. Fernandez Barbadillo,[93] P. Fernandez Martinez,[67] M. J. V. Fernoux,[104] J. Ferrando,[93] A. Ferrari,[167] P. Ferrari,[117,116] R. Ferrari,[73a] D. Ferrere,[56] C. Ferretti,[108] M. P. Fewell,[1] D. Fiacco,[75a,75b] F. Fiedler,[102] P. Fiedler,[135] S. Filimonov,[39] M. S. Filip,[28b,r] A. Filipčič,[95]

E. K. Filmer,[162a] F. Filthaut,[116] M. C. N. Fiolhais,[133a,133c,s] L. Fiorini,[169] W. C. Fisher,[109] T. Fitschen,[103] P. M. Fitzhugh,[138] I. Fleck,[147] P. Fleischmann,[108] T. Flick,[177] M. Flores,[34d,t] L. R. Flores Castillo,[64a] L. Flores Sanz De Acedo,[37] F. M. Follega,[78a,78b] N. Fomin,[33] J. H. Foo,[161] A. Formica,[138] A. C. Forti,[103] E. Fortin,[37] A. W. Fortman,[18a] L. Foster,[18a] L. Fountas,[9,u] D. Fournier,[66] H. Fox,[93] P. Francavilla,[74a,74b] S. Francescato,[61] S. Franchellucci,[56] M. Franchini,[24b,24a] S. Franchino,[63a] D. Francis,[37] L. Franco,[116] V. Franco Lima,[37] L. Franconi,[48] M. Franklin,[61] G. Frattari,[27] Y. Y. Frid,[157] J. Friend,[59] N. Fritzsche,[37] A. Froch,[56] D. Froidevaux,[37] J. A. Frost,[129] Y. Fu,[109] S. Fuenzalida Garrido,[140f] M. Fujimoto,[104] K. Y. Fung,[64a] E. Furtado De Simas Filho,[83e] M. Furukawa,[159] J. Fuster,[169] A. Gaa,[55] A. Gabrielli,[24b,24a] A. Gabrielli,[161] P. Gadow,[37] G. Gagliardi,[57b,57a] L. G. Gagnon,[18a] S. Gaid,[88b] S. Galantzan,[157] J. Gallagher,[1] E. J. Gallas,[129] A. L. Gallen,[167] B. J. Gallop,[137] K. K. Gan,[122] S. Ganguly,[159] Y. Gao,[52] A. Garabaglu,[142] F. M. Garay Walls,[140a,140b] C. García,[169] A. Garcia Alonso,[117] A. G. Garcia Caffaro,[178] J. E. García Navarro,[169] M. Garcia-Sciveres,[18a] G. L. Gardner,[131] R. W. Gardner,[40] N. Garelli,[164] R. B. Garg,[149] J. M. Gargan,[52] C. A. Garner,[161] C. M. Garvey,[34a] V. K. Gassmann,[164] G. Gaudio,[73a] V. Gautam,[13] P. Gauzzi,[75a,75b] J. Gavranovic,[95] I. L. Gavrilenko,[133a] A. Gavrilyuk,[38] C. Gay,[170] G. Gaycken,[126] E. N. Gazis,[10] A. Gekow,[122] C. Gemme,[57b] M. H. Genest,[60] A. D. Gentry,[115] S. George,[97] T. Geralis,[46] A. A. Gerwin,[123] P. Gessinger-Befurt,[37] M. E. Geyik,[177] M. Ghani,[173] K. Ghorbanian,[96] A. Ghosal,[147] A. Ghosh,[165] A. Ghosh,[7] B. Giacobbe,[24b] S. Giagu,[75a,75b] T. Giani,[117] A. Giannini,[62] S. M. Gibson,[97] M. Gignac,[139] D. T. Gil,[86b] A. K. Gilbert,[86a] B. J. Gilbert,[42] D. Gillberg,[35] G. Gilles,[117] D. M. Gingrich,[2,e] M. P. Giordani,[69a,69c] P. F. Giraud,[138] G. Giugliarelli,[69a,69c] D. Giugni,[71a] F. Giuli,[76a,76b] I. Gkialas,[9,u] L. K. Gladilin,[38] C. Glasman,[101] M. Glazewska,[20] G. Glemža,[48] M. Glisic,[126] I. Gnesi,[44b] Y. Go,[30] M. Goblirsch-Kolb,[37] B. Gocke,[49] D. Godin,[110] B. Gokturk,[22a] S. Goldfarb,[107] T. Golling,[56] M. G. D. Gololo,[34c] D. Golubkov,[38] J. P. Gombas,[109] A. Gomes,[133a,133b] G. Gomes Da Silva,[147] A. J. Gomez Delegido,[169] R. Gonçalo,[133a] L. Gonella,[21] A. Gongadze,[155c] F. Gonnella,[21] J. L. Gonski,[149] R. Y. González Andana,[52] S. González de la Hoz,[169] M. V. Gonzalez Rodrigues,[48] R. Gonzalez Suarez,[167] S. Gonzalez-Sevilla,[56] L. Goossens,[37] B. Gorini,[37] E. Gorini,[70a,70b] A. Gorišek,[95] T. C. Gosart,[131] A. T. Goshaw,[51] M. I. Gostkin,[39] S. Goswami,[124] C. A. Gottardo,[37] S. A. Gotz,[111] M. Gouighri,[36b] A. G. Goussiou,[142] N. Govender,[34c] R. P. Grabarczyk,[129] I. Grabowska-Bold,[86a] K. Graham,[35] E. Gramstad,[128] S. Grancagnolo,[70a,70b] C. M. Grant,[1] P. M. Gravila,[28f] F. G. Gravili,[70a,70b] H. M. Gray,[18a] M. Greco,[112] M. J. Green,[1] C. Grefe,[25] A. S. Grefsrud,[17] I. M. Gregor,[48] K. T. Greif,[165] P. Grenier,[149] S. G. Grewe,[112] A. A. Grillo,[139] K. Grimm,[32] S. Grinstein,[13,v] J.-F. Grivaz,[66] E. Gross,[175] J. Grosse-Knetter,[55] L. Guan,[108] G. Guerrieri,[37] R. Guevara,[128] R. Gugel,[102] J. A. M. Guhit,[108] A. Guida,[19] E. Guilloton,[173] S. Guindon,[37] F. Guo,[14,114c] J. Guo,[144a] L. Guo,[48] L. Guo,[114b,w] Y. Guo,[108] A. Gupta,[49] R. Gupta,[132] S. Gupta,[27] S. Gurbuz,[25] S. S. Gurdasani,[48] G. Gustavino,[75a,75b] P. Gutierrez,[123] L. F. Gutierrez Zagazeta,[131] M. Gutsche,[50] C. Gutschow,[98] C. Gwenlan,[129] C. B. Gwilliam,[94] E. S. Haaland,[128] A. Haas,[120] M. Habedank,[59] C. Haber,[18a] H. K. Hadavand,[8] A. Haddad,[41] A. Hadef,[50] A. I. Hagan,[93] J. J. Hahn,[147] E. H. Haines,[98] M. Haleem,[172] J. Haley,[124] G. D. Hallewell,[104] L. Halser,[20] K. Hamano,[171] M. Hamer,[25] S. E. D. Hammoud,[66] E. J. Hampshire,[97] J. Han,[143a] L. Han,[114a] L. Han,[62] S. Han,[18a] K. Hanagaki,[84] M. Hance,[139] D. A. Hangal,[42] H. Hanif,[148] M. D. Hank,[131] J. B. Hansen,[43] P. H. Hansen,[43] D. Harada,[56] T. Harenberg,[177] S. Harkusha,[179] M. L. Harris,[105] Y. T. Harris,[25] J. Harrison,[13] N. M. Harrison,[122] P. F. Harrison,[173] M. L. E. Hart,[98] N. M. Hartman,[112] N. M. Hartmann,[111] R. Z. Hasan,[97,137] Y. Hasegawa,[146] F. Haslbeck,[129] S. Hassan,[17] R. Hauser,[109] M. Haviernik,[136] C. M. Hawkes,[21] R. J. Hawkings,[37] Y. Hayashi,[159] D. Hayden,[109] C. Hayes,[108] R. L. Hayes,[117] C. P. Hays,[129] J. M. Hays,[96] H. S. Hayward,[94] M. He,[14,114c] Y. He,[48] Y. He,[98] N. B. Heatley,[96] V. Hedberg,[100] C. Heidegger,[54] K. K. Heidegger,[54] J. Heilman,[35] S. Heim,[48] T. Heim,[18a] J. G. Heinlein,[131] J. J. Heinrich,[126] L. Heinrich,[112] J. Hejbal,[134] M. Helbig,[50] A. Held,[176] S. Hellesund,[17] C. M. Helling,[170] S. Hellman,[47a,47b] L. Henkelmann,[33] A. M. Henriques Correia,[37] H. Herde,[100] Y. Hernández Jiménez,[151] L. M. Herrmann,[25] T. Herrmann,[50] G. Herten,[54] R. Hertenberger,[111] L. Hervas,[37] M. E. Hesping,[102] N. P. Hessey,[162a] J. Hessler,[112] M. Hidaoui,[36b] N. Hidic,[136] E. Hill,[161] S. J. Hillier,[21] J. R. Hinds,[109] F. Hinterkeuser,[25] M. Hirose,[127] S. Hirose,[163] D. Hirschbuehl,[177] T. G. Hitchings,[103] B. Hiti,[95] J. Hobbs,[151] R. Hobincu,[28e] N. Hod,[175] A. M. Hodges,[168] M. C. Hodgkinson,[145] B. H. Hodkinson,[129] A. Hoecker,[37] D. D. Hofer,[108] J. Hofer,[169] M. Holzbock,[37] L. B. A. H. Hommels,[33] V. Homsak,[129]

B. P. Honan,[103] J. J. Hong,[68] T. M. Hong,[132] B. H. Hooberman,[168] W. H. Hopkins,[6] M. C. Hoppesch,[168] Y. Horii,[113] M. E. Horstmann,[112] S. Hou,[154] M. R. Housenga,[168] A. S. Howard,[95] J. Howarth,[59] J. Hoya,[6] M. Hrabovsky,[125] T. Hryn'ova,[4] P. J. Hsu,[65] S.-C. Hsu,[142] T. Hsu,[66] M. Hu,[18a] Q. Hu,[62] S. Huang,[33] X. Huang,[14,114c] Y. Huang,[136] Y. Huang,[114b] Y. Huang,[102] Y. Huang,[14] Z. Huang,[66] Z. Hubacek,[135] M. Huebner,[25] F. Huegging,[25] T. B. Huffman,[129] M. Hufnagel Maranha De Faria,[83a] C. A. Hugli,[48] M. Huhtinen,[37] S. K. Huiberts,[17] R. Hulsken,[106] C. E. Hultquist,[18a] N. Huseynov,[12,x] J. Huston,[109] J. Huth,[61] R. Hyneman,[7] G. Iacobucci,[56] G. Iakovidis,[30] L. Iconomidou-Fayard,[66] J. P. Iddon,[37] P. Iengo,[72a,72b] R. Iguchi,[159] Y. Iiyama,[159] T. Iizawa,[159] Y. Ikegami,[84] D. Iliadis,[158] N. Ilic,[161] H. Imam,[36a] G. Inacio Goncalves,[83d] S. A. Infante Cabanas,[140c] T. Ingebretsen Carlson,[47a,47b] J. M. Inglis,[96] G. Introzzi,[73a,73b] M. Iodice,[77a] V. Ippolito,[75a,75b] R. K. Irwin,[94] M. Ishino,[159] W. Islam,[176] C. Issever,[19] S. Istin,[22a,y] K. Itabashi,[84] H. Ito,[174] R. Iuppa,[78a,78b] A. Ivina,[175] V. Izzo,[72a] P. Jacka,[134] P. Jackson,[1] P. Jain,[48] K. Jakobs,[54] T. Jakoubek,[175] J. Jamieson,[59] W. Jang,[159] S. Jankovych,[136] M. Javurkova,[105] P. Jawahar,[103] L. Jeanty,[126] J. Jejelava,[155a,z] P. Jenni,[54,aa] C. E. Jessiman,[35] C. Jia,[143a] H. Jia,[170] J. Jia,[151] X. Jia,[14,114c] Z. Jia,[114a] C. Jiang,[52] Q. Jiang,[64b] S. Jiggins,[48] M. Jimenez Ortega,[169] J. Jimenez Pena,[13] S. Jin,[114a] A. Jinaru,[28b] O. Jinnouchi,[141] P. Johansson,[145] K. A. Johns,[7] J. W. Johnson,[139] F. A. Jolly,[48] D. M. Jones,[152] E. Jones,[48] K. S. Jones,[8] P. Jones,[33] R. W. L. Jones,[93] T. J. Jones,[94] H. L. Joos,[55,37] R. Joshi,[122] J. Jovicevic,[16] X. Ju,[18a] J. J. Junggeburth,[37] T. Junkermann,[63a] A. Juste Rozas,[13,v] M. K. Juzek,[87] S. Kabana,[140e] A. Kaczmarska,[87] M. Kado,[112] H. Kagan,[122] M. Kagan,[149] A. Kahn,[131] C. Kahra,[102] T. Kaji,[159] E. Kajomovitz,[156] N. Kakati,[175] N. Kakoty,[13] I. Kalaitzidou,[54] S. Kandel,[8] N. J. Kang,[139] D. Kar,[34g] K. Karava,[129] E. Karentzos,[25] O. Karkout,[117] S. N. Karpov,[39] Z. M. Karpova,[39] V. Kartvelishvili,[93] A. N. Karyukhin,[38] E. Kasimi,[158] J. Katzy,[48] S. Kaur,[35] K. Kawade,[146] M. P. Kawale,[123] C. Kawamoto,[89] T. Kawamoto,[62] E. F. Kay,[37] F. I. Kaya,[164] S. Kazakos,[109] V. F. Kazanin,[38] J. M. Keaveney,[34a] R. Keeler,[171] G. V. Kehris,[61] J. S. Keller,[35] J. J. Kempster,[152] O. Kepka,[134] J. Kerr,[162b] B. P. Kerridge,[137] B. P. Kerševan,[95] L. Keszeghova,[29a] R. A. Khan,[132] A. Khanov,[124] A. G. Kharlamov,[38] T. Kharlamova,[38] E. E. Khoda,[142] M. Kholodenko,[133a] T. J. Khoo,[19] G. Khoriauli,[172] Y. Khoulaki,[36a] J. Khubua,[155b,a] Y. A. R. Khwaira,[130] B. Kibirige,[34g] D. Kim,[6] D. W. Kim,[47a,47b] Y. K. Kim,[40] N. Kimura,[98] M. K. Kingston,[55] A. Kirchhoff,[55] C. Kirfel,[25] F. Kirfel,[25] J. Kirk,[137] A. E. Kiryunin,[112] S. Kita,[163] O. Kivernyk,[25] M. Klassen,[164] C. Klein,[35] L. Klein,[172] M. H. Klein,[45] S. B. Klein,[56] U. Klein,[94] A. Klimentov,[30] T. Klioutchnikova,[37] P. Kluit,[117] S. Kluth,[112] E. Kneringer,[79] T. M. Knight,[161] A. Knue,[49] M. Kobel,[50] D. Kobylianskii,[175] S. F. Koch,[129] M. Kocian,[149] P. Kodyš,[136] D. M. Koeck,[126] T. Koffas,[35] O. Kolay,[50] I. Koletsou,[4] T. Komarek,[87] K. Köneke,[55] A. X. Y. Kong,[1] T. Kono,[121] N. Konstantinidis,[98] P. Kontaxakis,[56] B. Konya,[100] R. Kopeliansky,[42] S. Koperny,[86a] K. Korcyl,[87] K. Kordas,[158,bb] A. Korn,[98] S. Korn,[55] I. Korolkov,[13] N. Korotkova,[38] B. Kortman,[117] O. Kortner,[112] S. Kortner,[112] W. H. Kostecka,[118] M. Kostov,[29a] V. V. Kostyukhin,[147] A. Kotsokechagia,[37] A. Kotwal,[51] A. Koulouris,[37] A. Kourkoumeli-Charalampidi,[73a,73b] C. Kourkoumelis,[9] E. Kourlitis,[112] O. Kovanda,[126] R. Kowalewski,[171] W. Kozanecki,[126] A. S. Kozhin,[38] V. A. Kramarenko,[38] G. Kramberger,[95] P. Kramer,[25] M. W. Krasny,[130] A. Krasznahorkay,[105] A. C. Kraus,[118] J. W. Kraus,[177] J. A. Kremer,[48] N. B. Krengel,[147] T. Kresse,[50] L. Kretschmann,[177] J. Kretzschmar,[94] K. Kreul,[19] P. Krieger,[161] K. Krizka,[21] K. Kroeninger,[49] H. Kroha,[112] J. Kroll,[134] J. Kroll,[131] K. S. Krowpman,[109] U. Kruchonak,[39] H. Krüger,[25] N. Krumnack,[81] M. C. Kruse,[51] O. Kuchinskaia,[39] S. Kuday,[3a] S. Kuehn,[37] R. Kuesters,[54] T. Kuhl,[48] V. Kukhtin,[39] Y. Kulchitsky,[39] S. Kuleshov,[140d,140b] J. Kull,[1] M. Kumar,[34g] N. Kumari,[48] P. Kumari,[162b] A. Kupco,[134] T. Kupfer,[49] A. Kupich,[38] O. Kuprash,[54] H. Kurashige,[85] L. L. Kurchaninov,[162a] O. Kurdysh,[4] Y. A. Kurochkin,[38] A. Kurova,[38] M. Kuze,[141] A. K. Kvam,[105] J. Kvita,[125] N. G. Kyriacou,[108] C. Lacasta,[169] F. Lacava,[75a,75b] H. Lacker,[19] D. Lacour,[130] N. N. Lad,[98] E. Ladygin,[39] A. Lafarge,[41] B. Laforge,[130] T. Lagouri,[178] F. Z. Lahbabi,[36a] S. Lai,[55] J. E. Lambert,[171] S. Lammers,[68] W. Lampl,[7] C. Lampoudis,[158,bb] G. Lamprinoudis,[102] A. N. Lancaster,[118] E. Lançon,[30] U. Landgraf,[54] M. P. J. Landon,[96] V. S. Lang,[54] O. K. B. Langrekken,[128] A. J. Lankford,[165] F. Lanni,[37] K. Lantzsch,[25] A. Lanza,[73a] M. Lanzac Berrocal,[169] J. F. Laporte,[138] T. Lari,[71a] D. Larsen,[17] L. Larson,[11] F. Lasagni Manghi,[24b] M. Lassnig,[37] S. D. Lawlor,[145] R. Lazaridou,[173] M. Lazzaroni,[71a,71b] H. D. M. Le,[109] E. M. Le Boulicaut,[178] L. T. Le Pottier,[18a] B. Leban,[24b,24a] F. Ledroit-Guillon,[60] T. F. Lee,[162b] L. L. Leeuw,[34c] M. Lefebvre,[171] C. Leggett,[18a] G. Lehmann Miotto,[37]

M. Leigh,[56] W. A. Leight,[105] W. Leinonen,[116] A. Leisos,[158,cc] M. A. L. Leite,[83c] C. E. Leitgeb,[19] R. Leitner,[136] K. J. C. Leney,[45] T. Lenz,[25] S. Leone,[74a] C. Leonidopoulos,[52] A. Leopold,[150] J. H. Lepage Bourbonnais,[35] R. Les,[109] C. G. Lester,[33] M. Levchenko,[38] J. Levêque,[4] L. J. Levinson,[175] G. Levrini,[24b,24a] M. P. Lewicki,[87] C. Lewis,[142] D. J. Lewis,[4] L. Lewitt,[145] A. Li,[30] B. Li,[143a] C. Li,[108] C-Q. Li,[112] H. Li,[143a] H. Li,[103] H. Li,[15] H. Li,[62] H. Li,[143a] J. Li,[144a] K. Li,[14] L. Li,[144a] R. Li,[178] S. Li,[14,114c] S. Li,[144b,144a] T. Li,[5] X. Li,[106] Z. Li,[159] Z. Li,[14,114c] Z. Li,[62] S. Liang,[14,114c] Z. Liang,[14] M. Liberatore,[138] B. Liberti,[76a] K. Lie,[64c] J. Lieber Marin,[83e] H. Lien,[68] H. Lin,[108] S. F. Lin,[151] L. Linden,[111] R. E. Lindley,[7] J. H. Lindon,[37] J. Ling,[61] E. Lipeles,[131] A. Lipniacka,[17] A. Lister,[170] J. D. Little,[68] B. Liu,[14] B. X. Liu,[114b] D. Liu,[144b,144a] E. H. L. Liu,[21] J. K. K. Liu,[120] K. Liu,[144b] K. Liu,[144b,144a] M. Liu,[62] M. Y. Liu,[62] P. Liu,[14] Q. Liu,[144b,142,144a] X. Liu,[62] X. Liu,[143a] Y. Liu,[114b,114c] Y. L. Liu,[143a] Y. W. Liu,[62] Z. Liu,[66,dd] S. L. Lloyd,[96] E. M. Lobodzinska,[48] P. Loch,[7] E. Lodhi,[161] T. Lohse,[19] K. Lohwasser,[145] E. Loiacono,[48] J. D. Lomas,[21] J. D. Long,[42] I. Longarini,[165] R. Longo,[168] A. Lopez Solis,[13] N. A. Lopez-canelas,[7] N. Lorenzo Martinez,[4] A. M. Lory,[111] M. Losada,[119a] G. Löschcke Centeno,[152] X. Lou,[47a,47b] X. Lou,[14,114c] A. Lounis,[66] P. A. Love,[93] G. Lu,[14,114c] M. Lu,[66] S. Lu,[131] Y. J. Lu,[154] H. J. Lubatti,[142] C. Luci,[75a,75b] F. L. Lucio Alves,[114a] F. Luehring,[68] B. S. Lunday,[131] O. Lundberg,[150] J. Lunde,[37] N. A. Luongo,[6] M. S. Lutz,[37] A. B. Lux,[26] D. Lynn,[30] R. Lysak,[134] V. Lysenko,[135] E. Lytken,[100] V. Lyubushkin,[39] T. Lyubushkina,[39] M. M. Lyukova,[151] M. Firdaus M. Soberi,[52] H. Ma,[30] K. Ma,[62] L. L. Ma,[143a] W. Ma,[62] Y. Ma,[124] J. C. MacDonald,[102] P. C. Machado De Abreu Farias,[83e] R. Madar,[41] T. Madula,[98] J. Maeda,[85] T. Maeno,[30] P. T. Mafa,[34c,ee] H. Maguire,[145] V. Maiboroda,[66] A. Maio,[133a,133b,133d] K. Maj,[86a] O. Majersky,[48] S. Majewski,[126] R. Makhmanazarov,[38] N. Makovec,[66] V. Maksimovic,[16] B. Malaescu,[130] J. Malamant,[128] Pa. Malecki,[87] V. P. Maleev,[38] F. Malek,[60,ff] M. Mali,[95] D. Malito,[97] U. Mallik,[80,a] A. Maloizel,[5] S. Maltezos,[10] A. Malvezzi Lopes,[83d] S. Malyukov,[39] J. Mamuzic,[13] G. Mancini,[53] M. N. Mancini,[27] G. Manco,[73a,73b] J. P. Mandalia,[96] S. S. Mandarry,[152] I. Mandić,[95] L. Manhaes de Andrade Filho,[83a] I. M. Maniatis,[175] J. Manjarres Ramos,[91] D. C. Mankad,[175] A. Mann,[111] T. Manoussos,[37] M. N. Mantinan,[40] S. Manzoni,[37] L. Mao,[144a] X. Mapekula,[34c] A. Marantis,[158] R. R. Marcelo Gregorio,[96] G. Marchiori,[5] M. Marcisovsky,[134] C. Marcon,[71a] E. Maricic,[16] M. Marinescu,[48] S. Marium,[48] M. Marjanovic,[123] A. Markhoos,[54] M. Markovitch,[66] M. K. Maroun,[105] G. T. Marsden,[103] E. J. Marshall,[93] Z. Marshall,[18a] S. Marti-Garcia,[169] J. Martin,[98] T. A. Martin,[137] V. J. Martin,[52] B. Martin dit Latour,[17] L. Martinelli,[75a,75b] M. Martinez,[13,v] P. Martinez Agullo,[169] V. I. Martinez Outschoorn,[105] P. Martinez Suarez,[13] S. Martin-Haugh,[137] G. Martinovicova,[136] V. S. Martoiu,[28b] A. C. Martyniuk,[98] A. Marzin,[37] D. Mascione,[78a,78b] L. Masetti,[102] J. Masik,[103] A. L. Maslennikov,[39] S. L. Mason,[42] P. Massarotti,[72a,72b] P. Mastrandrea,[74a,74b] A. Mastroberardino,[44b,44a] T. Masubuchi,[127] T. T. Mathew,[126] J. Matousek,[136] D. M. Mattern,[49] J. Maurer,[28b] T. Maurin,[59] A. J. Maury,[66] B. Maček,[95] C. Mavungu Tsava,[104] D. A. Maximov,[38] A. E. May,[103] E. Mayer,[41] R. Mazini,[34g] I. Maznas,[118] S. M. Mazza,[139] E. Mazzeo,[71a,71b] J. P. Mc Gowan,[171] S. P. Mc Kee,[108] C. A. Mc Lean,[6] C. C. McCracken,[170] E. F. McDonald,[107] A. E. McDougall,[117] L. F. Mcelhinney,[93] J. A. Mcfayden,[152] R. P. McGovern,[131] R. P. Mckenzie,[34g] T. C. Mclachlan,[48] D. J. Mclaughlin,[98] S. J. McMahon,[137] C. M. Mcpartland,[94] R. A. McPherson,[171,p] S. Mehlhase,[111] A. Mehta,[94] D. Melini,[169] B. R. Mellado Garcia,[34g] A. H. Melo,[55] F. Meloni,[48] A. M. Mendes Jacques Da Costa,[103] L. Meng,[93] S. Menke,[112] M. Mentink,[37] E. Meoni,[44b,44a] G. Mercado,[118] S. Merianos,[158] C. Merlassino,[69a,69c] C. Meroni,[71a,71b] J. Metcalfe,[6] A. S. Mete,[6] E. Meuser,[102] C. Meyer,[68] J-P. Meyer,[138] Y. Miao,[114a] R. P. Middleton,[137] M. Mihovilovic,[66] L. Mijović,[52] G. Mikenberg,[175] M. Mikestikova,[134] M. Mikuž,[95] H. Mildner,[102] A. Milic,[37] D. W. Miller,[40] E. H. Miller,[149] L. S. Miller,[35] A. Milov,[175] D. A. Milstead,[47a,47b] T. Min,[114a] A. A. Minaenko,[38] I. A. Minashvili,[155b] A. I. Mincer,[120] B. Mindur,[86a] M. Mineev,[39] Y. Mino,[89] L. M. Mir,[13] M. Miralles Lopez,[59] M. Mironova,[18a] M. C. Missio,[116] A. Mitra,[173] V. A. Mitsou,[169] Y. Mitsumori,[113] O. Miu,[161] P. S. Miyagawa,[96] T. Mkrtchyan,[63a] M. Mlinarevic,[98] T. Mlinarevic,[98] M. Mlynarikova,[37] S. Mobius,[20] M. H. Mohamed Farook,[115] A. F. Mohammed,[14,114c] S. Mohapatra,[42] S. Mohiuddin,[124] G. Mokgatitswane,[34g] L. Moleri,[175] U. Molinatti,[129] L. G. Mollier,[20] B. Mondal,[147] S. Mondal,[135] K. Mönig,[48] E. Monnier,[104] L. Monsonis Romero,[169] J. Montejo Berlingen,[13] A. Montella,[47a,47b] M. Montella,[122] F. Montereali,[77a,77b] F. Monticelli,[92] S. Monzani,[69a,69c] A. Morancho Tarda,[43] N. Morange,[66] A. L. Moreira De Carvalho,[48] M. Moreno Llácer,[169] C. Moreno Martinez,[56] J. M. Moreno Perez,[23b]

P. Morettini,[57b] S. Morgenstern,[37] M. Morii,[61] M. Morinaga,[159] M. Moritsu,[90] F. Morodei,[75a,75b] P. Moschovakos,[37] B. Moser,[54] M. Mosidze,[155b] T. Moskalets,[45] P. Moskvitina,[116] J. Moss,[32] P. Moszkowicz,[86a] A. Moussa,[36d] Y. Moyal,[175] H. Moyano Gomez,[13] E. J. W. Moyse,[105] O. Mtintsilana,[34g] S. Muanza,[104] M. Mucha,[25] J. Mueller,[132] R. Müller,[37] G. A. Mullier,[167] A. J. Mullin,[33] J. J. Mullin,[51] A. E. Mulski,[61] D. P. Mungo,[161] D. Munoz Perez,[169] F. J. Munoz Sanchez,[103] W. J. Murray,[173,137] M. Muškinja,[95] C. Mwewa,[48] A. G. Myagkov,[38,l] A. J. Myers,[8] G. Myers,[108] M. Myska,[135] B. P. Nachman,[18a] K. Nagai,[129] K. Nagano,[84] R. Nagasaka,[159] J. L. Nagle,[30,gg] E. Nagy,[104] A. M. Nairz,[37] Y. Nakahama,[84] K. Nakamura,[84] K. Nakkalil,[5] H. Nanjo,[127] E. A. Narayanan,[45] Y. Narukawa,[159] I. Naryshkin,[38] L. Nasella,[71a,71b] S. Nasri,[119b] C. Nass,[25] G. Navarro,[23a] J. Navarro-Gonzalez,[169] A. Nayaz,[19] P. Y. Nechaeva,[38] S. Nechaeva,[24b,24a] F. Nechansky,[134] L. Nedic,[129] T. J. Neep,[21] A. Negri,[73a,73b] M. Negrini,[24b] C. Nellist,[117] C. Nelson,[106] K. Nelson,[108] S. Nemecek,[134] M. Nessi,[37,hh] M. S. Neubauer,[168] J. Newell,[94] P. R. Newman,[21] Y. W. Y. Ng,[168] B. Ngair,[119a] H. D. N. Nguyen,[110] J. D. Nichols,[123] R. B. Nickerson,[129] R. Nicolaidou,[138] J. Nielsen,[139] M. Niemeyer,[55] J. Niermann,[37] N. Nikiforou,[37] V. Nikolaenko,[38,l] I. Nikolic-Audit,[130] P. Nilsson,[30] I. Ninca,[48] G. Ninio,[157] A. Nisati,[75a] N. Nishu,[2] R. Nisius,[112] N. Nitika,[69a,69c] J-E. Nitschke,[50] E. K. Nkadimeng,[34b] T. Nobe,[159] T. Nommensen,[153] M. B. Norfolk,[145] B. J. Norman,[35] M. Noury,[36a] J. Novak,[95] T. Novak,[95] R. Novotny,[135] L. Nozka,[125] K. Ntekas,[165] N. M. J. Nunes De Moura Junior,[83b] J. Ocariz,[130] A. Ochi,[85] I. Ochoa,[133a] S. Oerdek,[48,ii] J. T. Offermann,[40] A. Ogrodnik,[136] A. Oh,[103] C. C. Ohm,[150] H. Oide,[84] M. L. Ojeda,[37] Y. Okumura,[159] L. F. Oleiro Seabra,[133a] I. Oleksiyuk,[56] G. Oliveira Correa,[13] D. Oliveira Damazio,[30] J. L. Oliver,[165] Ö. O. Öncel,[54] A. P. O'Neill,[20] A. Onofre,[133a,133e,jj] P. U. E. Onyisi,[11] M. J. Oreglia,[40] D. Orestano,[77a,77b] R. Orlandini,[77a,77b] R. S. Orr,[161] L. M. Osojnak,[131] Y. Osumi,[113] G. Otero y Garzon,[31] H. Otono,[90] G. J. Ottino,[18a] M. Ouchrif,[36d] F. Ould-Saada,[128] T. Ovsiannikova,[142] M. Owen,[59] R. E. Owen,[137] V. E. Ozcan,[22a] F. Ozturk,[87] N. Ozturk,[8] S. Ozturk,[82] H. A. Pacey,[129] K. Pachal,[162a] A. Pacheco Pages,[13] C. Padilla Aranda,[13] G. Padovano,[75a,75b] S. Pagan Griso,[18a] G. Palacino,[68] A. Palazzo,[70a,70b] J. Pampel,[25] J. Pan,[178] T. Pan,[64a] D. K. Panchal,[11] C. E. Pandini,[117] J. G. Panduro Vazquez,[137] H. D. Pandya,[1] H. Pang,[138] P. Pani,[48] G. Panizzo,[69a,69c] L. Panwar,[130] L. Paolozzi,[56] S. Parajuli,[168] A. Paramonov,[6] C. Paraskevopoulos,[53] D. Paredes Hernandez,[64b] A. Pareti,[73a,73b] K. R. Park,[42] T. H. Park,[112] F. Parodi,[57b,57a] J. A. Parsons,[42] U. Parzefall,[54] B. Pascual Dias,[41] L. Pascual Dominguez,[101] E. Pasqualucci,[75a] S. Passaggio,[57b] F. Pastore,[97] P. Patel,[87] U. M. Patel,[51] J. R. Pater,[103] T. Pauly,[37] F. Pauwels,[136] C. I. Pazos,[164] M. Pedersen,[128] R. Pedro,[133a] S. V. Peleganchuk,[38] O. Penc,[37] E. A. Pender,[52] S. Peng,[15] G. D. Penn,[178] K. E. Penski,[111] M. Penzin,[38] B. S. Peralva,[83d] A. P. Pereira Peixoto,[142] L. Pereira Sanchez,[149] D. V. Perepelitsa,[30,gg] G. Perera,[105] E. Perez Codina,[162a] M. Perganti,[10] H. Pernegger,[37] S. Perrella,[75a,75b] O. Perrin,[41] K. Peters,[48] R. F. Y. Peters,[103] B. A. Petersen,[37] T. C. Petersen,[43] E. Petit,[104] V. Petousis,[135] A. R. Petri,[71a,71b] C. Petridou,[158,bb] T. Petru,[136] A. Petrukhin,[147] M. Pettee,[18a] A. Petukhov,[82] K. Petukhova,[37] R. Pezoa,[140f] L. Pezzotti,[24b,24a] G. Pezzullo,[178] L. Pfaffenbichler,[37] A. J. Pfleger,[37] T. M. Pham,[176] T. Pham,[107] P. W. Phillips,[137] G. Piacquadio,[151] E. Pianori,[18a] F. Piazza,[126] R. Piegaia,[31] D. Pietreanu,[28b] A. D. Pilkington,[103] M. Pinamonti,[69a,69c] J. L. Pinfold,[2] B. C. Pinheiro Pereira,[133a] J. Pinol Bel,[13] A. E. Pinto Pinoargote,[130] L. Pintucci,[69a,69c] K. M. Piper,[152] A. Pirttikoski,[56] D. A. Pizzi,[35] L. Pizzimento,[64b] A. Plebani,[33] M.-A. Pleier,[30] V. Pleskot,[136] E. Plotnikova,[39] G. Poddar,[96] R. Poettgen,[100] L. Poggioli,[130] S. Polacek,[136] G. Polesello,[73a] A. Poley,[148] A. Polini,[24b] C. S. Pollard,[173] Z. B. Pollock,[122] E. Pompa Pacchi,[123] N. I. Pond,[98] D. Ponomarenko,[68] L. Pontecorvo,[37] S. Popa,[28a] G. A. Popeneciu,[28d] A. Poreba,[37] D. M. Portillo Quintero,[162a] S. Pospisil,[135] M. A. Postill,[145] P. Postolache,[28c] K. Potamianos,[173] P. A. Potepa,[86a] I. N. Potrap,[39] C. J. Potter,[33] H. Potti,[153] J. Poveda,[169] M. E. Pozo Astigarraga,[37] R. Pozzi,[37] A. Prades Ibanez,[76a,76b] J. Pretel,[171] D. Price,[103] M. Primavera,[70a] L. Primomo,[69a,69c] M. A. Principe Martin,[101] R. Privara,[125] T. Procter,[86b] M. L. Proffitt,[142] N. Proklova,[131] K. Prokofiev,[64c] G. Proto,[112] J. Proudfoot,[6] M. Przybycien,[86a] W. W. Przygoda,[86b] A. Psallidas,[46] J. E. Puddefoot,[145] D. Pudzha,[53] D. Pyatiizbyantseva,[116] J. Qian,[108] R. Qian,[109] D. Qichen,[103] Y. Qin,[13] T. Qiu,[52] A. Quadt,[55] M. Queitsch-Maitland,[103] G. Quetant,[56] R. P. Quinn,[170] G. Rabanal Bolanos,[61] D. Rafanoharana,[54] F. Raffaeli,[76a,76b] F. Ragusa,[71a,71b] J. L. Rainbolt,[40] J. A. Raine,[56] S. Rajagopalan,[30] E. Ramakoti,[39] L. Rambelli,[57b,57a] I. A. Ramirez-Berend,[35] K. Ran,[48,114c] D. S. Rankin,[131] N. P. Rapheeha,[34g] H. Rasheed,[28b] D. F. Rassloff,[63a] A. Rastogi,[18a] S. Rave,[102] S. Ravera,[57b,57a] B. Ravina,[37] I. Ravinovich,[175]

M. Raymond,[37] A. L. Read,[128] N. P. Readioff,[145] D. M. Rebuzzi,[73a,73b] A. S. Reed,[112] K. Reeves,[27] J. A. Reidelsturz,[177] D. Reikher,[126] A. Rej,[49] C. Rembser,[37] H. Ren,[62] M. Renda,[28b] F. Renner,[48] A. G. Rennie,[59] A. L. Rescia,[48] S. Resconi,[71a] M. Ressegotti,[57b,57a] S. Rettie,[37] W. F. Rettie,[35] E. Reynolds,[18a] O. L. Rezanova,[39] P. Reznicek,[136] H. Riani,[36d] N. Ribaric,[51] E. Ricci,[78a,78b] R. Richter,[112] S. Richter,[47a,47b] E. Richter-Was,[86b] M. Ridel,[130] S. Ridouani,[36d] P. Rieck,[120] P. Riedler,[37] E. M. Riefel,[47a,47b] J. O. Rieger,[117] M. Rijssenbeek,[151] M. Rimoldi,[37] L. Rinaldi,[24b,24a] P. Rincke,[167] G. Ripellino,[167] I. Riu,[13] J. C. Rivera Vergara,[171] F. Rizatdinova,[124] E. Rizvi,[96] B. R. Roberts,[18a] S. S. Roberts,[139] D. Robinson,[33] M. Robles Manzano,[102] A. Robson,[59] A. Rocchi,[76a,76b] C. Roda,[74a,74b] S. Rodriguez Bosca,[37] Y. Rodriguez Garcia,[23a] A. M. Rodríguez Vera,[118] S. Roe,[37] J. T. Roemer,[37] O. Røhne,[128] R. A. Rojas,[37] C. P. A. Roland,[130] A. Romaniouk,[79] E. Romano,[73a,73b] M. Romano,[24b] A. C. Romero Hernandez,[168] N. Rompotis,[94] L. Roos,[130] S. Rosati,[75a] B. J. Rosser,[40] E. Rossi,[129] E. Rossi,[72a,72b] L. P. Rossi,[61] L. Rossini,[54] R. Rosten,[122] M. Rotaru,[28b] B. Rottler,[54] D. Rousseau,[66] D. Rousso,[48] S. Roy-Garand,[161] A. Rozanov,[104] Z. M. A. Rozario,[59] Y. Rozen,[156] A. Rubio Jimenez,[169] V. H. Ruelas Rivera,[19] T. A. Ruggeri,[1] A. Ruggiero,[129] A. Ruiz-Martinez,[169] A. Rummler,[37] Z. Rurikova,[54] N. A. Rusakovich,[39] H. L. Russell,[171] G. Russo,[75a,75b] J. P. Rutherfoord,[7] S. Rutherford Colmenares,[33] M. Rybar,[136] P. Rybczynski,[86a] A. Ryzhov,[45] J. A. Sabater Iglesias,[56] H. F-W. Sadrozinski,[139] F. Safai Tehrani,[75a] S. Saha,[1] M. Sahinsoy,[82] B. Sahoo,[175] A. Saibel,[169] B. T. Saifuddin,[123] M. Saimpert,[138] G. T. Saito,[83c] M. Saito,[159] T. Saito,[159] A. Sala,[71a,71b] A. Salnikov,[149] J. Salt,[169] A. Salvador Salas,[157] F. Salvatore,[152] A. Salzburger,[37] D. Sammel,[54] E. Sampson,[93] D. Sampsonidis,[158,bb] D. Sampsonidou,[126] J. Sánchez,[169] V. Sanchez Sebastian,[169] H. Sandaker,[128] C. O. Sander,[48] J. A. Sandesara,[176] M. Sandhoff,[177] C. Sandoval,[23b] L. Sanfilippo,[63a] D. P. C. Sankey,[137] T. Sano,[89] A. Sansoni,[53] L. Santi,[37] C. Santoni,[41] H. Santos,[133a,133b] A. Santra,[175] E. Sanzani,[24b,24a] K. A. Saoucha,[88b] J. G. Saraiva,[133a,133d] J. Sardain,[7] O. Sasaki,[84] K. Sato,[163] C. Sauer,[37] E. Sauvan,[4] P. Savard,[161,e] R. Sawada,[159] C. Sawyer,[137] L. Sawyer,[99] C. Sbarra,[24b] A. Sbrizzi,[24b,24a] T. Scanlon,[98] J. Schaarschmidt,[142] U. Schäfer,[102] A. C. Schaffer,[66,45] D. Schaile,[111] R. D. Schamberger,[151] C. Scharf,[19] M. M. Schefer,[20] V. A. Schegelsky,[38] D. Scheirich,[136] M. Schernau,[140e] C. Scheulen,[56] C. Schiavi,[57b,57a] M. Schioppa,[44b,44a] B. Schlag,[149] S. Schlenker,[37] J. Schmeing,[177] E. Schmidt,[112] M. A. Schmidt,[177] K. Schmieden,[102] C. Schmitt,[102] N. Schmitt,[102] S. Schmitt,[48] L. Schoeffel,[138] A. Schoening,[63b] P. G. Scholer,[35] E. Schopf,[147] M. Schott,[25] S. Schramm,[56] T. Schroer,[56] H-C. Schultz-Coulon,[63a] M. Schumacher,[54] B. A. Schumm,[139] Ph. Schune,[138] H. R. Schwartz,[139] A. Schwartzman,[149] T. A. Schwarz,[108] Ph. Schwemling,[138] R. Schwienhorst,[109] F. G. Sciacca,[20] A. Sciandra,[30] G. Sciolla,[27] F. Scuri,[74a] C. D. Sebastiani,[37] K. Sedlaczek,[118] S. C. Seidel,[115] A. Seiden,[139] B. D. Seidlitz,[42] C. Seitz,[48] J. M. Seixas,[83b] G. Sekhniaidze,[72a] L. Selem,[60] N. Semprini-Cesari,[24b,24a] A. Semushin,[179] D. Sengupta,[56] V. Senthilkumar,[169] L. Serin,[66] M. Sessa,[76a,76b] H. Severini,[123] F. Sforza,[57b,57a] A. Sfyrla,[56] Q. Sha,[14] E. Shabalina,[55] H. Shaddix,[118] A. H. Shah,[33] R. Shaheen,[150] J. D. Shahinian,[131] M. Shamim,[37] L. Y. Shan,[14] M. Shapiro,[18a] A. Sharma,[37] A. S. Sharma,[170] P. Sharma,[30] P. B. Shatalov,[38] K. Shaw,[152] S. M. Shaw,[103] Q. Shen,[144a] D. J. Sheppard,[148] P. Sherwood,[98] L. Shi,[98] X. Shi,[14] S. Shimizu,[84] C. O. Shimmin,[178] I. P. J. Shipsey,[129,a] S. Shirabe,[90] M. Shiyakova,[39,kk] M. J. Shochet,[40] D. R. Shope,[128] B. Shrestha,[123] S. Shrestha,[122,ll] I. Shreyber,[39] M. J. Shroff,[171] P. Sicho,[134] A. M. Sickles,[168] E. Sideras Haddad,[34g,166] A. C. Sidley,[117] A. Sidoti,[24b] F. Siegert,[50] Dj. Sijacki,[16] F. Sili,[92] J. M. Silva,[52] I. Silva Ferreira,[83b] M. V. Silva Oliveira,[30] S. B. Silverstein,[47a] S. Simion,[66] R. Simoniello,[37] E. L. Simpson,[103] H. Simpson,[152] L. R. Simpson,[6] S. Simsek,[82] S. Sindhu,[55] P. Sinervo,[161] S. N. Singh,[27] S. Singh,[30] S. Sinha,[48] S. Sinha,[103] M. Sioli,[24b,24a] K. Sioulas,[9] I. Siral,[37] E. Sitnikova,[48] J. Sjölin,[47a,47b] A. Skaf,[55] E. Skorda,[21] P. Skubic,[123] M. Slawinska,[87] I. Slazyk,[17] V. Smakhtin,[175] B. H. Smart,[137] S. Yu. Smirnov,[140b] Y. Smirnov,[82] L. N. Smirnova,[38,l] O. Smirnova,[100] A. C. Smith,[42] D. R. Smith,[165] J. L. Smith,[103] M. B. Smith,[35] R. Smith,[149] H. Smitmanns,[102] M. Smizanska,[93] K. Smolek,[135] P. Smolyanskiy,[135] A. A. Snesarev,[39] H. L. Snoek,[117] S. Snyder,[30] R. Sobie,[171,p] A. Soffer,[157] C. A. Solans Sanchez,[37] E. Yu. Soldatov,[39] U. Soldevila,[169] A. A. Solodkov,[34g] S. Solomon,[27] A. Soloshenko,[39] K. Solovieva,[54] O. V. Solovyanov,[41] P. Sommer,[50] A. Sonay,[13] A. Sopczak,[135] A. L. Sopio,[52] F. Sopkova,[29b] J. D. Sorenson,[115] I. R. Sotarriva Alvarez,[141] V. Sothilingam,[63a] O. J. Soto Sandoval,[140c,140b] S. Sottocornola,[68] R. Soualah,[88a] Z. Soumaimi,[36e] D. South,[48] N. Soybelman,[175] S. Spagnolo,[70a,70b] M. Spalla,[112] D. Sperlich,[54] B. Spisso,[72a,72b]

D. P. Spiteri,[59] L. Splendori,[104] M. Spousta,[136] E. J. Staats,[35] R. Stamen,[63a] E. Stanecka,[87] W. Stanek-Maslouska,[48] M. V. Stange,[50] B. Stanislaus,[18a] M. M. Stanitzki,[48] B. Stapf,[48] E. A. Starchenko,[38] G. H. Stark,[139] J. Stark,[91] P. Staroba,[134] P. Starovoitov,[88b] R. Staszewski,[87] G. Stavropoulos,[46] A. Stefl,[37] P. Steinberg,[30] B. Stelzer,[148,162a] H. J. Stelzer,[132] O. Stelzer-Chilton,[162a] H. Stenzel,[58] T. J. Stevenson,[152] G. A. Stewart,[37] J. R. Stewart,[124] M. C. Stockton,[37] G. Stoicea,[28b] M. Stolarski,[133a] S. Stonjek,[112] A. Straessner,[50] J. Strandberg,[150] S. Strandberg,[47a,47b] M. Stratmann,[177] M. Strauss,[123] T. Strebler,[104] P. Strizenec,[29b] R. Ströhmer,[172] D. M. Strom,[126] R. Stroynowski,[45] A. Strubig,[47a,47b] S. A. Stucci,[30] B. Stugu,[17] J. Stupak,[123] N. A. Styles,[48] D. Su,[149] S. Su,[62] X. Su,[62] D. Suchy,[29a] K. Sugizaki,[131] V. V. Sulin,[38] M. J. Sullivan,[94] D. M. S. Sultan,[129] L. Sultanaliyeva,[38] S. Sultansoy,[3b] S. Sun,[176] W. Sun,[14] O. Sunneborn Gudnadottir,[167] N. Sur,[100] M. R. Sutton,[152] H. Suzuki,[163] M. Svatos,[134] P. N. Swallow,[33] M. Swiatlowski,[162a] T. Swirski,[172] I. Sykora,[29a] M. Sykora,[136] T. Sykora,[136] D. Ta,[102] K. Tackmann,[48,ii] A. Taffard,[165] R. Tafirout,[162a] Y. Takubo,[84] M. Talby,[104] A. A. Talyshev,[38] K. C. Tam,[64b] N. M. Tamir,[157] A. Tanaka,[159] J. Tanaka,[159] R. Tanaka,[66] M. Tanasini,[151] Z. Tao,[170] S. Tapia Araya,[140f] S. Tapprogge,[102] A. Tarek Abouelfadl Mohamed,[109] S. Tarem,[156] K. Tariq,[14] G. Tarna,[28b] G. F. Tartarelli,[71a] M. J. Tartarin,[91] P. Tas,[136] M. Tasevsky,[134] E. Tassi,[44b,44a] A. C. Tate,[168] G. Tateno,[159] Y. Tayalati,[36e,mm] G. N. Taylor,[107] W. Taylor,[162b] A. S. Tegetmeier,[91] P. Teixeira-Dias,[97] J. J. Teoh,[161] K. Terashi,[159] J. Terron,[101] S. Terzo,[13] M. Testa,[53] R. J. Teuscher,[161,p] A. Thaler,[79] O. Theiner,[56] T. Theveneaux-Pelzer,[104] D. W. Thomas,[97] J. P. Thomas,[21] E. A. Thompson,[18a] P. D. Thompson,[21] E. Thomson,[131] R. E. Thornberry,[45] C. Tian,[62] Y. Tian,[56] V. Tikhomirov,[82] Yu. A. Tikhonov,[39] S. Timoshenko,[38] D. Timoshyn,[136] E. X. L. Ting,[1] P. Tipton,[178] A. Tishelman-Charny,[30] K. Todome,[141] S. Todorova-Nova,[136] S. Todt,[50] L. Toffolin,[69a,69c] M. Togawa,[84] J. Tojo,[90] S. Tokár,[29a] O. Toldaiev,[68] G. Tolkachev,[104] M. Tomoto,[84,113] L. Tompkins,[149,nn] E. Torrence,[126] H. Torres,[91] E. Torró Pastor,[169] M. Toscani,[31] C. Tosciri,[40] M. Tost,[11] D. R. Tovey,[145] T. Trefzger,[172] P. M. Tricarico,[13] A. Tricoli,[30] I. M. Trigger,[162a] S. Trincaz-Duvoid,[130] D. A. Trischuk,[27] A. Tropina,[39] L. Truong,[34c] M. Trzebinski,[87] A. Trzupek,[87] F. Tsai,[151] M. Tsai,[108] A. Tsiamis,[158] P. V. Tsiareshka,[39] S. Tsigaridas,[162a] A. Tsirigotis,[158,cc] V. Tsiskaridze,[161] E. G. Tskhadadze,[155a] M. Tsopoulou,[158] Y. Tsujikawa,[89] I. I. Tsukerman,[38] V. Tsulaia,[18a] S. Tsuno,[84] K. Tsuri,[121] D. Tsybychev,[151] Y. Tu,[64b] A. Tudorache,[28b] V. Tudorache,[28b] S. Turchikhin,[57b,57a] I. Turk Cakir,[3a] R. Turra,[71a] T. Turtuvshin,[39,oo] P. M. Tuts,[42] S. Tzamarias,[158,bb] E. Tzovara,[102] Y. Uematsu,[84] F. Ukegawa,[163] P. A. Ulloa Poblete,[140c,140b] E. N. Umaka,[30] G. Unal,[37] A. Undrus,[30] G. Unel,[165] J. Urban,[29b] P. Urrejola,[140a] G. Usai,[8] R. Ushioda,[160] M. Usman,[110] F. Ustuner,[52] Z. Uysal,[82] V. Vacek,[135] B. Vachon,[106] T. Vafeiadis,[37] A. Vaitkus,[98] C. Valderanis,[111] E. Valdes Santurio,[47a,47b] M. Valente,[37] S. Valentinetti,[24b,24a] A. Valero,[169] E. Valiente Moreno,[169] A. Vallier,[91] J. A. Valls Ferrer,[169] D. R. Van Arneman,[117] T. R. Van Daalen,[142] A. Van Der Graaf,[49] H. Z. Van Der Schyf,[34g] P. Van Gemmeren,[6] M. Van Rijnbach,[37] S. Van Stroud,[98] I. Van Vulpen,[117] P. Vana,[136] M. Vanadia,[76a,76b] U. M. Vande Voorde,[150] W. Vandelli,[37] E. R. Vandewall,[124] D. Vannicola,[157] L. Vannoli,[53] R. Vari,[75a] E. W. Varnes,[7] C. Varni,[18b] D. Varouchas,[66] L. Varriale,[169] K. E. Varvell,[153] M. E. Vasile,[28b] L. Vaslin,[84] M. D. Vassilev,[149] A. Vasyukov,[39] L. M. Vaughan,[124] R. Vavricka,[136] T. Vazquez Schroeder,[13] J. Veatch,[32] V. Vecchio,[103] M. J. Veen,[105] I. Veliscek,[30] I. Velkovska,[95] L. M. Veloce,[161] F. Veloso,[133a,133c] S. Veneziano,[75a] A. Ventura,[70a,70b] S. Ventura Gonzalez,[138] A. Verbytskyi,[112] M. Verducci,[74a,74b] C. Vergis,[96] M. Verissimo De Araujo,[83b] W. Verkerke,[117] J. C. Vermeulen,[117] C. Vernieri,[149] M. Vessella,[165] M. C. Vetterli,[148,e] A. Vgenopoulos,[102] N. Viaux Maira,[140f] T. Vickey,[145] O. E. Vickey Boeriu,[145] G. H. A. Viehhauser,[129] L. Vigani,[63b] M. Vigl,[112] M. Villa,[24b,24a] M. Villaplana Perez,[169] E. M. Villhauer,[52] E. Vilucchi,[53] M. G. Vincter,[35] A. Visibile,[117] C. Vittori,[37] I. Vivarelli,[24b,24a] E. Voevodina,[112] F. Vogel,[111] J. C. Voigt,[50] P. Vokac,[135] Yu. Volkotrub,[86b] E. Von Toerne,[25] B. Vormwald,[37] K. Vorobev,[51] M. Vos,[169] K. Voss,[147] M. Vozak,[37] L. Vozdecky,[123] N. Vranjes,[16] M. Vranjes Milosavljevic,[16] M. Vreeswijk,[117] N. K. Vu,[144b,144a] R. Vuillermet,[37] O. Vujinovic,[102] I. Vukotic,[40] I. K. Vyas,[35] J. F. Wack,[33] S. Wada,[163] C. Wagner,[149] J. M. Wagner,[18a] W. Wagner,[177] S. Wahdan,[177] H. Wahlberg,[92] C. H. Waits,[123] J. Walder,[137] R. Walker,[111] W. Walkowiak,[147] A. Wall,[131] E. J. Wallin,[100] T. Wamorkar,[18a] A. Z. Wang,[139] C. Wang,[102] C. Wang,[11] H. Wang,[18a] J. Wang,[64c] P. Wang,[103] P. Wang,[98] R. Wang,[61] R. Wang,[6] S. M. Wang,[154] S. Wang,[14] T. Wang,[62] T. Wang,[62] W. T. Wang,[80] W. Wang,[14] X. Wang,[168] X. Wang,[144a] X. Wang,[48] Y. Wang,[114a] Y. Wang,[62] Z. Wang,[108] Z. Wang,[144b] Z. Wang,[108] C. Wanotayaroj,[84] A. Warburton,[106]

A. L. Warnerbring,[147] N. Warrack,[59] S. Waterhouse,[97] A. T. Watson,[21] H. Watson,[52] M. F. Watson,[21] E. Watton,[59] G. Watts,[142] B. M. Waugh,[98] J. M. Webb,[54] C. Weber,[30] H. A. Weber,[19] M. S. Weber,[20] S. M. Weber,[63a] C. Wei,[62] Y. Wei,[54] A. R. Weidberg,[129] E. J. Weik,[120] J. Weingarten,[49] C. Weiser,[54] C. J. Wells,[48] T. Wenaus,[30] B. Wendland,[49] T. Wengler,[37] N. S. Wenke,[112] N. Wermes,[25] M. Wessels,[63a] A. M. Wharton,[93] A. S. White,[61] A. White,[8] M. J. White,[1] D. Whiteson,[165] L. Wickremasinghe,[127] W. Wiedenmann,[176] M. Wielers,[137] R. Wierda,[150] C. Wiglesworth,[43] H. G. Wilkens,[37] J. J. H. Wilkinson,[33] D. M. Williams,[42] H. H. Williams,[131] S. Williams,[33] S. Willocq,[105] B. J. Wilson,[103] D. J. Wilson,[103] P. J. Windischhofer,[40] F. I. Winkel,[31] F. Winklmeier,[126] B. T. Winter,[54] M. Wittgen,[149] M. Wobisch,[99] T. Wojtkowski,[60] Z. Wolffs,[117] J. Wollrath,[37] M. W. Wolter,[87] H. Wolters,[133a,133c] M. C. Wong,[139] E. L. Woodward,[42] S. D. Worm,[48] B. K. Wosiek,[87] K. W. Woźniak,[87] S. Wozniewski,[55] K. Wraight,[59] C. Wu,[161] C. Wu,[21] J. Wu,[159] M. Wu,[114b] M. Wu,[116] S. L. Wu,[176] S. Wu,[14] X. Wu,[62] Y. Wu,[62] Z. Wu,[4] J. Wuerzinger,[112] T. R. Wyatt,[103] B. M. Wynne,[52] S. Xella,[43] L. Xia,[114a] M. Xia,[15] M. Xie,[62] A. Xiong,[126] J. Xiong,[18a] D. Xu,[14] H. Xu,[62] L. Xu,[62] R. Xu,[131] T. Xu,[108] Y. Xu,[142] Z. Xu,[52] Z. Xu,[114a] B. Yabsley,[153] S. Yacoob,[34a] Y. Yamaguchi,[84] E. Yamashita,[159] H. Yamauchi,[163] T. Yamazaki,[18a] Y. Yamazaki,[85] S. Yan,[59] Z. Yan,[105] H. J. Yang,[144a,144b] H. T. Yang,[62] S. Yang,[62] T. Yang,[64c] X. Yang,[37] X. Yang,[14] Y. Yang,[159] Y. Yang,[62] W-M. Yao,[18a] C. L. Yardley,[152] J. Ye,[14] S. Ye,[30] X. Ye,[62] Y. Yeh,[98] I. Yeletskikh,[39] B. Yeo,[18b] M. R. Yexley,[98] T. P. Yildirim,[129] P. Yin,[42] K. Yorita,[174] C. J. S. Young,[37] C. Young,[149] N. D. Young,[126] Y. Yu,[62] J. Yuan,[14,114c] M. Yuan,[108] R. Yuan,[144b,144a] L. Yue,[98] M. Zaazoua,[62] B. Zabinski,[87] I. Zahir,[36a] A. Zaio,[57b,57a] Z. K. Zak,[87] T. Zakareishvili,[169] S. Zambito,[56] J. A. Zamora Saa,[140d] J. Zang,[159] D. Zanzi,[54] R. Zanzottera,[71a,71b] O. Zaplatilek,[135] C. Zeitnitz,[177] H. Zeng,[14] J. C. Zeng,[168] D. T. Zenger Jr.,[27] O. Zenin,[38] T. Ženiš,[29a] S. Zenz,[96] D. Zerwas,[66] M. Zhai,[14,114c] D. F. Zhang,[145] G. Zhang,[14] J. Zhang,[143a] J. Zhang,[6] K. Zhang,[14,114c] L. Zhang,[62] L. Zhang,[114a] P. Zhang,[14,114c] R. Zhang,[176] S. Zhang,[91] T. Zhang,[159] X. Zhang,[144a] Y. Zhang,[142] Y. Zhang,[98] Y. Zhang,[62] Y. Zhang,[114a] Z. Zhang,[18a] Z. Zhang,[143a] Z. Zhang,[66] H. Zhao,[142] T. Zhao,[143a] Y. Zhao,[35] Z. Zhao,[62] Z. Zhao,[62] A. Zhemchugov,[39] J. Zheng,[114a] K. Zheng,[168] X. Zheng,[62] Z. Zheng,[149] D. Zhong,[168] B. Zhou,[108] H. Zhou,[7] N. Zhou,[144a] Y. Zhou,[15] Y. Zhou,[114a] Y. Zhou,[7] C. G. Zhu,[143a] J. Zhu,[108] X. Zhu,[144b] Y. Zhu,[144a] Y. Zhu,[62] X. Zhuang,[14] K. Zhukov,[68] N. I. Zimine,[39] J. Zinsser,[63b] M. Ziolkowski,[147] L. Živković,[16] A. Zoccoli,[24b,24a] K. Zoch,[61] T. G. Zorbas,[145] O. Zormpa,[46] and L. Zwalinski[37]

(ATLAS Collaboration)

[1]*Department of Physics, University of Adelaide, Adelaide, Australia*
[2]*Department of Physics, University of Alberta, Edmonton, Alberta, Canada*
[3a]*Department of Physics, Ankara University, Ankara, Türkiye*
[3b]*Division of Physics, TOBB University of Economics and Technology, Ankara, Türkiye*
[4]*LAPP, Université Savoie Mont Blanc, CNRS/IN2P3, Annecy, France*
[5]*APC, Université Paris Cité, CNRS/IN2P3, Paris, France*
[6]*High Energy Physics Division, Argonne National Laboratory, Argonne, Illinois, USA*
[7]*Department of Physics, University of Arizona, Tucson, Arizona, USA*
[8]*Department of Physics, University of Texas at Arlington, Arlington, Texas, USA*
[9]*Physics Department, National and Kapodistrian University of Athens, Athens, Greece*
[10]*Physics Department, National Technical University of Athens, Zografou, Greece*
[11]*Department of Physics, University of Texas at Austin, Austin, Texas, USA*
[12]*Institute of Physics, Azerbaijan Academy of Sciences, Baku, Azerbaijan*
[13]*Institut de Física d'Altes Energies (IFAE), Barcelona Institute of Science and Technology, Barcelona, Spain*
[14]*Institute of High Energy Physics, Chinese Academy of Sciences, Beijing, China*
[15]*Physics Department, Tsinghua University, Beijing, China*
[16]*Institute of Physics, University of Belgrade, Belgrade, Serbia*
[17]*Department for Physics and Technology, University of Bergen, Bergen, Norway*
[18a]*Physics Division, Lawrence Berkeley National Laboratory, Berkeley, California, USA*
[18b]*University of California, Berkeley, California, USA*
[19]*Institut für Physik, Humboldt Universität zu Berlin, Berlin, Germany*

[20]Albert Einstein Center for Fundamental Physics and Laboratory for High Energy Physics, University of Bern, Bern, Switzerland
[21]School of Physics and Astronomy, University of Birmingham, Birmingham, United Kingdom
[22a]Department of Physics, Bogazici University, Istanbul, Türkiye
[22b]Department of Physics Engineering, Gaziantep University, Gaziantep, Türkiye
[22c]Department of Physics, Istanbul University, Istanbul, Türkiye
[23a]Facultad de Ciencias y Centro de Investigaciónes, Universidad Antonio Nariño, Bogotá, Colombia
[23b]Departamento de Física, Universidad Nacional de Colombia, Bogotá, Colombia
[24a]Dipartimento di Fisica e Astronomia A. Righi, Università di Bologna, Bologna, Italy
[24b]INFN Sezione di Bologna, Bologna, Italy
[25]Physikalisches Institut, Universität Bonn, Bonn, Germany
[26]Department of Physics, Boston University, Boston, Massachusetts, USA
[27]Department of Physics, Brandeis University, Waltham, Massachusetts, USA
[28a]Transilvania University of Brasov, Brasov, Romania
[28b]Horia Hulubei National Institute of Physics and Nuclear Engineering, Bucharest, Romania
[28c]Department of Physics, Alexandru Ioan Cuza University of Iasi, Iasi, Romania
[28d]National Institute for Research and Development of Isotopic and Molecular Technologies, Physics Department, Cluj-Napoca, Romania
[28e]National University of Science and Technology Politechnica, Bucharest, Romania
[28f]West University in Timisoara, Timisoara, Romania
[28g]Faculty of Physics, University of Bucharest, Bucharest, Romania
[29a]Faculty of Mathematics, Physics and Informatics, Comenius University, Bratislava, Slovak Republic
[29b]Department of Subnuclear Physics, Institute of Experimental Physics of the Slovak Academy of Sciences, Kosice, Slovak Republic
[30]Physics Department, Brookhaven National Laboratory, Upton, New York, USA
[31]Universidad de Buenos Aires, Facultad de Ciencias Exactas y Naturales, Departamento de Física, y CONICET, Instituto de Física de Buenos Aires (IFIBA), Buenos Aires, Argentina
[32]California State University, Long Beach, California, USA
[33]Cavendish Laboratory, University of Cambridge, Cambridge, United Kingdom
[34a]Department of Physics, University of Cape Town, Cape Town, South Africa
[34b]iThemba Labs, Western Cape, South Africa
[34c]Department of Mechanical Engineering Science, University of Johannesburg, Johannesburg, South Africa
[34d]National Institute of Physics, University of the Philippines Diliman (Philippines), Quezon City, Philippines
[34e]University of South Africa, Department of Physics, Pretoria, South Africa
[34f]University of Zululand, KwaDlangezwa, South Africa
[34g]School of Physics, University of the Witwatersrand, Johannesburg, South Africa
[35]Department of Physics, Carleton University, Ottawa, Ontario, Canada
[36a]Faculté des Sciences Ain Chock, Université Hassan II de Casablanca, Casablanca, Morocco
[36b]Faculté des Sciences, Université Ibn-Tofail, Kénitra, Morocco
[36c]Faculté des Sciences Semlalia, Université Cadi Ayyad, LPHEA-Marrakech, Morocco
[36d]LPMR, Faculté des Sciences, Université Mohamed Premier, Oujda, Morocco
[36e]Faculté des sciences, Université Mohammed V, Rabat, Morocco
[36f]Institute of Applied Physics, Mohammed VI Polytechnic University, Ben Guerir, Morocco
[37]CERN, Geneva, Switzerland
[38]Affiliated with an institute formerly covered by a cooperation agreement with CERN
[39]Affiliated with an international laboratory covered by a cooperation agreement with CERN
[40]Enrico Fermi Institute, University of Chicago, Chicago, Illinois, USA
[41]LPC, Université Clermont Auvergne, CNRS/IN2P3, Clermont-Ferrand, France
[42]Nevis Laboratory, Columbia University, Irvington, New York, USA
[43]Niels Bohr Institute, University of Copenhagen, Copenhagen, Denmark
[44a]Dipartimento di Fisica, Università della Calabria, Rende, Italy
[44b]INFN Gruppo Collegato di Cosenza, Laboratori Nazionali di Frascati, Italy
[45]Physics Department, Southern Methodist University, Dallas, Texas, USA
[46]National Centre for Scientific Research "Demokritos," Agia Paraskevi, Greece
[47a]Department of Physics, Stockholm University, Stockholm, Sweden
[47b]Oskar Klein Centre, Stockholm, Sweden
[48]Deutsches Elektronen-Synchrotron DESY, Hamburg and Zeuthen, Germany
[49]Fakultät Physik, Technische Universität Dortmund, Dortmund, Germany

[50]*Institut für Kern- und Teilchenphysik, Technische Universität Dresden, Dresden, Germany*
[51]*Department of Physics, Duke University, Durham, North Carolina, USA*
[52]*SUPA—School of Physics and Astronomy, University of Edinburgh, Edinburgh, United Kingdom*
[53]*INFN e Laboratori Nazionali di Frascati, Frascati, Italy*
[54]*Physikalisches Institut, Albert-Ludwigs-Universität Freiburg, Freiburg, Germany*
[55]*II. Physikalisches Institut, Georg-August-Universität Göttingen, Göttingen, Germany*
[56]*Département de Physique Nucléaire et Corpusculaire, Université de Genève, Genève, Switzerland*
[57a]*Dipartimento di Fisica, Università di Genova, Genova, Italy*
[57b]*INFN Sezione di Genova, Genova, Italy*
[58]*II. Physikalisches Institut, Justus-Liebig-Universität Giessen, Giessen, Germany*
[59]*SUPA—School of Physics and Astronomy, University of Glasgow, Glasgow, United Kingdom*
[60]*LPSC, Université Grenoble Alpes, CNRS/IN2P3, Grenoble INP, Grenoble, France*
[61]*Laboratory for Particle Physics and Cosmology, Harvard University, Cambridge, Massachusetts, USA*
[62]*Department of Modern Physics and State Key Laboratory of Particle Detection and Electronics, University of Science and Technology of China, Hefei, China*
[63a]*Kirchhoff-Institut für Physik, Ruprecht-Karls-Universität Heidelberg, Heidelberg, Germany*
[63b]*Physikalisches Institut, Ruprecht-Karls-Universität Heidelberg, Heidelberg, Germany*
[64a]*Department of Physics, Chinese University of Hong Kong, Shatin, N.T., Hong Kong, China*
[64b]*Department of Physics, University of Hong Kong, Hong Kong, China*
[64c]*Department of Physics and Institute for Advanced Study, Hong Kong University of Science and Technology, Clear Water Bay, Kowloon, Hong Kong, China*
[65]*Department of Physics, National Tsing Hua University, Hsinchu, Taiwan*
[66]*IJCLab, Université Paris-Saclay, CNRS/IN2P3, 91405, Orsay, France*
[67]*Centro Nacional de Microelectrónica (IMB-CNM-CSIC), Barcelona, Spain*
[68]*Department of Physics, Indiana University, Bloomington, Indiana, USA*
[69a]*INFN Gruppo Collegato di Udine, Sezione di Trieste, Udine, Italy*
[69b]*ICTP, Trieste, Italy*
[69c]*Dipartimento Politecnico di Ingegneria e Architettura, Università di Udine, Udine, Italy*
[70a]*INFN Sezione di Lecce, Lecce, Italy*
[70b]*Dipartimento di Matematica e Fisica, Università del Salento, Lecce, Italy*
[71a]*INFN Sezione di Milano, Milano, Italy*
[71b]*Dipartimento di Fisica, Università di Milano, Milano, Italy*
[72a]*INFN Sezione di Napoli, Napoli, Italy*
[72b]*Dipartimento di Fisica, Università di Napoli, Napoli, Italy*
[73a]*INFN Sezione di Pavia, Pavia, Italy*
[73b]*Dipartimento di Fisica, Università di Pavia, Pavia, Italy*
[74a]*INFN Sezione di Pisa, Pisa, Italy*
[74b]*Dipartimento di Fisica E. Fermi, Università di Pisa, Pisa, Italy*
[75a]*INFN Sezione di Roma, Roma, Italy*
[75b]*Dipartimento di Fisica, Sapienza Università di Roma, Roma, Italy*
[76a]*INFN Sezione di Roma Tor Vergata, Roma, Italy*
[76b]*Dipartimento di Fisica, Università di Roma Tor Vergata, Roma, Italy*
[77a]*INFN Sezione di Roma Tre, Roma, Italy*
[77b]*Dipartimento di Matematica e Fisica, Università Roma Tre, Roma, Italy*
[78a]*INFN-TIFPA, Italy*
[78b]*Università degli Studi di Trento, Trento, Italy*
[79]*Universität Innsbruck, Department of Astro and Particle Physics, Innsbruck, Austria*
[80]*University of Iowa, Iowa City, Iowa, USA*
[81]*Department of Physics and Astronomy, Iowa State University, Ames, Iowa, USA*
[82]*Istinye University, Sariyer, Istanbul, Türkiye*
[83a]*Departamento de Engenharia Elétrica, Universidade Federal de Juiz de Fora (UFJF), Juiz de Fora, Brazil*
[83b]*Universidade Federal do Rio De Janeiro COPPE/EE/IF, Rio de Janeiro, Brazil*
[83c]*Instituto de Física, Universidade de São Paulo, São Paulo, Brazil*
[83d]*Rio de Janeiro State University, Rio de Janeiro, Brazil*
[83e]*Federal University of Bahia, Bahia, Brazil*
[84]*KEK, High Energy Accelerator Research Organization, Tsukuba, Japan*
[85]*Graduate School of Science, Kobe University, Kobe, Japan*
[86a]*AGH University of Krakow, Faculty of Physics and Applied Computer Science, Krakow, Poland*
[86b]*Marian Smoluchowski Institute of Physics, Jagiellonian University, Krakow, Poland*

[87]Institute of Nuclear Physics Polish Academy of Sciences, Krakow, Poland
[88a]Khalifa University of Science and Technology, Abu Dhabi, United Arab Emirates
[88b]University of Sharjah, Sharjah, United Arab Emirates
[89]Faculty of Science, Kyoto University, Kyoto, Japan
[90]Research Center for Advanced Particle Physics and Department of Physics, Kyushu University, Fukuoka, Japan
[91]L2IT, Université de Toulouse, CNRS/IN2P3, UPS, Toulouse, France
[92]Instituto de Física La Plata, Universidad Nacional de La Plata and CONICET, La Plata, Argentina
[93]Physics Department, Lancaster University, Lancaster, United Kingdom
[94]Oliver Lodge Laboratory, University of Liverpool, Liverpool, United Kingdom
[95]Department of Experimental Particle Physics, Jožef Stefan Institute and Department of Physics, University of Ljubljana, Ljubljana, Slovenia
[96]Department of Physics and Astronomy, Queen Mary University of London, London, United Kingdom
[97]Department of Physics, Royal Holloway University of London, Egham, United Kingdom
[98]Department of Physics and Astronomy, University College London, London, United Kingdom
[99]Louisiana Tech University, Ruston, Louisiana, USA
[100]Fysiska institutionen, Lunds universitet, Lund, Sweden
[101]Departamento de Física Teorica C-15 and CIAFF, Universidad Autónoma de Madrid, Madrid, Spain
[102]Institut für Physik, Universität Mainz, Mainz, Germany
[103]School of Physics and Astronomy, University of Manchester, Manchester, United Kingdom
[104]CPPM, Aix-Marseille Université, CNRS/IN2P3, Marseille, France
[105]Department of Physics, University of Massachusetts, Amherst, Massachusetts, USA
[106]Department of Physics, McGill University, Montreal, Quebec, Canada
[107]School of Physics, University of Melbourne, Victoria, Australia
[108]Department of Physics, University of Michigan, Ann Arbor, Michigan, USA
[109]Department of Physics and Astronomy, Michigan State University, East Lansing, Michigan, USA
[110]Group of Particle Physics, University of Montreal, Montreal, Quebec, Canada
[111]Fakultät für Physik, Ludwig-Maximilians-Universität München, München, Germany
[112]Max-Planck-Institut für Physik (Werner-Heisenberg-Institut), München, Germany
[113]Graduate School of Science and Kobayashi-Maskawa Institute, Nagoya University, Nagoya, Japan
[114a]Department of Physics, Nanjing University, Nanjing, China
[114b]School of Science, Shenzhen Campus of Sun Yat-sen University, China
[114c]University of Chinese Academy of Science (UCAS), Beijing, China
[115]Department of Physics and Astronomy, University of New Mexico, Albuquerque, New Mexico, USA
[116]Institute for Mathematics, Astrophysics and Particle Physics, Radboud University/Nikhef, Nijmegen, Netherlands
[117]Nikhef National Institute for Subatomic Physics and University of Amsterdam, Amsterdam, Netherlands
[118]Department of Physics, Northern Illinois University, DeKalb, Illinois, USA
[119a]New York University Abu Dhabi, Abu Dhabi, United Arab Emirates
[119b]United Arab Emirates University, Al Ain, United Arab Emirates
[120]Department of Physics, New York University, New York, New York, USA
[121]Ochanomizu University, Otsuka, Bunkyo-ku, Tokyo, Japan
[122]The Ohio State University, Columbus, Ohio, USA
[123]Homer L. Dodge Department of Physics and Astronomy, University of Oklahoma, Norman, Oklahoma, USA
[124]Department of Physics, Oklahoma State University, Stillwater, Oklahoma, USA
[125]Palacký University, Joint Laboratory of Optics, Olomouc, Czech Republic
[126]Institute for Fundamental Science, University of Oregon, Eugene, Oregon, USA
[127]Graduate School of Science, University of Osaka, Osaka, Japan
[128]Department of Physics, University of Oslo, Oslo, Norway
[129]Department of Physics, Oxford University, Oxford, United Kingdom
[130]LPNHE, Sorbonne Université, Université Paris Cité, CNRS/IN2P3, Paris, France
[131]Department of Physics, University of Pennsylvania, Philadelphia, Pennsylvania, USA
[132]Department of Physics and Astronomy, University of Pittsburgh, Pittsburgh, Pennsylvania, USA
[133a]Laboratório de Instrumentação e Física Experimental de Partículas—LIP, Lisboa, Portugal
[133b]Departamento de Física, Faculdade de Ciências, Universidade de Lisboa, Lisboa, Portugal
[133c]Departamento de Física, Universidade de Coimbra, Coimbra, Portugal
[133d]Centro de Física Nuclear da Universidade de Lisboa, Lisboa, Portugal
[133e]Departamento de Física, Escola de Ciências, Universidade do Minho, Braga, Portugal
[133f]Departamento de Física Teórica y del Cosmos, Universidad de Granada, Granada, Spain

[133g]*Departamento de Física, Instituto Superior Técnico, Universidade de Lisboa, Lisboa, Portugal*
[134]*Institute of Physics of the Czech Academy of Sciences, Prague, Czech Republic*
[135]*Czech Technical University in Prague, Prague, Czech Republic*
[136]*Charles University, Faculty of Mathematics and Physics, Prague, Czech Republic*
[137]*Particle Physics Department, Rutherford Appleton Laboratory, Didcot, United Kingdom*
[138]*IRFU, CEA, Université Paris-Saclay, Gif-sur-Yvette, France*
[139]*Santa Cruz Institute for Particle Physics, University of California Santa Cruz, Santa Cruz, California, USA*
[140a]*Departamento de Física, Pontificia Universidad Católica de Chile, Santiago, Chile*
[140b]*Millennium Institute for Subatomic Physics at High Energy Frontier (SAPHIR), Santiago, Chile*
[140c]*Instituto de Investigación Multidisciplinario en Ciencia y Tecnología, y Departamento de Física, Universidad de La Serena, La Serena, Chile*
[140d]*Universidad Andres Bello, Department of Physics, Santiago, Chile*
[140e]*Instituto de Alta Investigación, Universidad de Tarapacá, Arica, Chile*
[140f]*Departamento de Física, Universidad Técnica Federico Santa María, Valparaíso, Chile*
[141]*Department of Physics, Institute of Science, Tokyo, Japan*
[142]*Department of Physics, University of Washington, Seattle, Washington, USA*
[143a]*Institute of Frontier and Interdisciplinary Science and Key Laboratory of Particle Physics and Particle Irradiation (MOE), Shandong University, Qingdao, China*
[143b]*School of Physics, Zhengzhou University, Zhengzhou, China*
[144a]*State Key Laboratory of Dark Matter Physics, School of Physics and Astronomy, Shanghai Jiao Tong University, Key Laboratory for Particle Astrophysics and Cosmology (MOE), SKLPPC, Shanghai, China*
[144b]*State Key Laboratory of Dark Matter Physics, Tsung-Dao Lee Institute, Shanghai Jiao Tong University, Shanghai, China*
[145]*Department of Physics and Astronomy, University of Sheffield, Sheffield, United Kingdom*
[146]*Department of Physics, Shinshu University, Nagano, Japan*
[147]*Department Physik, Universität Siegen, Siegen, Germany*
[148]*Department of Physics, Simon Fraser University, Burnaby, British Columbia, Canada*
[149]*SLAC National Accelerator Laboratory, Stanford, California, USA*
[150]*Department of Physics, Royal Institute of Technology, Stockholm, Sweden*
[151]*Departments of Physics and Astronomy, Stony Brook University, Stony Brook, New York, USA*
[152]*Department of Physics and Astronomy, University of Sussex, Brighton, United Kingdom*
[153]*School of Physics, University of Sydney, Sydney, Australia*
[154]*Institute of Physics, Academia Sinica, Taipei, Taiwan*
[155a]*E. Andronikashvili Institute of Physics, Iv. Javakhishvili Tbilisi State University, Tbilisi, Georgia*
[155b]*High Energy Physics Institute, Tbilisi State University, Tbilisi, Georgia*
[155c]*University of Georgia, Tbilisi, Georgia*
[156]*Department of Physics, Technion, Israel Institute of Technology, Haifa, Israel*
[157]*Raymond and Beverly Sackler School of Physics and Astronomy, Tel Aviv University, Tel Aviv, Israel*
[158]*Department of Physics, Aristotle University of Thessaloniki, Thessaloniki, Greece*
[159]*International Center for Elementary Particle Physics and Department of Physics, University of Tokyo, Tokyo, Japan*
[160]*Graduate School of Science and Technology, Tokyo Metropolitan University, Tokyo, Japan*
[161]*Department of Physics, University of Toronto, Toronto, Ontario, Canada*
[162a]*TRIUMF, Vancouver, British Columbia, Canada*
[162b]*Department of Physics and Astronomy, York University, Toronto, Ontario, Canada*
[163]*Division of Physics and Tomonaga Center for the History of the Universe, Faculty of Pure and Applied Sciences, University of Tsukuba, Tsukuba, Japan*
[164]*Department of Physics and Astronomy, Tufts University, Medford, Massachusetts, USA*
[165]*Department of Physics and Astronomy, University of California Irvine, Irvine, California, USA*
[166]*University of West Attica, Athens, Greece*
[167]*Department of Physics and Astronomy, University of Uppsala, Uppsala, Sweden*
[168]*Department of Physics, University of Illinois, Urbana, Illinois, USA*
[169]*Instituto de Física Corpuscular (IFIC), Centro Mixto Universidad de Valencia—CSIC, Valencia, Spain*
[170]*Department of Physics, University of British Columbia, Vancouver, British Columbia, Canada*
[171]*Department of Physics and Astronomy, University of Victoria, Victoria, British Columbia, Canada*
[172]*Fakultät für Physik und Astronomie, Julius-Maximilians-Universität Würzburg, Würzburg, Germany*
[173]*Department of Physics, University of Warwick, Coventry, United Kingdom*
[174]*Waseda University, Tokyo, Japan*

[175]*Department of Particle Physics and Astrophysics, Weizmann Institute of Science, Rehovot, Israel*
[176]*Department of Physics, University of Wisconsin, Madison, Wisconsin, USA*
[177]*Fakultät für Mathematik und Naturwissenschaften, Fachgruppe Physik, Bergische Universität Wuppertal, Wuppertal, Germany*
[178]*Department of Physics, Yale University, New Haven, Connecticut, USA*
[179]*Yerevan Physics Institute, Yerevan, Armenia*

[a]Deceased.
[b]Also at Department of Physics, King's College London, London, United Kingdom.
[c]Also at Institute of Physics, Azerbaijan Academy of Sciences, Baku, Azerbaijan.
[d]Also at Imam Mohammad Ibn Saud Islamic University, Saudi Arabia.
[e]Also at TRIUMF, Vancouver, British Columbia, Canada.
[f]Also at Department of Physics, University of Thessaly, Greece.
[g]Also at An-Najah National University, Nablus, Palestine.
[h]Also at Department of Physics, University of Fribourg, Fribourg, Switzerland.
[i]Also at Department of Physics, Westmont College, Santa Barbara, California, USA.
[j]Also at Departament de Fisica de la Universitat Autonoma de Barcelona, Barcelona, Spain.
[k]Also at University of Sienna, Italy.
[l]Also at Affiliated with an institute formerly covered by a cooperation agreement with CERN.
[m]Also at The Collaborative Innovation Center of Quantum Matter (CICQM), Beijing, China.
[n]Also at Faculty of Physics, Sofia University, "St. Kliment Ohridski," Sofia, Bulgaria.
[o]Also at Università di Napoli Parthenope, Napoli, Italy.
[p]Also at Institute of Particle Physics (IPP), Canada.
[q]Also at Department of Physics, Bolu Abant Izzet Baysal University, Bolu, Türkiye.
[r]Also at Faculty of Physics, University of Bucharest, Romania.
[s]Also at Borough of Manhattan Community College, City University of New York, New York, New York, USA.
[t]Also at National Institute of Physics, University of the Philippines Diliman (Philippines), Quezon City, Philippines.
[u]Also at Department of Financial and Management Engineering, University of the Aegean, Chios, Greece.
[v]Also at Institucio Catalana de Recerca i Estudis Avancats, ICREA, Barcelona, Spain.
[w]Also at Henan University, China.
[x]Also at CMD-AC UNEC Research Center, Azerbaijan State University of Economics (UNEC), Azerbaijan.
[y]Also at Yeditepe University, Physics Department, Istanbul, Türkiye.
[z]Also at Institute of Theoretical Physics, Ilia State University, Tbilisi, Georgia.
[aa]Also at CERN, Geneva, Switzerland.
[bb]Also at Center for Interdisciplinary Research and Innovation (CIRI-AUTH), Thessaloniki, Greece.
[cc]Also at Hellenic Open University, Patras, Greece.
[dd]Also at Department of Modern Physics and State Key Laboratory of Particle Detection and Electronics, University of Science and Technology of China, Hefei, China.
[ee]Also at Department of Mathematical Sciences, University of South Africa, Johannesburg, South Africa.
[ff]Also at Department of Physics, Stellenbosch University, South Africa.
[gg]Also at University of Colorado Boulder, Department of Physics, Boulder, Colorado, USA.
[hh]Also at Département de Physique Nucléaire et Corpusculaire, Université de Genève, Genève, Switzerland.
[ii]Also at Institut für Experimentalphysik, Universität Hamburg, Hamburg, Germany.
[jj]Also at Centre of Physics of the Universities of Minho and Porto (CF-UM-UP), Minho and Porto, Portugal.
[kk]Also at Institute for Nuclear Research and Nuclear Energy (INRNE) of the Bulgarian Academy of Sciences, Sofia, Bulgaria.
[ll]Also at Washington College, Chestertown, Maryland, USA.
[mm]Also at Institute of Applied Physics, Mohammed VI Polytechnic University, Ben Guerir, Morocco.
[nn]Also at Department of Physics, Stanford University, Stanford, California, USA.
[oo]Also at Institute of Physics and Technology, Mongolian Academy of Sciences, Ulaanbaatar, Mongolia.